Alma Mater Studiorum – Università degli Studi di Bologna

Scuola di Scienze Matematiche, Fisiche e Naturali

Dipartimento di Chimica "G. Ciamician"

DOTTORATO DI RICERCA IN

CHIMICA

Ciclo XXVII

Settore concorsuale di afferenza 03/B1

Settore scientifico-disciplinare di afferenza: CHIM 03

OPTIMIZATION OF MOLECULAR AND CRYSTALLINE FORMS OF DRUGS, AGROCHEMICALS, PESTICIDES IN RELATION TO ACTIVITY, BIOAVAILABILITY, PATENTABILITY AND TO THE FABRICATION OF POLYMORPHS, SOLVATES, CO-CRYSTALS WITH GREEN CHEMISTRY METHODS

presentata da: Dott. **Saverio Nanna**

Coordinatore Dottorato
Prof. **Aldo Roda**

Relatore
Prof. **Fabrizia Grepioni**

Esame finale - Anno 2014/2015

INDEX

PREFACE

This doctorate is supported by Regione Emilia Romagna as a part of a Spinner PhD project coordinated by the University of Parma.

The aim of the project is:

I. Production of polymorphs, solvates, hydrates and co-crystals with green chemistry methods;
II. Optimization of molecular and crystalline forms of drugs and pesticides in relation to activity, bioavailability and patentability.

During the first and second year, we selected APIs (active pharmaceutical ingredients) in order to study and rationalize the relationships between crystal structure and properties of the drugs in solid state and solution. In the last decades, a growing interest in the solid-state properties of the drugs in addition to their solution chemistry has blossomed. The achievement of the desired and/or the more stable polymorph during the production process can be a challenge for the industry; in this sense, crystallization environment plays a key role in the polymorphs discrimination.

The study of crystalline forms could be a valuable step to produce new polymorphs with better physical-chemical properties such as solubility, permeability, thermal stability, habit, bulk density, compressibility, friability, hygroscopicity and dissolution rate in order to have potential industrial applications.

A further way to improve these properties is the synthesis of co-crystals, i.e. solids that are crystalline materials composed of two or more molecules, which are in stoichiometric ratio and – as pure substances - are solid at ambient conditions.

Polymorph screening and synthesis of solvates and molecular/ionic co-crystals were performed according to green chemistry principles (grinding, kneading in addition to the traditional methods from solution). Part of this project was developed in collaboration with chemical/pharmaceutical companies such as BASF (Germany) and UCB (Belgium). These projects focused on the one hand on the optimization of conditions and parameters of crystallization processes (in terms of additives, concentration and temperature)[Braga D. et al. Cryst. Growth Des. 2014, 14, 5729−5736; Braga D. et al. Cryst. Growth Des., 2014, 14(3), pp1430–1437], and on the other hand on the synthesis and characterization of ionic co-crystals of piracetam derivatives[Grepioni F. et al. CrystEngComm, 2014, 16, 5887–5896].

During the period of research abroad spent in Ann Arbor (University of Michigan,USA), the stability in aqueous solution at the equilibrium of some ionic co-crystals (ICCs) of piracetam was investigated in collaboration with Professor Nair Rodriguez-Hormedo (department of Pharmaceutical Sciences). This study was useful to understand the relationship between solid-state properties and those in solution, to design new materials that reflect some of their properties in solution.

The following techniques were used for the characterization of solid products:

(i) X-ray diffraction from single crystal (SCXRD), the 'gold standard' in terms of structural characterisation;

(ii) X-ray powders diffraction (XRPD), provides the 'fingerprint' diffraction pattern characteristic of a crystalline solid form and, in favourable circumstances, allows structure solution or Rietveld refinement procedure;

(iii) Variable Temperature X-ray powders diffraction (VTXRPD), a valuable technique to assess the thermal properties of crystalline solid forms;

(iv) differential scanning calorimetry (DSC), useful in detecting phase changes with and without change in mass (loss of a volatile co-crystal component and polymorphic transition/melting respectively);

(v) thermogravimetric analysis (TG), useful in recording sample mass loss during heating process in order to quantify the mass loss and have indications on stoichiometry, especially in the presence of volatile co-crystal components;

(vi) hot-stage microscopy (HSM), used for a visual and instrumental evaluation of the thermal processes and complementary to the previous techniques cited;

(vii) measurements of dissolution rate (IDR), necessary to understand how fast is the dissolution of the crystalline form;

(viii) inductive coupling plasma with optical emission as detector (ICP-OES), employed during my period of research abroad for quantitative measurements in solution of inorganic salts;

(ix) UV-Spectrophotometer used during the period of research abroad used for quantitative measurements in solution of organic molecules.

In this thesis Chapter 1 introduces the concepts of crystal engineering and polymorphism and their effect on the pharmaceutical field in terms of the improvement of solid-state properties; Chapter 2 is focused on results and discussions.

Chapter 1

Introduction

INTRODUCTION

1.1 CRYSTAL ENGINEERING

In 1989, Desiraju defined crystal engineering as "*the understanding of intermolecular interactions in the context of crystal packing and in the utilisation of such understanding in the design of new solids with desired physical and chemical properties*"[1].

Crystal engineering has its roots in the 1960s with G. M. J. Schmidt and its studies of solid-state photo-cyclization reactions [2-5], which are a bright example of supramolecular control over chemical properties, and are still fascinating the world of crystal engineering. Crystal engineering deals with design, synthesis and characterization of crystalline materials with desired properties.

Schmidt's work is recognized as the first attempt to rationally design crystals with a purpose [2,6]. It is right to point out that supramolecular chemistry [7] was crucial in the development of crystal engineering, a field of research that includes all traditional chemistry branches, becoming ''*an all-purpose mature discipline, a science without borders, where the motivations can well be utilitarian and economical, but also aesthetical (when not artistic) and/or fuelled by pure, quintessential, scientific curiosity*''.[8]

The aim of the design and synthesis of new crystals is to obtain supramolecular organization with desired properties [9-25,50]

According to Jean-Marie Lehn, [26] supramolecular chemistry is: "*chemistry beyond the molecule bearing on the organised entities of higher complexity that result from the association of two or more chemical species held together by intermolecular forces*".

Therefore, we should think about a crystal as a supramolecular entity with a higher level of complexity with respect to molecules.[27,28]

Margaret Etter [29] in 1987 wrote: "*Organizing molecules into predictable arrays is the first step in a systematic approach to designing organic solid-state materials*".

1.1.1 Crystal packing and intermolecular interactions

Dunitz wrote: "*A crystal is, in a sense, the supramolecule par excellence: a lump of matter, of macroscopic dimensions, millions of molecules long, held together in a periodic arrangement by just the same kind of interactions as are responsible for molecular recognition and complexation at all levels - ion-ion, ion-dipole, dipole-dipole interactions, hydrogen bonding, London forces, and so on*". The understanding and the control of intramolecular interactions is a master key in the scenario of supramolecular synthesis.

In organic synthesis, but also in general, in order to develop a synthetic strategy, it is useful to apply a retrosynthetic approach in which the molecular structure can be simplified into a basic unit called *synthon* [30], which can be used as a synthetic tool to build complex supramolecular architectures.

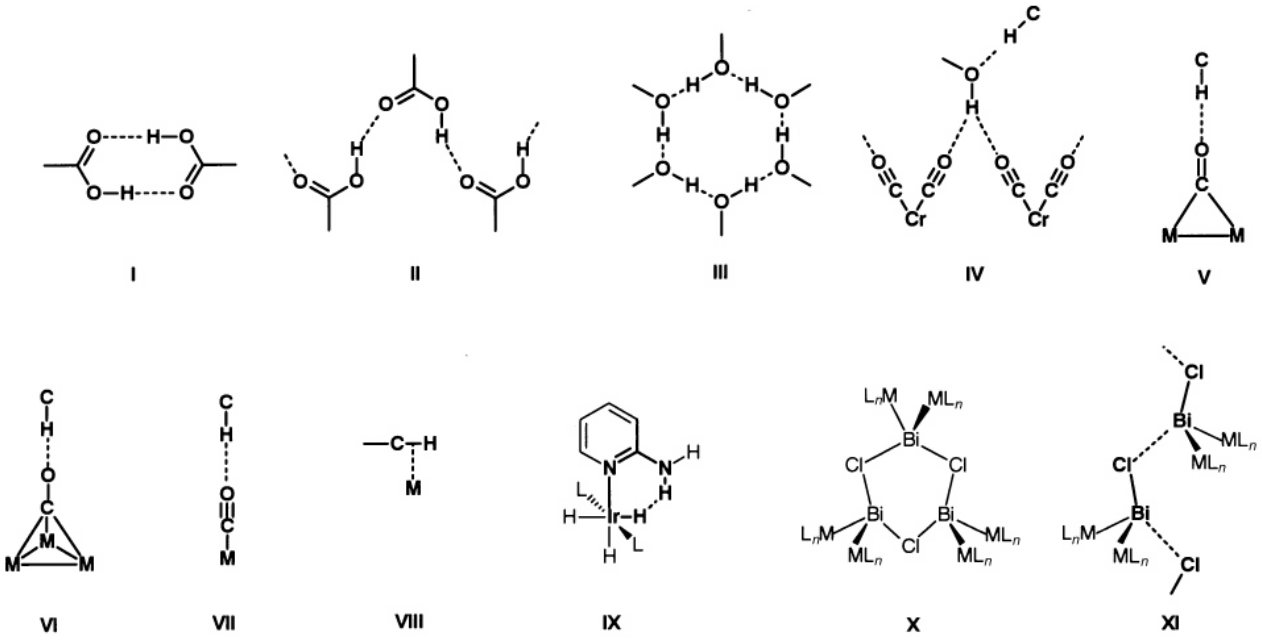

Scheme 1. Representative scheme of some supramolecular synthons. Reproduced from [31]

Another useful concept, complementary to *supramolecular synthons* [32,33], that has become of considerable practical importance in crystal engineering is the *tecton* defined by Wuest [34] as moieties ''whose interactions are dominated by specific attractive forces that induce the assembly of aggregates with controlled geometries''.[35]

1.1.2 Hydrogen Bonding

The hydrogen bond (HB) plays a key role in crystal engineering [36], as it is both an electrostatic and a directional interaction.

Various definitions of HB have followed [37] starting from Pimentel and McClellan who claimed: "*a hydrogen bond exists if 1) there is evidence of a bond, and 2) there is evidence that this bond sterically involves a hydrogen atom already bonded to another atom*"[36b]. Subsequently Etter[38], from an elaboration of Linus Pauling's definition, wrote: "*hydrogen bond is an interaction that directs the association of a covalently bound hydrogen atom with one or more other atoms, groups of atoms, or molecules into an aggregate structure that is sufficiently stable to make it convenient for the chemist to consider it as an independent chemical species*".

A further interpretation defines the "classical" HB as an interaction between a donor (X-H) and an acceptor (Y) with X an electronegative atom and Y an electronegative and electron rich atom. [39]

Jeffrey and Saenger [36] stated: "*the use of a van der Waals distance cutoff criterion carries the wrong implication that hydrogen bonds become van der Waals interactions at longer distances*". In this sense, HB is stabilized at distances greater than the sum of the radii of vdW; the vdW interactions decrease more rapidly with respect to the distance (r^{-6}) than the electrostatic interactions (r^{-1}). According to Jeffrey [36], HB is considered moderate in strength if the energies are in the range of 4-15 kcal/mol:HB is stronger if the energy is greater than 15 kcal/mol; HB is weaker if the energy is less than 4 kcal/mol. [53].

The strength of an hydrogen bond depends also on the pKa of both component involved in the bond and on the resonance-assisted hydrogen bonding (RAHB) mechanism [54,55]. Weak and moderate hydrogen bonds also play an important role in the landscape of the non-covalent interactions in the absence of strong HBs. The most common weak HB interactions are C-H···N, C-H···O, C-H···X (X= Cl,F), N-H···π …[40]. The strength of the weak HBs is directly proportional to the acidity or basicity of the acceptor groups like nitrogen, oxygen and halogens.

There is no clear demarcation between strong and weak hydrogen bonds, as the strongest of the weakest and the weakest of the strongest have comparable energy. The distance as a parameter of

strength of HB interaction is one of the features to be considered; the other one is the directionality, indeed HB can distinguished from vdW interaction for its preference for linearity. [36, 43, 44-47]

The presence of ionic charges on hydrogen bond acceptor and hydrogen bond donator reinforces the electrostatic dipole-dipole component of HB. This particular type of hydrogen bond is called Charge Assisted hydrogen Bond (CAHB)[41,48,49]. Charge-assisted hydrogen bonds are easily obtained via proton transfer in acid-base reactions and combine HB directionality with the strength of Coulombic forces. This type of hydrogen bond can be a valuable resource to design and synthesize 1D, 2D as well as 3D networks.

1.2 POLYMORPHISM

A polymorph is a solid crystalline phase of a given compound resulting from the possibility of at least two crystalline arrangements of the molecules of that compound in the solid state. [51]

Polymorphism represents one of the most fascinating phenomena of solid state chemistry because of its intrinsic difficulties to be predicted and rationalized.[52] The relationship between nucleation phase and crystalline growth is often unclear, indeed there are many examples of appearing and disappearing polymorphs[53]. Klaproth in 1788 was the first to identify the polymorphs of calcium carbonate (calcite, vaterite and aragonite) [54], but crystal polymorphism was recognized with Mitscherlich only in 1823 [55], when he observed the difference in physical and chemical properties in different crystals of arsenates and phosphates.[56,57] Benzamide was the first polymorphic organic compound studied [58] in 1832; in the last decades, due to the surge of interest and patenting issues in the pharmaceutical, agrochemical and pigment industries, polymorphism has become a central field of investigation for the solid-state scientific community. [59-65]

Sirota wrote in 1982: “Polymorphism is now believed to be characteristic of all substances, its actual non-occurance arising from the fact that a polymorphic transition lies above the melting point of the substance or in the area of as yet unattainable values of external equilibrium factor or other conditions providing for the transition”[66].

1.2.1 Conformational polymorphism

According to the IUPAC definition, a conformation is “the spatial arrangement of the atoms affording distinction between stereoisomers which can be interconverted by rotations about formally single bonds”. On the other side, a conformer is defined as “one of a set of stereoisomers, each of which is characterized by a conformation corresponding to a distinct potential energy minimum”.[67]

In 1962, Eliel stated that conformation “is used to denote any one of the infinite number of momentary arrangements of the atoms in space that result from rotation about single bonds”.[68] in 1985, Glusker and Trueblood define it as “One of the likely shapes of a molecule. Generally applied to molecules for which there is a possibility for rotation about bonds. Different rotational positions about bonds are represented by torsion angles.”[69]

Dunitz included another component, the energy: “we can be reasonably confident that any particular arrangement of atoms observed in a molecular crystal cannot be far from an equilibrium structure of the isolated molecule. X-ray analysis thus provides information about the preferred conformations of molecules although it has nothing to say about the energy differences between conformations or the energy barriers that separate them.”[70]

Cruz-Cabeza and Bernstein incorporated the term energy into the definition of conformer: “Any change in a given single rotatable bond (henceforth R- bond) of a molecule always affords a new conformation, but it affords a new conformer only if the conformational change goes through a potential energy barrier into a different potential energy well. Intermolecular interactions present in organic crystals are generally not sufficient to significantly perturb bond lengths and bond angles, but for those molecules that do exhibit torsional degrees of freedom, various polymorphs can exhibit different molecular conformations and, more importantly, different conformers.” [71]

Conformers correspond to distinct energy minima of the gas-phase potential energy surface (gas-PES). In a crystal the energy minima correspond to the minima of the sum of the intra- and intermolecular energies. The presence of neighbouring molecules and the effect of these molecules on the molecular conformations changes dramatically the environment with respect to the gas phase. When there is a

variation of a torsion angle, the molecule of interest has a new conformation; moreover, according to the authors [71], the molecule can be considered conformer if there is a noteworthy change in potential energy as a consequence of the new conformation. On the other hand, when flexible molecules tend to adapt themselves to the crystal environment varying slightly their conformation, there is a small conformational energy penalty reflected in a "conformational adjustament", see figure 1.

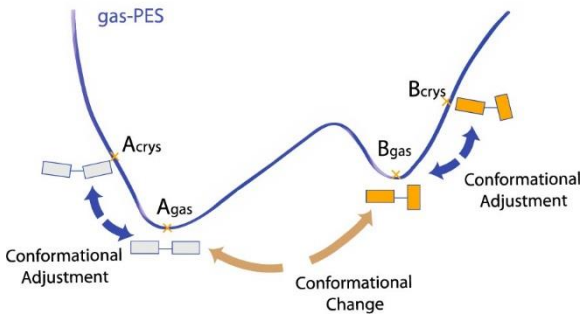

Figure 1. Schematic representation of "conformational change" and "conformational adjustment" [71].

It is worth stressing that the high occurrence of conformational polymorphism in APIs [72] is usually due to and facilitated by the flexibility of molecular structures [73].

1.2.2 Multiple crystal forms

The outcome of a crystallization process is hard to predict and can consist of new polymorphs, solvates, hydrates, salts and co-crystals[74] as well as solid solutions[75] and eutectics[76]. All these crystal forms are summarized in Figure 2.

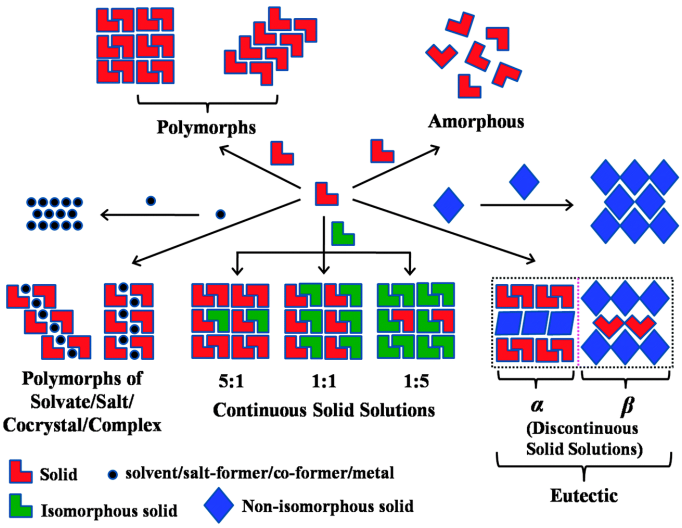

Figure 2. Schematic representation of the structural relationship between polymorphs, solvates, co-crystals, salts, amorphous, continuous and discontinuous solid solution.

The aim of the exploration of a polymorphic system is to find the most stable form and verify the existance of interconverting (enantiotropism) or non interconverting (monotropism) forms as a function of temperature – see figure 3.

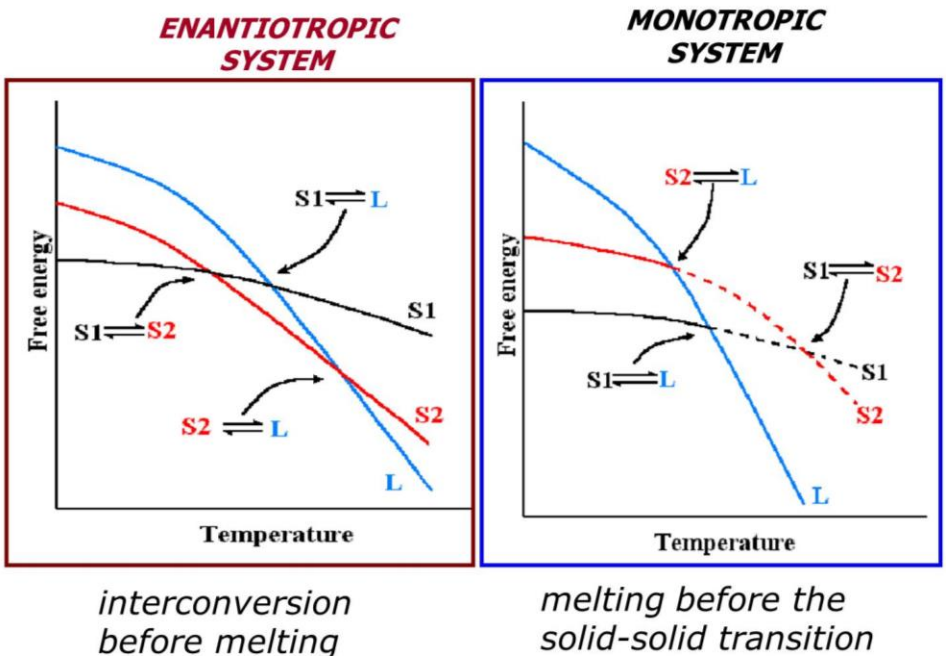

Figure 3. Qualitative E/T diagram for a dimorphic *enantiotropic* system (left), and for a dimorphic *monotropic* system (right).

Polymorphism can dramatically influence solubility but also other physical-chemical properties, like thermal and mechanical stability, permeability, hygroscopicity, habit, bulk density and so on.

Also the synthesis and study of co-crystals has gained importance in research and innovation in pharmaceutical and material science fields.[77,78-81] Pharmaceutical co-crystals investigation represents an opportunity to produce a stable crystalline solid starting from an amorphous or hard-to-crystallise API. Pharmaceutical co-crystal are composed by at least one API and the coformer should be

chosen so as to show no adverse side effects. Moreover, it should be approved by the USA Food and Drug Administration (FDA, for the US market)) or approved as Generally Regarded as Safe (GRAS). [82]

Co-crystals are composed by at least two components, which are present in stoichiometric ratio and are solid – as pure forms – at ambient condition. The practical application of pharmaceutical co-crystals depends on how a co-crystal is considered: it could be considered a physical mixture (regulated by current compendial guidelines), or a new chemical entity [83]. In this regard, the FDA has released (April 2013) a guidance for industry on the regulatory classification of pharmaceutical co-crystals for applicants for New Drug Applications (NDAs), in which is stated: "*In a co-crystal, the molecular association between an API and its excipient(s) occurs within the same crystal lattice and is governed by nonionic interactions, unlike the ionic interactions required for salt formation of an API. Therefore, within the Agency's current regulatory framework, co-crystals are classified as dissociable "API—excipient" molecular complexes (with the neutral guest compound being the excipient)*" [84]. In this sense, ionic co-crystals, [85] for which the co-former is an inorganic salt, are located in between co-crystals and salt definitions. Moreover, we deduce from these statements that the borderline between co-crystal and physical mixture is not well marked and it is reflected on the fact that no commercial pharmaceutical co-crystals have been approved so far for sale as drug substances.

Ideally, it is necessary to apply different methods in the research of polymorphs in order to minimize some risks linked to the presence of new unpredictable polymorphs, as shown by Jones and co-workers[86] or polymorphs obtained thorough fast crystallization methods which can lead to kinetic polymorphs, able to transform to a more stable form upon storage. An example is given by 1,3,5-trinitrobenzene[87] and its elusive thermodynamic form, ignored for 125 years.

Below are listed the most used crystallization techniques for a polymorph/multiple forms screening.

Crystallization from solution

Crystallization from solution is the most common method for air stable polymorph screening. It is performed preparing a near saturated solution with mixtures of solvents of different polarities in which the rate of evaporation of the solvent can be varied by changing the temperature.

Crystallization by thermal gradient

This method is alternative to the previous one; the near saturated solution at high temperature is kept in a sealed vial and the crystallization process depends on the temperature gradient applied upon cooling.

Solvent/Vapour diffusion

This method is used with to samples that are air and/or solvent sensitive. The solid sample, pure or as a mixture, is exposed to solvent vapours or moisture.

Solid-state synthesis

As an alternative to solvent-based crystallization techniques, solid-state synthesis (manual or mechanical grinding) has been extensively used for crystals and co-crystals screening [88]. Grinding with a catalytic amount of solvent (kneading) added to the reactants can also be employed. [89] These two methods usually improve the reaction rate, as temperature increases upon grinding; continuous contact between the different components is also achieved.

Hydrothermal and solvothermal synthesis

Hydrothermal or solvothermal synthesis are techniques widely used for the synthesis of inorganic or metal-organic material[90] but also employed for crystal and co-crystal polymorph screening. For example, Wang et al. applied this technique to prepare a co-crystal involving 1,2-bis(4-pyridyl)ethylene (BPE) and 4,4'-dihydroxybenzophenone (DHB).[91]

High-Pressure Crystallization Process

Fabbiani et al. described how pressure can be used to explore polymorphism, and provided examples of compounds studied at high pressure.[92,93]

REFERENCES:

[1] G. R. Desiraju and R. Parthasarathy, J. Am. Chem. Soc.,1989, 111, 8725.

[2] G. M. J. Schmidt, Pure Appl. Chem., 1971,27, 647–678.

[3] M. D. Cohen and G. M. J. Schmidt, J. Chem. Soc., 1996-2000 (1964).

[4] M. D. Cohen, G. M. J. Schmidt, and F. I. Sonntag, J. Chem. Soc., 2000-2013 (1964).

[5] G. M. J. Schmidt, ibid., 2014-2021 (1964).

[6]L. R. MacGillivray, CrystEngComm,2002, 4, 37; L. R. Macgillivray, G. S. Papaefstathiou, T. Friscic, T. D. Hamilton, D. K. Bucar, Q. Chu, D. B. Varshney and I. G. Georgiev, Acc. Chem. Res., 2008, 41, 280–291.

[7] J. M. Lehn, Angew. Chem., Int. Ed. Engl., 1990, 29, 1304; J. M. Lehn, Supramolecular Chemistry: Concepts and Perspectives, VCH, Weinheim, 1995; J. W. Steed and J. L. Atwood, Supramolecular Chemistry, Wiley & Sons, 2000.

[8] D. Braga, J. Miller, G. R. Desiraju, A. G. Orpen and S. L. Price, CrystEngComm, 2002, 4, 500.

[9] A. I. Kitaigorodskii, Molecular Crystals and Molecules, Academic Press, New York, 1973.

[10] J. M. Thomas, Nature 1981, 289, 633 – 634.

[11] L. Addadi, M. Lahav, Pure Appl. Chem. 1979, 51, 1269 – 1284.

[12] G. Wegner, Z. Naturforsch. B 1969, 24, 824 – 832.

[13] Crystal Engineering. From Molecules and Crystals to Materials (Eds.: D. Braga, F. Grepioni, A. G. Orpen), Kluwer, Dordrecht, 1999.

[14] Frontiers in Crystal Engineering (Eds.: E. R. Tiekink, J. J.Vittal), Wiley, Chichester, 2005.

[15] C. V. K. Sharma, Cryst. Growth Des. 2002, 2, 465 – 474.

[16] D. Braga, F. Grepioni, Chem. Commun. 2005, 3635 – 3645.

[17] A. D. Burrows, Encyclopedia of Supramolecular Chemistry,Vol. 1 (Eds.: J. Atwood, J. Steed), Marcel Dekker, New York, 2004, pp. 319 – 325.

[18] P. Coppens, S. L. Zheng, M. Gembicky, M. Messerschmidt, P. M. Dominiak, CrystEngComm 2006, 8, 735 – 741.

[19] R. Bishop, Synlett 1999, 1351 – 1358.

[20] K. Biradha, CrystEngComm 2003, 5, 374 – 384.

[21] S. A. Dalrymple, G. K. H. Shimizu, J. Mol. Struct. 2006, 796, 95 – 106.

[22] P. Erk, H. Hengelsberg, M. F. Haddow, R. van Gelder, CrystEngComm 2004, 6, 474 – 483.

[23] J. M. Lehn, Angew. Chem. 1988, 100, 91 – 116; Angew. Chem. Int. Ed. Engl. 1988, 27, 89 – 112.

[24] J. D. Dunitz, Pure Appl. Chem. 1991, 63, 177 – 185.

[25] G. M.Whitesides, E. E. Simanek, J. P. Mathias, C. T. Seto, D. N. Chin, M. Mammen, D. M. Gordon, Acc. Chem. Res. 1995, 28, 37 – 44.

[26] Nobel lecture, December 8, 1987

[27] M. C. T. Fyfe, J. F. Stoddart, Acc. Chem. Res. 1997, 30, 393 – 401.

[28] G. R. Desiraju, Curr. Sci. 2005, 88, 374 – 380.

[29] Thomas W. Panunto , Zofia Urbanczyk-Lipkowska , Ruth Johnson , Margaret C. Etter J. Am. Chem. Soc., 1987, 109 (25), pp 7786–7797.

[30] E.J.Corey, Pure Appl.Chem, 1967, 14, 19; E.J.Corey, Chem.Soc.rev. 1998, 17,111.

[31] G. R. Desiraju, J. Chem. Soc., Dalton Trans., 2000, 3745.

[32] M. W. Hosseini, Acc. Chem. Res., 2005, 38, 313–323; M. W. Hosseini, CrystEngComm, 2004, 6, 318–322.

[33] S. A. Barnett, A. J. Blake and N. R. Champness, CrystEngComm, 2003, 5, 134–136; C. B. Aakeroy, A. M. Beatty and B. A. Helfrich, Angew. Chem., Int. Ed., 2001, 40, 3240; C. B. Aakeroy, M. Fasulo, N. Schultheiss, J. Desper and C. Moore, J. Am. Chem. Soc., 2007, 129, 13772–13773.

[34] P. Brunet, M. Simard and J. D. Wuest, J. Am. Chem. Soc., 1997, 119, 2737.

[35] J. Hamblin, S. P. Argent, A. J. Blake, C. Wilson and N. R. Champness, CrystEngComm, 2008, 10, 1782.

[36] Braga, D.; Grepioni, F. Hydrogen Bonding Interactions with the CO-Ligand in the Solid State. Acc. Chem. Res. 1997, 30, 81; T. Steiner, Angew. Chem. Int. Ed. 2002, 41, 48-76; G. C. Pimentel, A. L. McClellan, The Hydrogen Bond, Freeman, San Francisco, 1960 ; L. Pauling, The Nature of the Chemical Bond, 3rd ed., Cornell University Press, Ithaca, 1963; W. C. Hamilton, J. A. Ibers, Hydrogen Bonding in Solids, Benjamin, New York, 1968; G. A. Jeffrey, W. Saenger, Hydrogen Bonding in Biological Structures, Springer, Berlin, 1991; G. A. Jeffrey, An Introduction to Hydrogen Bonding, Oxford University Press, Oxford, 1997; S. Scheiner, Hydrogen Bonding. A Theoretical Perspective, Oxford University Press, Oxford, 1997; G. R. Desiraju, T. Steiner, The Weak Hydrogen Bond in Structural

Chemistry and Biology, Oxford University Press, Oxford, 1999; The Hydrogen Bond (Ed.: D. Hadzi), Pergamon, New York, 1957; The Hydrogen Bond. Recent Developments in Theory and Experiment, Vols. 1-3 (Eds.: P. Schuster, G. Zundel, C. Sandorfy), North-Holland, Amsterdam, 1976; Theoretical Treatments of Hydrogen Bonding (Ed.: D. Hadzi),Wiley, Chichester, 1997.

[37] Aakeroy, C. B.; Seddon, K. R. The Hydrogen Bond and Crystal Engineering. Chem. Soc. Rev. 1993, 397.

[38] Etter, M. C. Encoding and Decoding Hydrogen-Bond Patterns of Organic Compounds. Acc. Chem. Res. 1990, 23, 120.

[39] Gordon, M. S.; Jensen, J. H. Understanding The Hydrogen Bond Using Quantum Chemistry. Acc. Chem. Res. 1996, 29, 536.

[40]D.R. Armstrong, S. Bennett, M.G. Davidson, R. Snaith, D. Stalke, D.s. Wright, J.Chem.Soc. Commun. 1992,262; M.A. Viswamitra, R.Radhakrishnan, G.R. Desiraju, J. Am. Chem. Soc. 1993, 115, 4868.

[41] P. Gilli, V. Ferretti, V. Bertolasi, G. Gilli, J. Am. Chem. Soc 1994, 116, 909-915.

[42] F.Fillaux, N. Leygue, J. Tomkinson, A. Cousson, W. Paulus, Chem. Phys. 1999, 244, 387-403.

[43] J.Kroon, J.A. Kanters, Nature, 1974, 248, 667-669.

[44] H.H.J. Savage, J. Finney, Nature 1986, 322, 717-720.

[45] D. Braga, F. Grepioni, E. Tedesco, Organometalics 1998, 17, 2669-2672.

[46] C.B. Aakeroy, T.A. Evans, K.R. Seddon, I. Palinko, New J. Chem. 1999, 23, 145-152; P.K. Thallapally, A. Nangia, CrystEngComm 2001, 27.

[47] V.R. Thalladi, H.C. Weiss, D.Blaser, R. Boese, A. Nangia, G.R. Desiraju, J. Am. Chem. Soc. 1998, 120, 8702-8710.

[48] Speakman J.C. 1972 Struct Bond 12, 141.

[49] Grabowsky S.J. 2006 Annu Rep Prop Chem Sect C, 102, 131.

[50] G.R. Desiraju Angew. Chem. Int. Ed. 2007, 46, 8342 – 8356

[51] W. C. McCrone, Physics and Chemistry of the Organic Solid State Vol. 2 in Interscience, New York, p. 725, 1965.

[52] J. Bernstein, Polymorphism in molecular crystals. Oxford University Press, Oxford, 2002, p.352

[53] JD Dunitz, J Bernstein, Acc Chem Res, 1995, 28, 193-200.

[54] MH Klaproth, bergmannische J, 1798, I, 294-299.

[55] E Mitscherlich 1823 Abhl Akad Berlin 43

[56] Mitscherlich, E. Ann. Chim. Phys. 1822, 19, 350.

[57] Mitscherlich, E. Ann. Chim. Phys. 1823, 24, 264.

[58] Liebig, J.; Wöhler, F. Ann. Pharm. III 1832, 249, 514.

[59] Hartley, H. Polymorphism: An Historical Account; Holywell Press: Oxford, U.K., 1902.

[60] Deffet, L. Repertoire des Composes Editions Desoer: Liege, Belgium, 1942.Organiques Polymorphes

[61] Groth, P. Chemische Krystallographie; Wilhelm Engelmann: Leipzig, Germany, 1906; Vol. I.

[62] Groth, P. Chemische Krystallographie; Wilhelm Engelmann: Leipzig, Germany, 1908; Vol. II.

[63] Groth, P. Chemische Krystallographie; Wilhelm Engelmann: Leipzig, Germany, 1910; Vol. III.

[64] Groth, P. Chemische Krystallographie; Wilhelm Engelmann: Leipzig, Germany, 1917; Vol. IV.

[65] Groth, P. Chemische Krystallographie; Wilhelm Engelmann: Leipzig, Germany, 1919; Vol. V.

[66] NN Sirota, Cryst Res technol, 1982, 17, 661-691.

[67] Nagase, H.; Ogawa, N.; Endo, T.; Shiro, M.; Ueda, H.; Sakurai, M. J. Phys. Chem. B 2008, 112, 9105.

[68] Eliel, E. L. Sterochemistry of Carbon Compounds; McGraw-Hill: New York, 1962.

[69] Glusker, J. P.; Trueblood, K. N. Crystal Structure Analysis: A Primer; Oxford University Press: New York, 1985.

[70] Dunitz, J. D. X-ray Analysis and the Structure of Organic Molecules; Cornell University Press: Ithaca, NY, 1979.

[71] A.J. Cruz-Cabeza and J. Bernstein, Chem. Rev. 2014, 114, 2170−2191.

[72] Vippagunta, S. R.; Brittain, H. G.; Grant, D. J. W. Adv. Drug Delivery Rev. 2001, 48, 3.

[73] Vistoli, G.; Pedretti, A.; Testa, B. Drug Discovery Today 2008, 13, 285.

[74] S. Aitipamula, P. S. Chow and R. B. H. Tan, CrystEngComm, 2012, 14, 2381.

[75] (a) M. A. Oliveira, M. L. Peterson and D. Klein, Cryst. Growth Des., 2008, 8, 4487; (b) M. Dabros, P. L. Emery and V.R. Thalladi, Angew. Chem., Int. Ed., 2007, 46, 4132.

[76] (a) S. Cherukuvada and A. Nangia, CrystEngComm, 2012, 14, 2579; (b) N. R. Goud, K. Suresh, P. Sanphui and A. Nangia, Int. J. Pharm., 2012, 439, 63; (c) E. Lu, N. Rodríguez-Hornedo and R. Suryanarayanan, CrystEngComm, 2008, 10, 665; (d) J. Lu, Y.-P. Li, J. Wang, Z. Li, S. Rohani and C.-B. Ching, J. Cryst. Growth, 2011, 407, 63.

[77] S. Cherukuvada and A. Nangia, Chem. Commun., 2014, 50, 906.

[78] Etter MC, Reutzel SM, Choo CG, J. Am Chem Soc, 1993, 115, 4411-4412.

[79] Zaworotko MJ, Crystal Growth & Design, 2007, 7, 4-9.

[80] Hickey MB, Peterson ML, Scoppettuolo LA, Morisette SL, Vetter A, Guzman H, Remenar JF, Zhang Z, Tawa MD, Haley S, Zaworotko MJ, Almarsson O, Eur. J. Pharm Biopharm, 2007, 67, 112-119.

[81] Trask AV, Mol Pharm, 2007, 4, 301-309.

[82] GRAS list, accessed 06 July 2012.

[83] Brittain, H. G. (2011) Cocrystal Systems of Pharmaceutical Interest, Cryst. Growth Des., 2010, 12, 1046-1054.

[84] U.S. Department of Health and Human Services Food and Drug Administration Center for Drug Evaluation and Research (CDER) April 2013 CMC, Guidance for Industry Regulatory Classification of Pharmaceutical Co-Crystals

[85] (a) Braga, D.; Grepioni, F.; Maini, L.; Prosperi, S.; Gobetto, R.; Chierotti, M. R. Chem.Commun. 2010, 46, 7715–7717.(b) D. Braga, F. Grepioni, G. I. Lampronti, L. Maini and A. Turrina, Cryst. Growth Des., 2011, 11, 5621–5627. (c) D. Braga, F. Grepioni, L. Maini, G. I. Lampronti, D. Capucci and C. Cuocci, CrystEngComm, 2012, 14, 3521–3527. (d) D. Braga, F.

Grepioni, L. Maini, D. Capucci, S. Nanna, J. Wouters, L. Aerts and L. Quéré, Chem. Commun., 2012, 48, 8219–8221 (e) J. Wouters, F. Grepioni, D. Braga, R. M. Kaminski, S. Rome, L. Aerts and L. Quéré, CrystEngComm, 2013, 15, 8898–8902. (f) Fabrizia Grepioni, Johan Wouters, Dario Braga, Saverio Nanna, Baptiste Fours,Gérard Coquerel, Geraldine Longfils, Sandrine Rome, Luc Aerts and Luc Quéré, CrystEngComm, 2014,16, 5887–5896.

[86] M. D. Eddleston, S. Sivachelvam and W. Jones, CrystEngComm, 2013, 15, 175.

[87] P. K. Thallapally, R. K. R. Jetti, A. K. Katz, H. L. Carrell, K. Singh, K. Lahiri, S. R. Kotha, R. Boese, G. R. Desiraju, Angew. Chem. 2004, 116, 1169 – 1175; Angew. Chem. Int. Ed. 2004, 43, 1149 – 1155.

[88] A. Delori, T. Friščić and W. Jones, CrystEngComm, 2012, 14, 2350.

[89] A. V. Trask, W. D. S. Motherwell and W. Jones, Chem. Commun., 2004, 890.

[90] O. M. Yaghi, M. O'Keeffe, N. W. Ockwig, H. K. Chae, M. Eddaoudi and J. Kim, Nature, 2003, 423, 705.

[91] J. Wang, L. Ding and C. Yang, CrystEngComm, 2007, 9, 591.

[92] F. P. A. Fabbiani, D. R. Allan, W. I. F. David, S. A. Moggach, S. Parsons and C. R. Pulham, CrystEngComm, 2004, 6, 504.

[93] Francesca P. A. Fabbiani and Colin R. Pulham, Chem. Soc. Rev., 2006, 35, 932–942.

Chapter 2

Results and discussions

2 RESULTS AND DISCUSSIONS

2.1 FOLIC ACID: AN INVESTIGATION OF SOLID-STATE PROPERTIES AND CRYSTAL FORMS [1]

2.1.1 Introduction

Understanding structural diversity, in particular the formation and behavior of polymorphs, amorphous forms, solvates and co-crystals/salts, is critical for establishing uniqueness in a pharmaceutical patent or more in general in the pharmaceutical fields, as well as optimizing conditions for tablet compression and powder flow required for pharmaceutical compounding [1]. There is a strong interest in the application of crystal engineering approach to the pharmaceutical fields for the preparation of new formulation of active pharmaceutical ingredients (APIs), in particular co-crystals, that often show physical and chemical properties (solubility, intrinsic dissolution rate, melting point, color, etc) different from those of their separate components. At the same time, the co-crystallization process does not affect the integrity of the molecular compounds. Another way to obtain useful change in the physical and chemical properties of new APIs is to obtain the amorphous solids. The importance of amorphous pharmaceutical compounds stems from useful properties such as higher stand solubility, higher dissolution rate and sometimes better compression characteristics than the corresponding crystals; to common occurrence, because the amorphous solids can be produced by standard pharmaceutical processes and are common form of certain materials (e.g., proteins, peptides, some sugars and polymers). Another important, but not useful, characteristic is that the amorphous solids are generally less physically and chemically stable than corresponding crystals [2].

Recently a new class of co-crystals has been reported [3] that are called ICCs (Ionic CoCrystals) formed by an organic molecule and an inorganic salt [4], like an alkali or an alkali earth halide. ICCs can be obtained either by classic crystallization methods or by solid-state reactions between solid components (grinding and kneading [5]) with no or limited solvent involvement. Using the solvent free methods of synthesis, were obtained powders directly in solid state in agreement with green chemistry principles.

[1] Saverio Nanna, Laura Chelazzi, Fabrizia Grepioni, Dario Braga (Manuscript in preparation)

In this work we have used salts of alkali and alkaline earth metals as co-formers. Using inorganic compounds in the formulation of API [4] makes possible to create a synergic effect between physical chemical properties of the single solid components (inorganic and organic matter). However, there is also another positive effect because of amorphous characteristics; therefore preparing "amorphous ICCs (Ionic CoCrystals)" with solvent free methods can be a useful tool to change in synergic way the physical properties of API. Summarizing there are many benefits using this approach on preparing eventually new formulation of active pharmaceutical ingredients:

- Synthesis methods (solvent free);
- Synergic effect between ionic compound and organic matter (API);
- Properties of amorphous compound respect of crystalline powders.

We studied Folic acid ((2*S*)-2-[(4-{[(2-amino-4-hydroxypteridin-6-yl)methyl]amino}phenyl)formamido]pentanedioic acid (FA – Scheme 1), vitamin B9, that is the synthetic form of folate, which is a generic name to explain the different forms of vitamin pteroylglutamates (with various levels of reduction of the pteridine ring). This vitamin and its biologically active derivatives acts as coenzymes for synthesis and metabolism of many amino acids and nucleotides by single carbon transfer reactions. This is a very important process in metabolic pathways and a folic acid deficiency can lead to various illnesses. In detail, an insufficient level of vitamin B9 can lead to various diseases related to side effects such as neural tube defects (NTDs) [6], pregnancy complications, cancer, cardiovascular diseases [7]. Folic acid and its derivatives are also used in therapies for organic mental disturbance like senile and pre-senile primary degenerative dementia of Alzhheimer type [8]. Vitamin B9 is not produced by human body and therefore must be taken through the diet; folic acid that derives from the food is classified as food folate that exists predominantly in the polyglutamyl form containing up to seven glutamate residues [9]. In order to make it available to the intestinal absorption, a process that involves the hydrolysis of folate polyglutamates is necessary [10]. This process, together with other factors (for example low thermal stability of certain food folate), determines in general a lower bioavailability than synthetic folic acid fortified food [11]. The concept of bioavailability is therefore a very important key to human health and is used in special cases such as pregnancies, in which insufficient level of folic acid in the body is dangerous; it is therefore necessary

to take major amounts of folic acid [12]. The bioavailability of folate is defined as the ratio between the quantity of ingested folate and the one made available for metabolic processes. Folic acid and its derivatives, for which solution studies are known, are administered individually as salts (lithium, sodium, potassium, magnesium folate) [13].

We focused on solid-state and dissolution properties of folic acid ionic co-crystals and salts, in order to further improve bioavailability and thermal stability of the native vitamin (synthetic folic acid); salts and co-crystals have been prepared via direct reaction of folic acid in the solid-state, with no – or very limited amounts of – solvent (grinding and kneading). The obtained compounds were analyzed through X-ray powder diffraction (XRPD), differential scanning calorimetry (DSC) and thermogravimetric analysis (TGA) and variable-temperature X-ray powder diffraction (XRPD) to characterize thermal stability compared to native vitamin. Intrinsic dissolution rate (IDR) of each synthesis product was also measured.

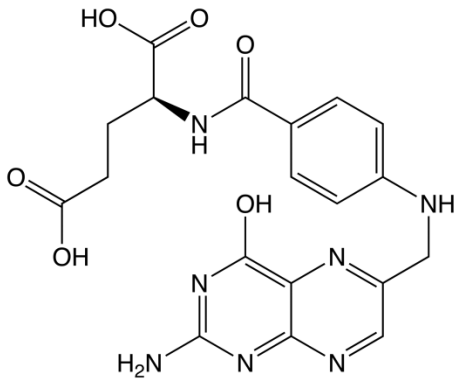

Scheme 1 – Folic acid molecule

2.1.2 Experimental Details And Structure Determination From Xrpd Data

All reagents and solvents were purchased from Sigma-Aldrich and used without further purification.

Solid State Synthesis. Salts of folic acid with NaOH and $Ca(OH)_2$ were obtained by manually kneading the two reagents in a ratio 1:2 in a agate mortar for 20 min with few drops of water; all reactions were quantitative. Salts and co-crystals of folic acid with LiOH and LiCl (with a molar ratio 1:2) were obtained by ball milling (using a Retsch MM200 grinder mill operated at a frequency of 20 Hz) and the reagents

were milled for 30 min with few drops of water, the reactions were quantitative. To obtain the co-crystal of folic acid with Na_2CO_3, the two reagents were manually ground in a agate mortar without solvent with a molar ratio 1:2; the reaction was quantitative (Table 1).

Table 1 - Reagents, synthesis methods and products obtained.

Reagents	**molar ratio**	**solid-state technique**	**Product**
$FAH_2 \cdot 2H_2O$ + LiCl	1:2	Ball milling	$FAH_2 \cdot LiCl \cdot nH_2O$
$FAH_2 \cdot 2H_2O$ + $Ca(OH)_2$	1:2	Kneading (H_2O)	$CaFA \cdot nH_2O$
$FAH_2 \cdot 2H_2O$ + Na_2CO_3	1:1	Grinding	$CaFA \cdot nH_2O$
$FAH_2 \cdot 2H_2O$ + NaOH	1:2	Kneading (H_2O)	$Na_2FA \cdot nH_2O$
$FAH_2 \cdot 2H_2O$ + LiOH	1:2	Ball milling	$Li_2FA \cdot nH_2O$

TGA. TGA measurements were performed using a Perkin-Elmer TGA7 in the temperature ranges 40-460 °C and 37-450 °C for the folic acid and the salts/co-crystal, respectively, under N_2 gas flow, at a heating rate of 5°C min^{-1}.

DSC. DSC measurements were performed with a Perkin-Elmer Diamond. Samples (3-10 mg) were placed in open aluminium pans. Heating were carried out at 5°C min^{-1} for all the samples, in the temperature range 25-300°C.

IDR. Dissolution rate in physiological solution at room temperature was measured for folic acid, the salts and the co-crystal. Measurements were carried out with a Varian Cary 50 Spectrophotometer equipped with a fiber optic dip probe. Four standard solutions in physiological solution (0.1 M NaCl) at concentrations 2.00, 4.00, 6.00, 8.00 $mg \cdot L^{-1}$ were used to calculate a calibration curve for all the samples (correlation coefficient was 0.9988). Absorbance of the solutions was measured, the linear part of the spectrum between 0.1 and 0.6 min utilized, and its slope calculated, corresponding to the dissolution rate in time interval, expressed in Abs min^{-1}. The Abs min^{-1} values were then interpolated in the calibration curve to find the dissolution rate of the analytes expressed as $g \cdot sec^{-1}$.

XRPD Experiments. For structure solution and refinement of folic acid and riboflavin, a X-ray powder diffractogram in the 2θ range 3-70° (step size 0.02°, time/step 15 s, VxA 40x40) were collected on D8 Bruker diffractometer equipped with a primary Ge monochromator for Cu Kα1 and a Sol-X solid state detector in Debye-Scherrer geometry on a capillary with 0.05 mm of diameter.

For phase identification purposes, X-ray powder diffractograms in the 2θ range 3-70° (step size 0.02°; time/step 20 s; 0.04° rad soller; VxA 40x40) were collected on a Panalytical X'Pert PRO automated diffractometer equipped with an X'Celerator detector in Bragg-Brentano geometry, using Cu Kα radiation without a monochromator.

Variable Temperature X-ray Diffraction. X ray powder diffractograms in the 2θ range 3-70° were collected on a Panalytical X'Pert PRO automated diffractometer equipped with an X'Celerator detector and an Anton Paar TTK 450 system for measurements at controlled temperature. The data were collected in open air in Bragg-Brentano geometry using a Cu Kα radiation without a monochromator.

Structure Determination

Folic acid·2H₂O. Powder diffraction data were analyzed with the software Highscore plus. 15 peaks were chosen in the 2θ range 3-40°, and unit cell parameters were found thanks to the algorithm DICVOL [14]. For Folic acid was found a monoclinic unit cell with a volume of 2033.3(4) $Å^3$. In the asymmetric unit were found the presence of one molecule of folic acid and two molecules of water. Space group determination with Highscore plus resulted in space group $P2_12_12_1$, with Z = 4, Z' = 1. The structure was solved by simulated annealing using all independent ions and molecules. Simulated annealing, that runs with structure fragments, was performed with EXPO2010, the updated version of EXPO2009 [15], using one folic acid molecule and two independent water molecules. Ten runs for simulated annealing trial were set, and a cooling rate (defined as the ratio T_n/T_{n-1}) of 0.95 was used. Best solutions were chosen for Rietveld refinements, which was performed with the software TOPAS [16]. A shifted Chebyshev function with 16 parameters and a Pseudo-Voigt function were used to fit background and peak shape, respectively. Soft constraints were applied for all bond distances and angles of the folic acid molecule, and a planar group restraint was applied to the aromatic ring. An overall thermal parameter was adopted for all atoms of the folic acid molecules. All the hydrogen atoms were fixed in calculated

positions. Refinement converged with χ^2 = 1.28 and R_{wp} = 9.68 (Table 2). Figure 1 shows the experimental, calculated and difference diffraction patterns.

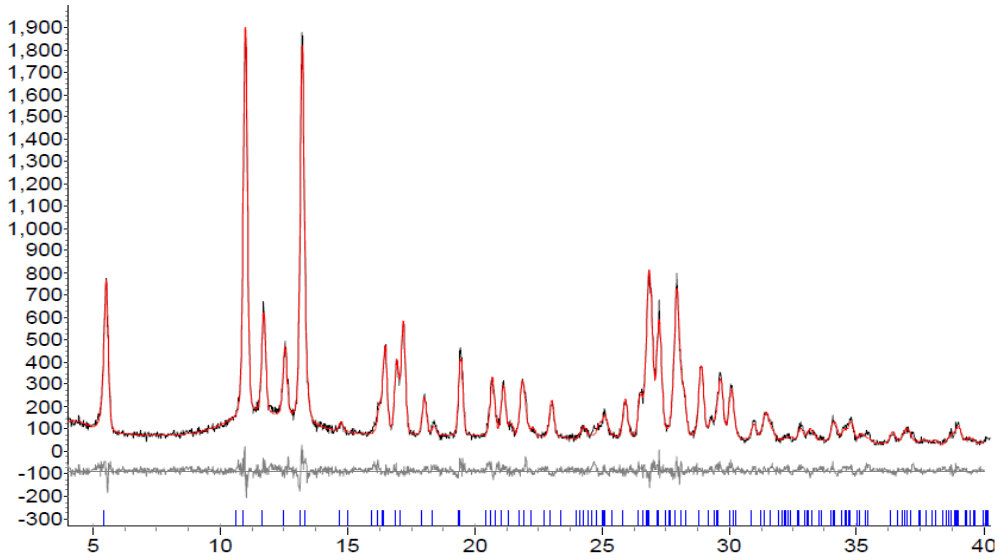

Figure 1 - Experimental (black curve), calculated (red curve), and difference (grey curve) powder pattern for folic acid · $2H_2O$. Peak positions are marked in blue.

Determination of the unit cell parameters (Pawley refinement) of the folic acid (anhydrous form) at high temperature. Powder diffraction data were analyzed with the software Highscore plus. 15 peaks were chosen in the 2θ range 3-40°, and unit cell parameters were found thanks to the algorithm DICVOL. For the anhydrous form of the Folic acid was found a monoclinic unit cell with a volume of 3170.4(7) $Å^3$. The volume is consistent with the presence of three folic acid molecules in the asymmetric unit. The Pawley fit was performed with the software TOPAS. A shifted Chebyshev with 8 coefficients and a pseudo-Voigt function were used to fit background and peak shape, respectively. Refinement converged with χ^2 = 1.40 and R_{wp} = 3.23 (Table 2). Figure 2 shows the experimental, calculated and difference diffraction patterns.

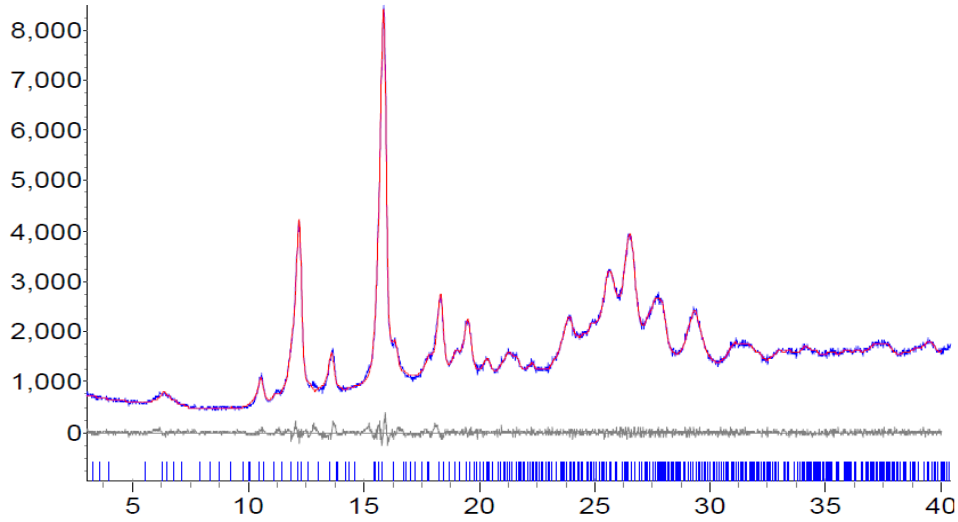

Figure 2 – Experimental (blue curve), calculated (red curve), and difference (gray curve) powder pattern for HT folic acid. Peak positions are marked in blue.

Table 2 – Details of data collection and structure refinement of folic acid, and Pawley fit of the anhydrous form.

	Folic acid · $2H_2O$ **Structure refinement**	**Folic acid HT (anhydrous form)** **Pawley fit**
Chemical formula	C_{19} H_{23} N_7 O_8	C_{19} H_{19} N_7 O_6
M_r	477.40	336.25
temp/K	293	293
wavelength (Å)	1.54056	1.54056
crystal system	orthorhombic	monoclinic
space group	$P2_12_12_1$	$P\ 2_1$
a/Å	8.6163(9)	28.812(3)

b/Å	32.428(4)	4.424(9)
c/Å	7.2771(5)	26.37(2)
β/deg	-	109.38(2)
V/Å^3	2033.3(4)	3170.4(7)
Z	4	6
Rwp	9.68	3.23
χ^2	1.28	1.40

[N.B.: *Science* data: RT, single crystal; R1 (all data) = 0.184, R1 (observed) 0.146]

2.1.3 Results And Discussion

The structure solution of Folic acid

The structure of Folic acid was solved in 1980 [17] by single crystal X-ray diffraction with an orthorhombic unit cell and R value based on the observed data of 0.146. The authors of this work give a description of the structure and a figure without the atomic coordinates. With the intent of study the relationships between the structure and the properties of folic acid and its ionic co-crystals and salts, we managed to obtain the atomic coordinates and a more detailed structure. Due to the impossibility to obtain single crystals of a suitable dimension to study by single crystal X-ray diffraction, we decided to try to solve the structure with X-ray powder diffraction. We obtained two different structure that differ only for the conformation of the glutamic moiety and after the refinement it was clear that one structure has a better result than the other and the result was in disagreement with that obtained with the single-crystal X-ray diffraction. Single crystal X-ray diffraction is surely the principle techniques to obtain reliable structural data, but sometimes a single crystal is not representative of the bulk of products and the study of the bulk is only possible using X-ray powder diffraction. The use and the synergy of different techniques can be a useful tool to solve complex problem and

Folic acid·2H$_2$O. Figure 4 shows a schematic representation of the structure of Folic Acid (FA) · 2H$_2$O. The crystal structure was described in the literature [17] in 1980, but only cell parameters were deposited in the Cambridge Structural Database (refcode *FOLCAH*). As described in Mastropaolo et al., each folic acid is hydrogen-bonded to two other folic acid and two water molecule .

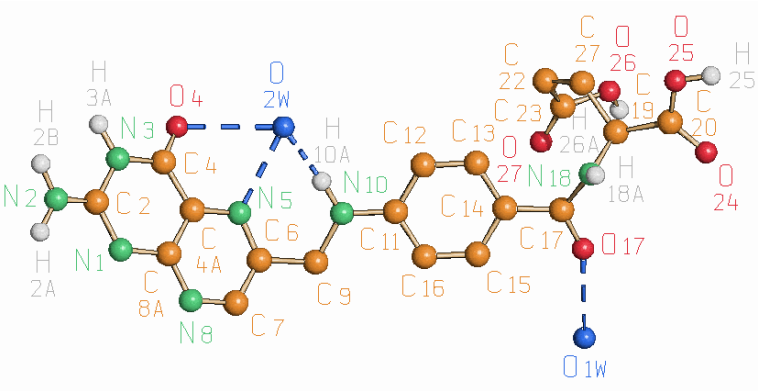

Figure 3. Schematic representation of Folic acid structure hydrogen-bonded to two water molecule. Colour codes: orange, carbon; red, folic acid oxygen; blue, water oxygen; green, nitrogen; grey, hydrogen (in the scheme some hydrogen atoms involved in inter and intra molecular interactions are reported).

The pteridine ring and the glutamic acid residue of each folic acid molecule are linked to the glutamic acid residue and the pteridine ring of the two adjacent folic acid molecules respectively. The p-aminobenzoyl group of one molecule of folic acid is almost below the pteridine ring of the symmetry related folic acid molecule. Zig-zag chains of folic acid are linked together by a bridged water along the b axes and these chains form a 3D network stabilized by hydrogen bond interaction (Figure 4).

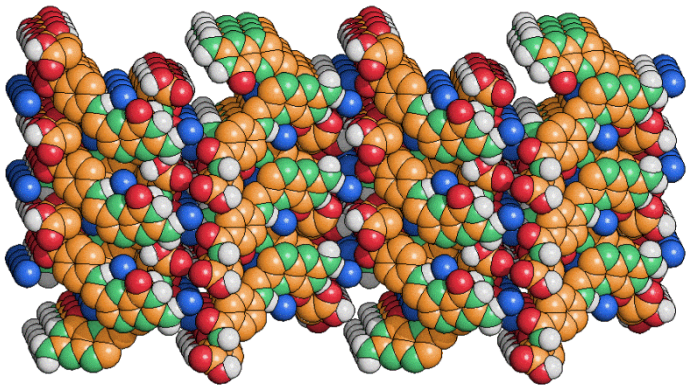

(a) (view down the *c*-axis)

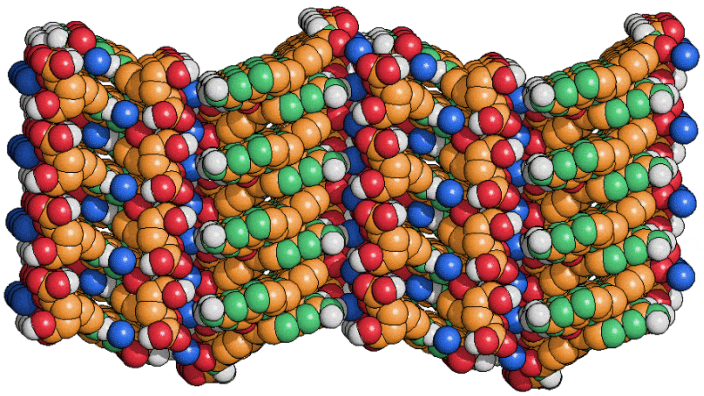

(b) (view down the *a*-axis)

Figure 4. Packing pattern for folic acid with two water molecules - (a) view down the c-axis – (b) view down the a-axis. Colour codes: orange, carbon; red, folic acid oxygen; blue, water oxygen; green, nitrogen; grey, hydrogen.

Variable temperature X-ray powder diffraction experiments of the dihydrate form has been carried out to verify the crystal structure stability after the dehydration process (Figure 5). The loss of water and the subsequent solid-solid transition to the anhydrous phase has been observed at 150°C. After cooling at 25°C, the restoration to the hydrate phase occurred in few minutes; the crystallinity of the folic acid increases with increasing of time (Figure 5). So far, we have not managed to determine the structure of the HT form (anhydrous form) due to the low quality of the diffraction pattern.

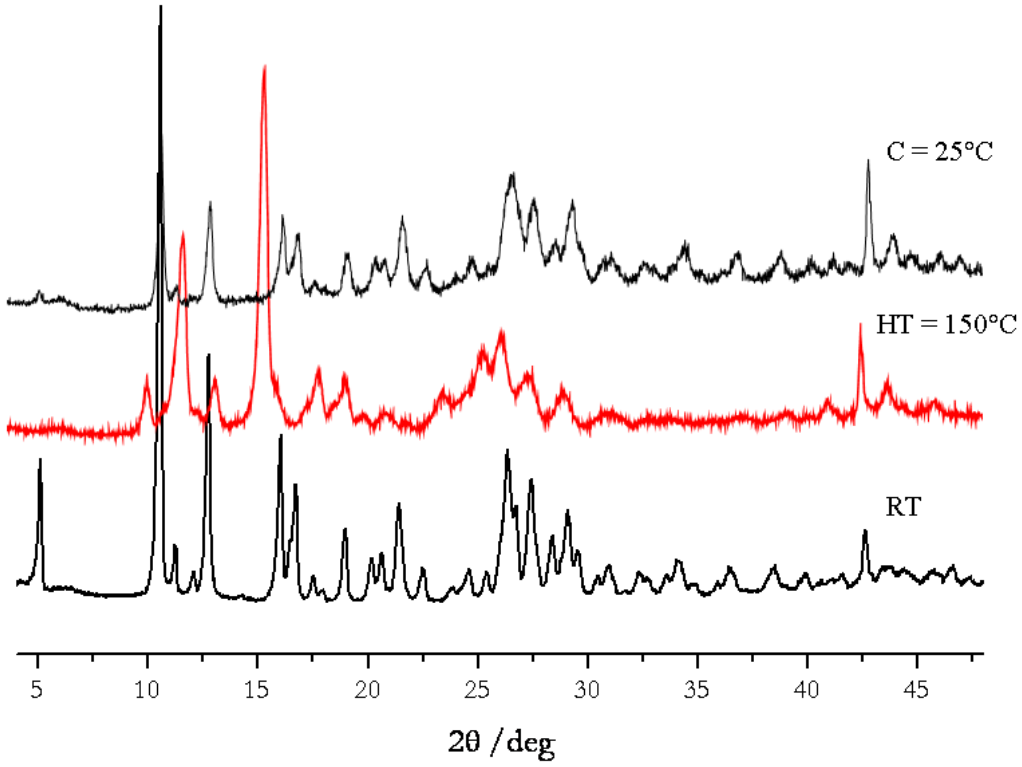

Figure 5. XRPD patterns for folic acid at room temperature (bottom curve), at 150°C (red curve) and at room temperature after cooling (top curve).

Our aim was to obtain folic acid salts or co-crystals using inorganic salts as coformers with solvent free methods. Synthesis products were analyzed by XRPD and the diffraction powder patterns were characteristic of an amorphous phase. In some cases, diffraction pattern shows the presence of the inorganic salt due to the different stoichiometric ratio and the presence of the reagents used for the synthesis due to the incomplete reaction between them (Figure 6).

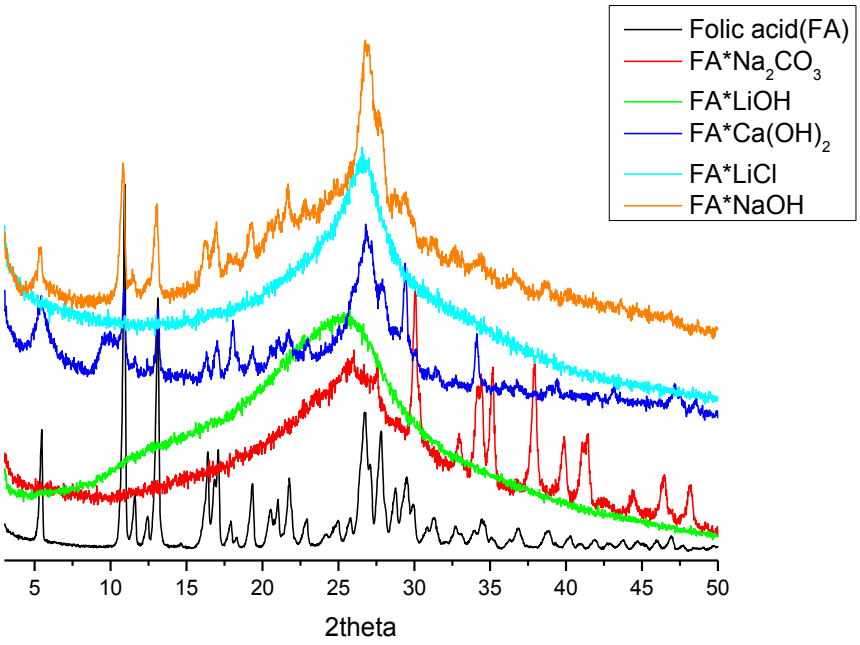

Figure 6. XRPD patterns of folic acid and its salts and co-crystals.

Due to the amorphous patterns of synthesis products, the samples have been characterized by TGA/DSC and IDR in order to verify the complete reaction between reagents, and to compare thermal stability and dissolution rate respect to the native vitamin. Comparing TGA experiments of our products with commercial folic acid, has been observed an improvement of thermal stability. This phenomenon suggests the presence of salts and co-crystals due to the occurred complete reaction. In figure 7 is shown the comparison between the TGA experiment of native folic acid [18] and FA·LiOH; in the FA·LiOH plot there is no peaks related to folic acid and the decomposition of salt occurs at about 350 °C (100°C more stable than pure folic acid). However there are no peaks related to folic acid for none of the samples studied because only traces of the two components have not reacted. The only sign of the presence of small quantity of FA is a small change in the slope at about 250°C corresponding to the temperature of melting and degradation of FA (see SI – figure S1). For the inorganic salts, the m.p. temperature occurs at higher degree respect to the temperature analysis.

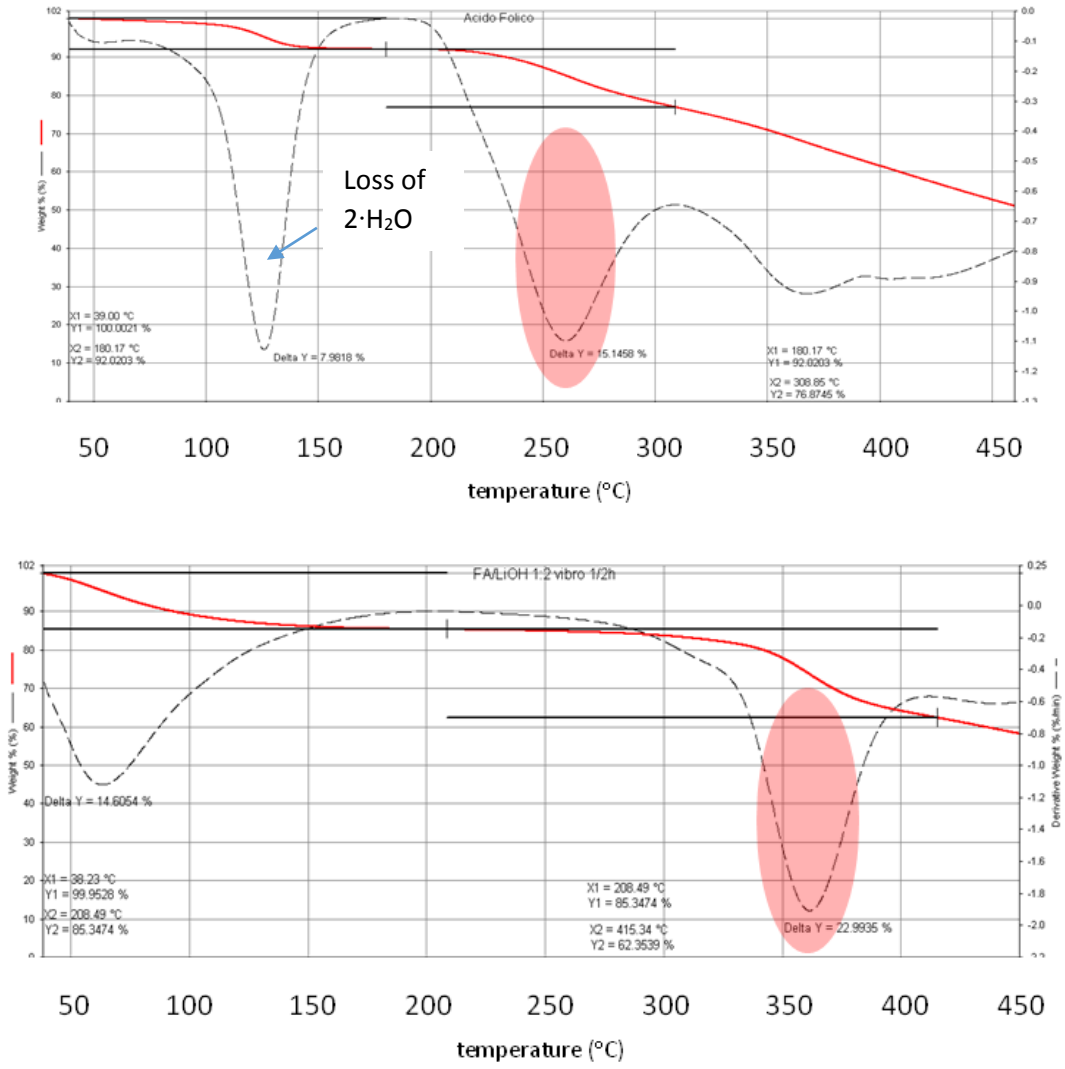

Figure 7. Thermogravimetric analysis (TGA) of folic acid (a) and FA·LiOH (b)

As stated in the introduction, new formulations synthesized directly in the solid state, has been tested in order to verify their physical properties in solution, in particular the intrinsic dissolution rate; the possibility to increase this property respect to the native vitamin could be a very interesting aspect for the possible application in the pharmaceutical field.

IDR measurements show an increase of IDR of salts and co-crystals up to eight times value of pure folic acid (see Table 3 and Figure 8).

Table 3 - IDR measurements

	G/sec
FA	1.26796E-05
FA·Na_2CO_3	3.92932E-05
FA·LiCl	1.59004E-05
FA·LiOH	8.62485E-05
FA·NaOH	4.96336E-05
FA·$Ca(OH)_2$	1.67479E-05

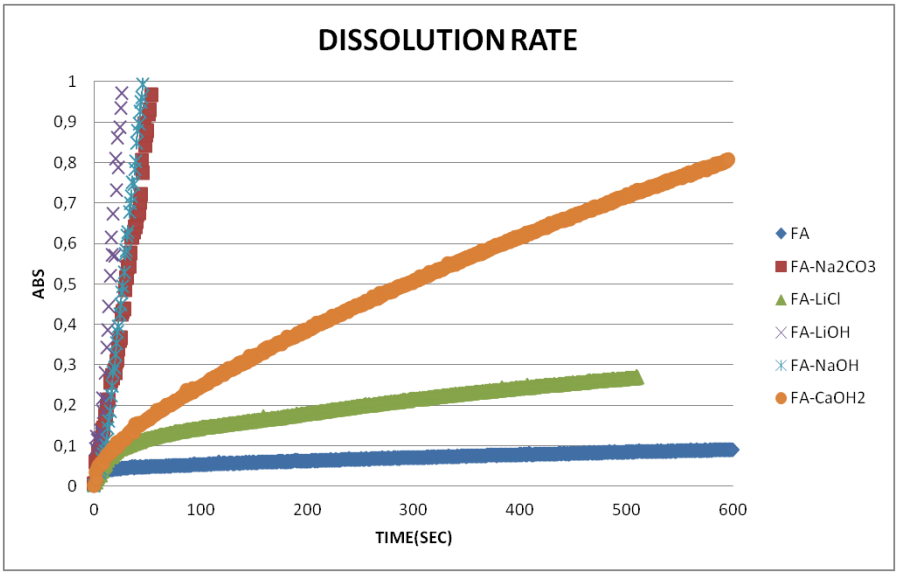

Figure 8. Intrinsic dissolution rate (IDR) measurements of Folic acid and its salts and co-crystals.

2.1.4 Conclusions

In this paper, we have reported the structure of folic acid solved by XRPD and the discover of the high temperature phase. The structure solution by X-ray powder diffraction data is a useful tool in case of Salts and co-crystals of folic acid with inorganic salts were synthesized by solvent free methods and characterized by TGA/DSC and were tested their intrinsic dissolution rate. This study highlights the importance of using different routes of preparation to obtain new APIs. In particular, the solid-solid reaction can be used to produce new forms with different physical chemical parameters. This aspect together with the possibility to obtain stable amorphous phase over time, without changing the chemical entity, could be an interesting way to obtain new useful results in the pharmaceutical field.

SUPPORTING INFORMATION

Below are reported the Thermogravimetric analysis (TGA) of the reaction product of folic acid with LiCl, Na_2CO_3 , NaOH and $Ca(OH)_2$ respectively.

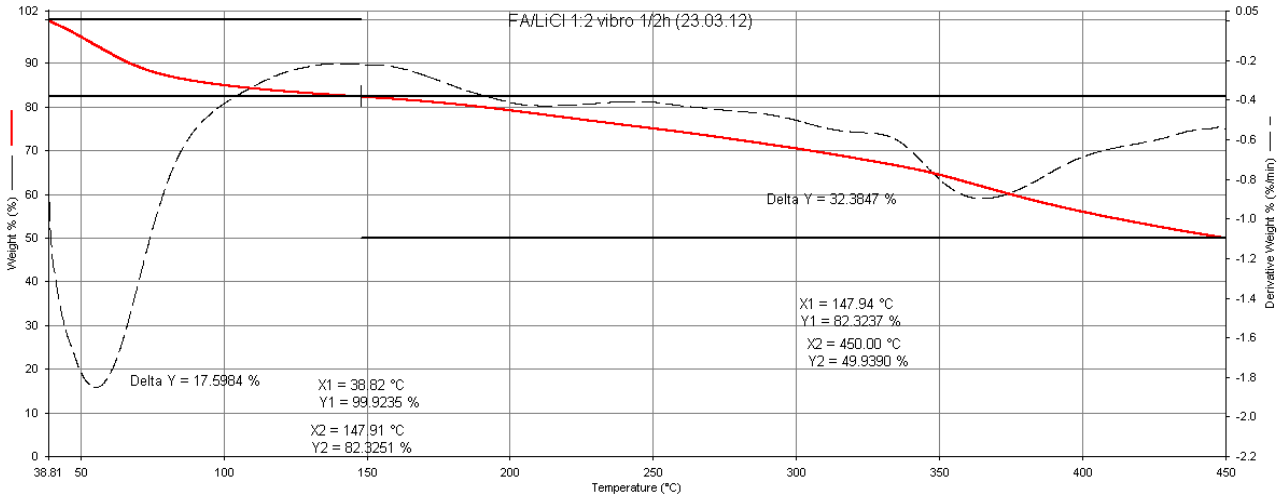

(a)

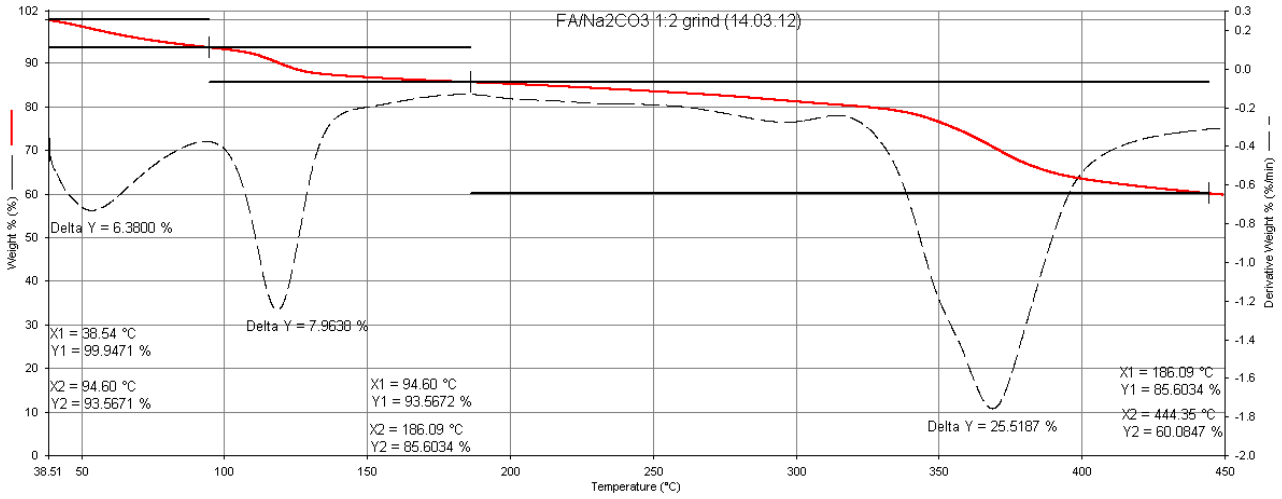
FA/Na2CO3 1:2 grind (14.03.12)
Weight % (%)
Derivative Weight % (%/min)
Temperature (°C)
Delta Y = 6.3800 %
Delta Y = 7.9638 %
X1 = 38.54 °C
Y1 = 99.9471 %
X2 = 94.60 °C
Y2 = 93.5671 %
X1 = 94.60 °C
Y1 = 93.5672 %
X2 = 186.09 °C
Y2 = 85.6034 %
Delta Y = 25.5187 %
X1 = 186.09 °C
Y1 = 85.6034 %
X2 = 444.35 °C
Y2 = 60.0847 %

(b)

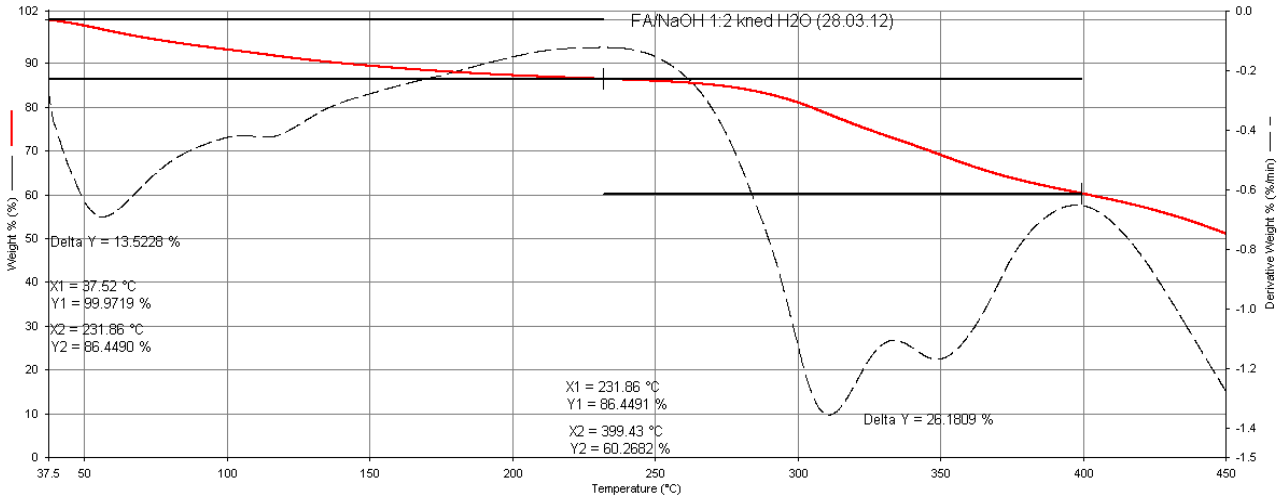
FA/NaOH 1:2 kned H2O (28.03.12)
Weight % (%)
Derivative Weight % (%/min)
Temperature (°C)
Delta Y = 13.5228 %
X1 = 37.52 °C
Y1 = 99.9719 %
X2 = 231.86 °C
Y2 = 86.4490 %
X1 = 231.86 °C
Y1 = 86.4491 %
X2 = 399.43 °C
Y2 = 60.2682 %
Delta Y = 26.1809 %

(c)

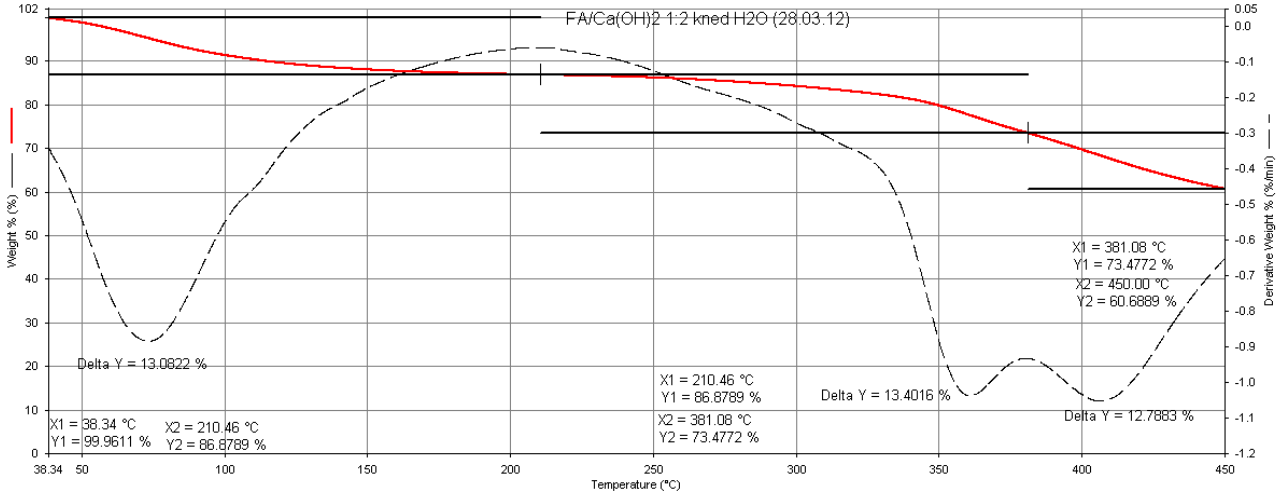
FA/Ca(OH)2 1:2 kned H2O (28.03.12)
Weight % (%)
Derivative Weight % (%/min)
Temperature (°C)
Delta Y = 13.0822 %
X1 = 38.34 °C
Y1 = 99.9611 %
X2 = 210.46 °C
Y2 = 86.8789 %
X1 = 210.46 °C
Y1 = 86.8789 %
X2 = 381.08 °C
Y2 = 73.4772 %
Delta Y = 13.4016 %
X1 = 381.08 °C
Y1 = 73.4772 %
X2 = 450.00 °C
Y2 = 60.6889 %
Delta Y = 12.7883 %

(d)

Figure S1. Thermogravimetric analysis (TGA) of (a) FA·LiCl, (b) FA·Na_2CO_3 , (c) FA·NaOH and (d) FA·$Ca(OH)_2$.

REFERENCES

[1] Chieng, N.; Rades, T.; Aaltonen, J. An overview of recent studies on the analysis of pharmaceutical polymorphs. *J. Pharm. Biomed. Anal.* 2011, 55, 618-644.

[2] Yu, L. Amorphous pharmaceutical solids: preparation, characterization and stabilization. *Advanced Drug Delivery Review*. 2001, 48, 27-42.

[3] Braga, D.; Grepioni, F.; Maini, L.; Prosperi, S.; Gobetto, R.; Chierotti, M.R. From unexpected reactions to a new family of ionic co-crystals: the case of barbituric acid with alkali bromides and caesium iodide. *Chem. Comm.* 2010, 46, 7715 – 7717.

[4] Braga, D.; Grepioni, F.; Lampronti, G.I.; Maini, L.; Turrina, A. Ionic Co-crystals of Organic Molecules with Metal Halides: A new Prospect in the Solid Formulation of Active Pharmaceutical ingredients. *Cryst. Growth Des.* 2011, 11, 5621-5627.

[5] (a) Karki, S.; Friščić, T.; Jones, W. Control and interconversion of cocrystal stoichiometry in grinding: stepwise mechanism for the formation of a hydrogen-bonded cocrystal. *CrystEngComm*, 2009, 11, 470 D. (b) Braga, D.; Giaffreda, S.L.; Rubini, K.; Grepioni, F.; Chierotti, M.R.; Gobetto, R. Solvent effect in a “solvent free” reaction. *CrystEngComm*, 2007, 9, 39. Add ChemSocRev

[6] (a) Perrin, P., Herry, G. Composition, kits and methods for nutrition supplementation. *US Patent* 8,183,227 B1 5/2012. (b) Tamura, T.; Picciano, M.F. Folate and human reproduction *Am. J. Clin. Nutr*. 2006, 83(5), 993-1016. (c) Czeizel, A.E.; Dudás, N. Prevention of the first occurrence of neural-tube defects by periconceptional vitamin supplementation *Engl. J. Med.* 1992, 327(26), 1832-1835. (d) Blencowe, H.; Cousens, S.; Modell, B.; Lawn, J. Folic acid to reduce neonatal mortality from neaural tube disorders *Int. J. Epidemiol.* 2010, 39, i110-i121. (e) Pitkin, R. M. Folate and neural tube defects. *Am. J. Clin. Nutr.* 2007, 85, 285S-288S.

[7] Wakat, D. Dietary supplements for the cardiovascular system. *US Patent* 6,054,128 4/2000.

[8] (a) Rampersaud, G. C.; Kauwell G. P. A.; Bailey L. B. Folate: A key to optimizing health and reducing disease risk in the elderly. *J. Am. College Nutr.* 2003, 22, 1-8. (b) Le Grazie, C. Pharmaceutical compositions containing 5-methyltetrahydrofolic acid, 5-formyltetrahydrofolic acid and their pharmaceutically acceptable salt in controlled-release form active in the therapy of organic mental disturbance. *US Patent* ,5,059,595 10/1991.

[9] (a) Melse-Boonstra, A.; De Bree, A.; Verhoef, P.; Bjorke-Monsen, A.L.; Verschuren, W. M. M. Dietary monoglutamate and polyglutamate folate are both associated with plasma folate concentrations in Dutch men and women aged 20-65 y. *J. Nutr.* 2002, 132, 1307-1312. (b) Stockstad, E. L. R.; Shin, Y. S.; Tamura, T. Distribution of folate forms in food and folate availability. *National Academy of Sciences* 1977, 56-58.

[10] Gregory, J.F. Case study: Folate Bioavailability. *J. Nutr.* 2001, 131, 1376S-1382S.

[11] (a) Institute of Medicine. Dietary reference intakes for thiamin, riboflavin, niacin, vitamin B_6, folate, vitamin B_{12}, panthotenic acid, biotin, and choline. Washington, DC: National Academy press, 2000, 196-305. (b) Pfeiffer, C.M.; Rogers, L.M.; Bailey, L.B.; Gregory, J.F. Absorption of folate from fortified cereal-grain products and of supplemental folate consumed with or without food determined by using a dual-label stable-isotope protocol *Am. J. Clin. Nutr.* 1997, 66, 1388-1397. (c) McNulty, H.; Pentieva, K. . Folate bioavailability *Proceedings of the Nutrition Society* 2004, 63, 529-536 (d) Winkels, R.M.; Brouwer, I.A.; Siebelink, E.; katan, M.B.; Verhoef, P. Bioavailability of food folates is 80% of that of folic acid. *Am. J. Clin. Nutr.* 2007, 85, 465-473.

[12] Brouwer, I.A.; van Dusseldorp, M.; West, C.E.; Steegers-Theunissen, R.P.M. Bioavailability and bioefficacy of folate and folic acid in man *Nutr. Res. Reviews* 2001, 14, 267-293.

[13] (a) Rapin J.R. Nouveaux sels de lithium, les compositions pharmaceutiques a base de ces sels de lithium et leurs applications comme medicament. *Institut national de la propriété industrielle* 2,816,944 11/2000 (b) Kafrissen, M.E. Folic acid-containing pharmaceutical compositions, and related methods and delivery systems WO 9953910 10/1999 (c) Haeger, B.E. Stable infectable pharmaceutical formulation for folic acid and leucovorin and method EP application 0,416,232 03/1991 (d) Omini,

C.F.; Giuseppe, Z. Pharmaceutical formulations designed to supplement the diet of anorexic patients. 0,067,988 3/2006, US Patent.

[14] Boultif, A. and Louer, D. Powder pattern indexing with dichotomy method. *J. Appl. Cryst.* 2004, 37, 724-731.

[15] Altomare, A.; Camalli, M.; Cuocci, C.; Giacovazzo, C.; Moliterni, A. and Rizzi, R. EXPO2009: structure solution by powder data in direct and reciprocal space. *J. Appl. Cryst.* 2009, 42, 1197-1202.

[16] Bruker-AXS, DIFFRACPlus TOPAS : TOPAS 4.2 Technical Reference, Bruker-AXS GmbH, Karlsruhe, Germany (2008).

[17] Mastropaolo, D.; Camerman, A.; Camerman, N. Folic acid: crystal structure and implications for enzyme binding. *Science* 1980, 210, 334-336.

[18] Vora, A., Riga, A., Dollimore, D., Kenneth, S.A. Thermal stability of folic acid. *Therm. Acta,* 2002, 392-393, 209-220.

2.2 FOLIC ACID REVISITED: A SYNERGIC COMPUTATIONAL, SPECTROSCOPIC AND STRUCTURAL APPROACH IN THE SOLID-STATE. [2]

2.2.1 Introduction

Folic acid ((2S)-2-[(4-{[(2-amino-4-hydroxypteridin-6-yl)methyl]amino}phenyl)formamido]pentanedioic acid (FA – Scheme 1) is the vitamin B9, that is the synthetic form of folate, which is a generic name to explain the different forms of vitamin pteroylglutamates (with various levels of reduction of the pteridine ring). This vitamin and its biologically active derivatives act as coenzymes for synthesis and metabolism of many amino acids and nucleotides by single carbon transfer reactions. This is a very important process in metabolic pathways and a folic acid deficiency can lead to various illnesses. In detail, an insufficient level of vitamin B9 can lead to various diseases related to side effects such as neural tube defects (NTDs) [1], pregnancy complications, cancer, cardiovascular diseases [2]. Vitamin B9 is not produced by human body and therefore must be taken through the diet in form of tablets. The upside of understanding the solid state of molecules is reflected into the deep comprehension of the relationships between structure and properties. The administration of folic acid could be a blind test without the acknowledgement of its intrinsic properties in solid state.

Scheme 1. Folic acid molecule.

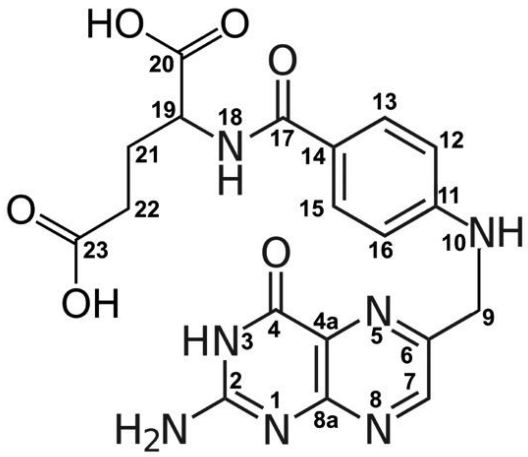

[2] Saverio Nanna, Laura Chelazzi, Fabrizia Grepioni, Dario Braga, Lorenzo Maschio, Paola Taddei (Manuscript in preparation)

2.2.2 Results And Discussion

The structure of Folic acid was solved in 1980 [3] by single crystal X-ray diffraction with an orthorhombic unit cell and R value based on the observed data of 0.146. The structure was described only by a stereo-view figure and no atomic coordinates were provided. With the intent of studying the relationships between the structure and the properties of folic acid, we managed to obtain the atomic coordinates and a more detailed structure. We were not able to obtain single crystals of a suitable dimension for a single crystal X-ray diffraction study, and for this reason we managed to solve the structure with X-ray powder diffraction. Folic acid is not a simple molecule to be solved by powder data due to the presence of several degrees of freedom in the glutamic moiety. We obtained two different solutions that differ just for the conformation of the glutamic moiety; one conformation that reflects the structure described in literature (**FOL2**, Figure 1, top), seems to be less accurate than the other conformation calculated (**FOL1**,Figure 1, bottom).

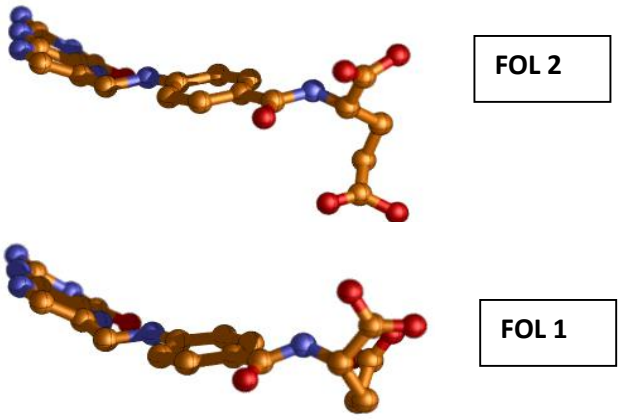

Figure 1. Different conformation of the glutamic moiety of the two solutions.

Powder diffraction data were analyzed with the software Highscore plus. 15 peaks were chosen in the 2θ range 3-40°, and unit cell parameters were found thanks to the algorithm DICVOL [4]. For Folic acid was found a monoclinic unit cell with a volume of 2033.3(4) $Å^3$. In the asymmetric unit the presence of one molecule of folic acid and two molecules of water was found. Space group determination with Highscore plus resulted in space group $P2_12_12_1$, with Z = 4, Z' = 1. The structure was solved by simulated annealing using all independent ions and molecules. Simulated annealing, that runs with structure fragments, was performed with EXPO2010, the updated version of EXPO2009 [5], using one folic acid

molecule and two independent water molecules. Ten runs for simulated annealing trial were set, and a cooling rate (defined as the ratio T_n/T_{n-1}) of 0.95 was used. Best solutions were chosen for Rietveld refinements, which was performed with the software TOPAS [6]. A shifted Chebyshev function with 16 parameters and a Pseudo-Voigt function were used to fit background and peak shape, respectively. Soft constraints were applied for all bond distances and angles of the folic acid molecule, and a planar group restraint was applied to the aromatic ring. An overall thermal parameter was adopted for all atoms of the folic acid molecules. All the hydrogen atoms were fixed in calculated positions. Refinement converged with χ^2 = 1.28 and Rwp = 9.68 . Figure 2 shows the experimental, calculated and difference diffraction patterns.

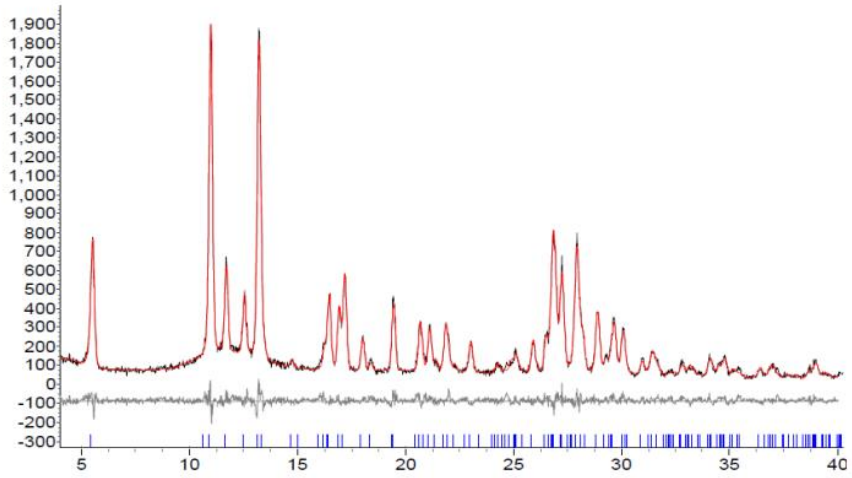

Figure 2. Experimental (black curve), calculated (red curve), and difference (grey curve) powder pattern for folic acid·$2H_2O$. Peak positions are marked in blue.

With flexible molecules, X-ray powder diffraction could be a useful tool to obtain the crystal structure but there is need of a synergic contribution of other complementary techniques. The characterization of the samples has been achieved through combination of *ab initio* calculations and Raman spectroscopy.

DFT calculation have been carried out using the CRYSTAL ab initio program[7], that uses a gaussian basis set. The method adopted for all calculations was a B3LYP hybrid functional, that has proven to provide remarkably good results in the evaluation of the vibrational properties of several crystalline compounds [8], including such complex structures as Metal-Organic Frameworks[9,10]. A 6-31G** basis was used

for geometry optimizations and frequency calculations, while a cc-pVTZ basis set was also adopted for the evaluation of relative stability (see below). Empirical D2[11] dispersion correction has been also included as reparametrized for solids by Civalleri et al.[12] The two structures have been fully optimized (unit cell and atomic positions), with the resulting lattice parameters (in Angstrom):

	a	b	c	Vol
FOL1	8.5019	31.1668	7.5000	1987.32
FOL2	8.7628	34.2373	6.7595	2027.95
Exp. FOL1	8.6163	32.4284	7.2771	2033.34
Exp. FOL2	8.6168	32.4337	7.2788	2034.25

It can be noticed that the FOL1 structure results in a more compressed volume with respect to the experiment. This is most likely to be ascribed to basis set incompleteness effects that are accounted for in the Raman spectrum calculation (vide infra) by suitable shifting of the computed wavenumbers. The volume of FOL2 structure is more similar to the experimental one but the lattice is considerably distorted, with a very compressed c parameter and overestimated a and b lattice components.

The relative stabilities of the two crystalline phases have been computed by standard counterpoise methods to account for Basis Set Superposition Error (BSSE) effects. As shown in earlier works[13], the 6-31G**/B3LYP level is often sufficient for a good estimate of formation energies of crystals.

In table 1 we report, for the two adopted basis sets:

1) the relative stability (per formula unit) between the two crystalline structures, evaluated as the difference between the total crystalline energy divided by the number of formula units in the cell.

$$\Delta E_{cry} = (E_{cry}^{fol1} - E_{cry}^{fol2})/4$$

2) the conformational energy, evaluated as the difference between the total energy of the Folic acid molecule, in the conformation adopted in the two different crystalline structures

$$\Delta E_{conf} = E_{mol}^{fol1} - E_{mol}^{fol2}$$

3) Finally, the zero point vibrational contribution (per formula unit) has been evaluated (only at the 6-31G** level) thanks to the availability of the computed full vibrational spectrum of the two crystals:

$$\Delta E_{vib} = (E_{vib}^{fol1} - E_{vib}^{fol2})/4$$

Table 1. Computed relative energies (values in kJ/mol) of the two crystalline phases of Folic acid, as obtained with 6-31G** and cc-pVTZ basis sets using the B3LYP Hamiltonian. See text for the definition of energy contributions

	6-31G**	cc-pVTZ
ΔE_{cry}	-14.06	-16.56
ΔE_{conf}	17.69	10.03
ΔE_{vib}	-0.72	

As a side note, we recall that use of augmented basis sets, such as cc-pVTZ, is not possible in crystalline systems since diffuse functions lead to linear dependencies and numerical issues in the calculation.

The Raman spectra have been calculated thanks to an entirely analytical method for the evaluation of transition intensities [14,15], that has been recently implemented in the CRYSTAL code. [7] This method, that is unique among solid state quantum chemistry programs, uses a Coupled-Perturbed Hartee-Fock/Kohn Sham (CPHF/KS) approach to evaluate the perturbation in the density due to the electric field, and combines it with analytical first order gradients to obtain the needed third-order derivatives. The derived equations, do not need gradients of the electronic density, thus making the computational effort optimal.

Structure FOL1 was found to be substantially more stable than the FOL2, by an amount of 17.3 kJ/mol per unit formula. This, despite the fact that the molecule itself is in a configuration that is, according to our calculations, less stable by about 10 kJ/mol. The latter result can be of interest in understanding the kinetics of the crystal formation.

Vibrational Raman spectroscopy represents a powerful tool to investigate and identify substances because it provides fingerprint spectra that are unique to each specific compound and its molecular packing. No Raman studies and vibrational assignments for solid folic acid have been reported in the literature. On the other hand, surface-Enhanced Raman spectroscopic (SERS) studies in aqueous solutions have been aimed at setting up analytical methods to selectively detect folic acid in water and biological samples [16]; moreover, resonance Raman studies in aqueous solutions have allowed to clarify the binding of folate and methotrexate to dihydrofolate reductases [17-19]. Due to the lack of solid-state Raman studies on folic acid, the Raman spectrum

of this compound was recorded (FT-Raman, λ_{exc} = 1064 nm, laser power at the sample 40 mW) and was compared with the spectra obtained for **FOL1** and **FOL2** by theoretical calculations. In figure 3, the full spectrum in the range 1800-50 cm-1 is reported, as measured and computed for the two structures and the band wavenumber values and assignments were compared as well (Table 2). Intensity of the peaks is in arbitrary units, and the computational spectra have been renormalized so that the tallest peak of the blue spectrum (80 cm-1) has the same height as the corresponding experimental one. Computed frequencies have been downscaled, as customary since long in ab initio vibrational frequency calculations,[20] by a factor 0.985, and upshifted by 45 cm-1 in order to compensate for underestimation of lattice volume, as discussed above. The experimental Raman spectrum was recorded on a Bruker MultiRam FT-Raman spectrometer equipped with a cooled Ge-diode detector. The excitation source was a Nd3+-YAG laser (1064 nm) in the backscattering (180°) configuration. The focused laser beam diameter was about 100 μm and the spectral resolution 4 cm-1. The spectrum was recorded with a laser power at the sample of about 40 mW.

Table 2. Experimental and calculated wavenumber values and assignments of the most significant Raman bands

Assignments based on solid model compounds	*Assignments based on folic acid and model compounds in solution*	*Experimental wavenumber value (cm^{-1})*	*Calculated wavenumber value (cm^{-1}) and assignment* ***FOL1***	*Calculated wavenumber value (cm^{-1}) and assignment* ***FOL2***
C=O stretching Glu [21]		1710	1705 C=O stretching Glu	1747 C=O stretching Glu
C=O stretching Glu [21]	Pter protonated N5=C6 stretching[19]; C=O stretching PABA-Glu[25]	1664	1672 C=O stretching Pter ring	1675 C=O stretching Pter ring

NH_2 scissoring biopterin [23]	Pter unprotonated N5=C6 stretching[13]; Amide I (C=O stretching) tetrahydrofolate[25]	1637	1631 NH_2 scissoring + H_2O scissoring	1642 (very weak) NH_2 scissoring + N1=C2 stretching
CC stretching PABA[15]*;* ν3o+ν21 *C=C stretching Pter modes*[24]	PABA[17], benzoyl ring mode of 1,4-disubstituted benzene[18]; Pter in methotrexate[17,26]; ν8a PABA-Glu[25]	1607	1601 C=C stretching benzene ring + H_2O and NH_2 scissoring 1595 C=C stretching benzene ring + NH_2 scissoring	1608 C=C stretching benzene ring + H_2O scissoring 1603 H_2O scissoring + NH_2 scissoring
ν5 *Pter mode* [24]*; pyrimidine ring quadrant stretching biopterin* [23]	*PABA* [17]; *ν8b PABA-Glu* [25]	1570	1568 C=N Pter ring stretching	1573 NH_2 scissoring
CH_2 wagging Glu[21]; ν11 and ν12 Pter modes[24]; C-H in plane bending biopterin[23]	PABA[17]; Pter ring vibration[26]; Pter ring stretching C-N; Pter in methotrexate[17,26]	1357	1351 Pter C=N stretching + CH_2 wagging, Pter ring breathing	
CC and C-OH stretching PABA[22]; CH_2 twisting Glu[21]; ν13 Pter mode[24]; C-H out-of-plane	PABA[17]; Amide III PABA-Glu[25]; Amide III folate[25]	1291	1290 C-H wagging mainly Glu	1282 C4a=C8a stretching

bending biopterin[23]				
	Pter in methotrexate[17]	1251	1258 N-H wagging	1230 N-H and C-H wagging
CH in plane bending PABA[22]; ν15 and ν22+ν23 Pter modes[24]	C9-N10 stretching[18]; ν9a PABA-Glu[25]	1193-1179	1193-1178 CH + CH_2 + NH wagging	1181 CH_2 wagging
		153	162 Pter flexural modes 143 Pter torsional modes	178 Pter flexural modes 140 Pter torsional modes
		119	120 H_2O translational mode	127 H_2O translational mode 110 benzene ring rotation
		82	80 torsional modes Glu	85 (weak) torsional modes (C6-C9)

PABA= *p*-aminobenzoic acid; Glu = glutamic acid; Pter = pteridine; PABA-Glu= *p*-aminobenzoylglutamate

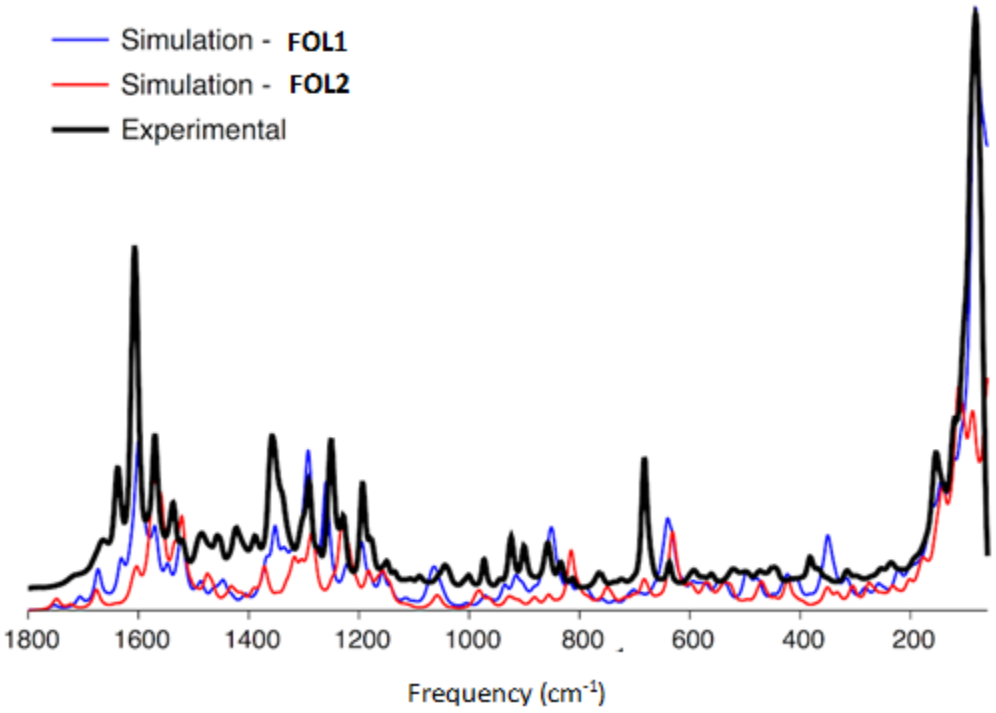

Figure 3. Experimental and calculated Raman spectra, **FOL1** (blue trace) and **FOL2** (red trace).

The spectrum calculated for **FOL1** (blue trace) showed a better agreement with the experimental data (black trace), especially in the low-wavenumber region, where lattice vibrations fall, and in the 1750-1100 cm^{-1} range. The assignments obtained from theoretical calculations showed a good agreement with those reported in the literature for solid model compounds[19-24] as well as for folate and model compounds in solution [17-19,25,26] (see Table 2). The obtained results represent a strong evidence supporting the **FOL1** newly proposed crystal structure.

2.2.3 Conclusions

It was pointed out how the synergic combination of different techniques at the solid state could be a power-full tool to solve complicated structural problems. The structure of folic acid was solved with X-ray powder diffraction and ab initio calculations reporting for the first time the Raman spectra with peaks assignment too.

REFERENCES:

[1] (a) Perrin, P.; Herry, G. Composition, kits and methods for nutrition supplementation. US Patent 8,183,227 B1 5/2012. (b) Tamura, T.; Picciano, M.F. Am. J. Clin. Nutr. 2006, 83, 993-1016. (c) Czeizel, A.E.; Dudás, Engl. J. Med. 1992, 327, 1832-1835. (d) Blencowe, H.; Cousens, S.; Modell, B.; Lawn, J. Int. J. Epidemiol. 2010, 39, i110-i121. (e) Pitkin, R. M. Am. J. Clin. Nutr. 2007, 85, 285S-288S.

[2] Wakat, D. Dietary supplements for the cardiovascular system. US Patent 6,054,128 4/2000.

[3] Mastropaolo, D.; Camerman, A.; Camerman, N. Science 1980, 210, 334-336.

[4] Boultif, A.; Louer, D. J. Appl. Cryst. 2004, 37, 724-731.

[5] Altomare, A.; Camalli, M.; Cuocci, C.; Giacovazzo, C.; Moliterni, A.; Rizzi, R. J. Appl. Cryst. 2009, 42, 1197-1202.

[6] Bruker-AXS, DIFFRACPlus TOPAS : TOPAS 4.2 Technical Reference, Bruker-AXS GmbH, Karlsruhe, Germany, 2008.

[7] Dovesi R.; Orlando, R.; Erba, A.; Zicovich-Wilson, C.M.; Civalleri, B.; Casassa, S.; Maschio, L.; Ferrabone, M.; De La Pierre, M.; D'Arco, P.; Noël, Y.; Causà, M.; Rérat, M.; Kirtman, B. Int. J. Quantum Chem. 2014, 114, 1287-1317.

[8] M. De La Pierre, R. Orlando, L. Maschio, K. Doll, P. Ugliengo, R. Dovesi, Performance of six functionals (LDA, PBE, PBESOL, B3LYP, PBE0, and WC1LYP) in the simulation of vibrational and dielectric properties of crystalline compounds. The case of forsterite Mg_2SiO_4. J. Comput. Chem., 2011, 32, 1775–1784.

[9] B. Civalleri, F. Napoli, Y. Noel, C. Roetti, R. Dovesi, Crystengcomm, 2006, 8, 364-37.

[10] L. Valenzano, B. Civalleri, S. Chavan, S. Bordiga, M. H. Nilsen, S. Jakobsen, K. P. Lillerud, C. Lamberti Chemistry of Materials, 2011 23 (7), 1700-1718

[11] S. Grimme, J. Comput. Chem., 2006, 27, 1787–1799

[12] B. Civalleri, C. M. Zicovich-Wilson, L. Valenzano, P. Ugliengo, Crystengcomm, 2008, 10, 405-410.

[13] L. Maschio, B. Civalleri, P. Ugliengo, A. Gavezzotti, J. Phys. Chem. A, 2011, 115, 11179-11186.

[14] L. Maschio, B. Kirtman, M. Rérat, R. Orlando, R. Dovesi.
"Ab initio analytical Raman intensities for periodic systems through a coupled perturbed Hartree-Fock/Kohn-Sham method in an atomic orbital basis. I. Theory." J. Chem. Phys., 2013, 139, 164101

[15] L. Maschio, B. Kirtman, M. Rérat, R. Orlando, R. Dovesi.
"Ab initio analytical Raman intensities for periodic systems through a coupled perturbed Hartree-Fock/Kohn-Sham method in an atomic orbital basis. II. Validation and comparison with experiments." J. Chem. Phys., 2013, 139, 164102.

[16] Stokes, R.J.; McBride, E.; Wilson, C.G.; Girkin, J.M.; Smith, W.E. Appl. Spectrosc. 2008, 62, 371-376.

[17] Ozaki, Y.; King, R.W.; Carey, P.R. Biochemistry 1981, 20, 3219-3225.

[18] Saperstein, D.D.; Rein, A.J.; Poe, M.; Leahy, M.F. J. Am. Chem. Soc. 1978, 100, 4296-4300.

[19] Chen, Y.Q.; Kraut, J.; Blackley, R.L.; Callender, R. Biochemistry 1994, 33, 7021-7026.

[20] J. A. Pople, A. P. Scott, M. W. Wong, L. Radom, Israel Journal of Chemistry, 1993, 33, 345-350

[21] Shurvell, H.F.; Bergin, F.J. J. Raman Spectrosc. 1989, 20, 163-168.

[22] Yang, X.; Wang, X.; Ching C.B. J. Raman Spectrosc. 2009, 40, 870-875.

[23] Moore, J.; Wood, J.M.; Schallreuter K.U. Biochemistry 1999, 38, 15317-15324.

[24] Hurst, J.K.; Wormell, P.; Bacskay, B.; Lacey, A.R. J. Phys. Chem. A 2000, 104, 7386-7397.

[25] Austin, J.C.; Fitzhugh, A.; Villafranca, J.E.; Spiro, T.G. Biochemistry 1995, 34, 7678-7685.

[26] Seng, G.; Bolard, J.; Chinsky, L.; Turpin, P.Y. J. Raman Spectrosc. 1982, 13, 100-102.

2.3 IONIC CO-CRYSTALS OF PIRACETAM: FROM SOLID TO SOLUTION [3]

2.3.1 Introduction

Ionic co-crystals (ICCs) [1] represent a new class of co-crystals of pharmaceutical interest, constituted by an organic molecule and an inorganic salt, like an alkali or alkaline earth halide. These compounds are characterized by the fact that the organic molecule, solid as a pure compound at ambient conditions, acts as a sort of solvating molecule toward the ions, competing with water molecules for ions coordination.[2] Here we report the study of the stability, at the equilibrium, in organic and aqueous solution of ICCs composed by piracetam with LiCl, LiBr, $CaCl_2$ and $SrCl_2$, respectively. Piracetam (PIR), 3a 2-oxo-1-pyrrolidine acetamide, is currently approved in over 100 countries for use in adults and the elderly for the treatment of vertigo and events associated with ageing. It belongs to a family of cognition enhancing medicines called nootropics, and was synthesized in 1964 by scientists at UCB. The inorganic salts used, on the other hand, have been chosen for their nontoxicity and potential applications in the pharmaceutical field. These systems were synthesized through crystallization from solution or by solid-state reactions between solid components with no (grinding) or limited (kneading) solvent addition. Their crystalline structures, solid state properties (thermal stability) as well as the intrinsic dissolution rate (IDR) studies have been published by the Crystal Engineering Group at Unibo.[2b,d] No studies in solution at equilibrium on ionic co-crystals are known from the literature. Ionic co-crystals of Piracetam with LiCl have been studied in solution through kinetic measurements of dissolution in physiological solution [2d]; kinetic and equilibrium solubility measurements represent two complementary resources, useful to classify a drug and a corresponding co-crystal from a solubility point of view. Going beyond this aspect, a synergic approach between kinetic and equilibrium measurements yields either a deep knowledge of the system, as a learning model, and the opportunity to approach other scenarios that would otherwise not be accessible. Here we report solubility and stability in solution studies, which exploit the methods for equilibrium measurements of co-crystal solubility, developed by Rodrigruez et al. [1] Solubility as well as permeability are a critical point in the

[3] Saverio Nanna, Fabrizia Grepioni, Rodriguez Nair-Hornedo (Manuscript in preparation)

pharmaceutical development of a drug, as they are reflected on the oral absorption according to the biopharmaceutics classification system (BCS). Piracetam belongs to class I of BCS, i.e. it is a drug soluble as well as permeable. The aim of this study is (1) to investigate the co-crystal solubility in order to figure out the solution chemistry and the behaviour of ICCs related to the properties of the pure components, (2) to study the solubilizing effect of salts on piracetam due to the solute-solute and solvent-solute interactions, and (3) to explore how the interactions in solution effect the solid state properties in terms of hygroscopicity.

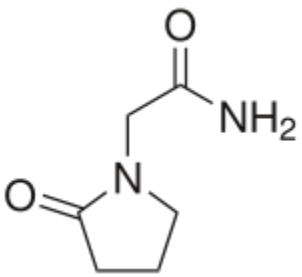

Scheme 1 Piracetam molecule.

2.3.2 Experimental Section

Materials.

Piracetam (PIR) and all the other reagents were purchased from Sigma-Aldrich and used without further purification.

Preparation of Ionic Co-Crystals.

Grinding experiments in an agate mortar for 20 min were performed on commercial piracetam (commercial Form III) (1,1 g, 7,5 mmol - see SI – figures S1-S5) with LiCl (0,3 g, 7,5 mmol) and LiBr (0,7 g, 7,5 mmol) respectively. Kneading (with a catalytic amount of water) experiments of commercial piracetam (0,8 g , 5,4 mmol) with $CaCl_2$ (0,3 g, 2,7 mmol) and $SrCl_2 \cdot 6(H_2O)$ (0,7 g, 2,7 mmol) were also carried out (see Table 1). ICCs were produced also from solution adding an excess of PIR to a nearly saturated solution of co-former (inorganic salt).

Solubility of ICCs and ICCs components.

The solubility of PIR in water and in ethanol at the equilibrium was determined at 25 ± 0.5 °C. The solubility studies of the ICCs in water and ethanol were performed carrying out, either slurry experiments of ICC (method 1), either slurry experiments using the eutectic approach (method 2). [1] The experiments, relative to the method 2, were conducted by adding an excess of ICC [PIR·LiCl·2(H_2O) (**1)**, PIR·LiBr·2(H_2O) (**2)**, PIR_2·$CaCl_2$·2(H_2O) (**3)** respectively] and PIR at the same time in 8 mL glass vials. The suspensions were magnetically stirred and withdrawn each 24h; the solid phase, filtered and dried, was characterized by XRPD and DSC. Once solid phase is stable for 48 h, the concentrations were measured by UV-spectrophotometer and ICP-OES as described below.

UV-spectrophotometer.

[PIR] was measured by Agilent 8453 UV- Visible spectrophotometer.

The Agilent 8453 spectrophotometer is a single-beam, microprocessor-controlled, UV-visible spectrophotometer with collimating optics. *Performance specifications* - Wavelength range 190–1100 nm - Slit width 1 nm - Resolution > 1.6 - Wavelength accuracy < ± 0.5 nm - Wavelength reproducibility < ± 0.02 nm.

I**CP-OES.**

The concentration of inorganic salts was monitored through ICP-OES.

Spectrometer specifications. "The OPTIMA 2000 ICP-OES uses a unique double-monochromator optical system. The first, or preselection monochromator (focal length of 0.3 meter and a Stigmatic Littrow configuration), selects a small portion of the spectrum around the analytical line of interest.The second, the Echelle-based (focal length of 0.3 meter and a Stigmatic Littrow configuration) high dispersion monochromator, disperses the narrow wavelength range onto the DBI-CCD. The spectral range is 160–900 nm. The slew rate is less than 3 seconds to cover the spectral range, and the measured resolution is <0.009 nm @ 200 nm. The prism and Echelle grating are rotated less than ± 2 degrees to access any wavelength, dramatically improving analytical speed. The UV-sensitive, dual backside-illuminated CCD detector is cooled directly using a single-stage integrated Peltier cooler operated at approximately -8°C.The detector housing is hermetically sealed

and is filled with dry nitrogen to eliminate condensation. The detector has two photosensitive segments containing 176 by 128 pixels.

ICP system specifications. The OPTIMA 2000 ICP-OES features a 40-MHz, free-running, solid-state (no power amplifier tube needed) RF generator, adjustable from 750 to 1500 watts, in 1-watt increments. Water recirculating cooling system works at 4 L/min flow capacity at 310 to 550 kPa and a temperature between 15°C and 25°C.

X-ray powder diffraction

X-ray powder diffraction diffractograms of solid phases were collected with a benchtop Rigaku Miniflex X-ray diffractometer (Rigaku, Danverse, MA) using Cu Kα radiation (λ= 1.54Å), a tube voltage if 30kV, and a tube current of 15 mA. Data were collected from 5 to 40° at a continuous scan rate of 2.5°/min.

Differential scanning calorimetry (DSC).

Solid phases collected from the slurry studies were dried and analyzed by differential scanning calorimetry (DSC) using a TA instrument (Newark, DE) 2910MDSC system equipped with a refrigerated cooling unit. DSC experiments were performed by heating the samples at a rate of 5-10 °C/min under a continuously purged dry nitrogen atmosphere (flow rate 50 mL/min). Samples were scanned over the range 30-250°C. Standard aluminum sample pans were used for all measurements.

2.3.3 Results And Discussion

The first step was to assess the solubility of PIR in water at 25°C through UV-spectroscopy; solubility in ethanol at RT (room temperature) is known from literature [3]. Slurry experiments in water at 25 ± 0.1°C were carried out (see Table 1).

Table 1. Solubility at 25±0.1°C of piracetam (Form III – commercial form)

Solvent	[PIR] (M) (mean ± range)
H_2O	$3{,}7 \times 10^{0} \pm 3 \times 10^{-3}$
Ethanol	$2{,}1 \times 10^{-1} \pm 2 \times 10^{-4}$

$$PIR \cdot LiCl \cdot 2(H_2O)_{(solid)} \Longleftrightarrow PIR_{(soln)} + Li^{+}_{(soln)} + Cl^{-}_{(soln)} + 2(H_2O)$$

$$PIR \cdot LiBr \cdot 2(H_2O)_{(solid)} \Longleftrightarrow PIR_{(soln)} + Li^{+}_{(soln)} + Br^{-}_{(soln)} + 2(H_2O)$$

$$PIR_2 \cdot CaCl_2 \cdot 2(H_2O)_{(solid)} \Longleftrightarrow 2PIR_{(soln)} + Ca^{2+}_{(soln)} + 2Cl^{-}_{(soln)} + 2(H_2O)$$

$$PIR_2 \cdot SrCl_2 \cdot 3(H_2O)_{(solid)} \Longleftrightarrow 2PIR_{(soln)} + Sr^{2+}_{(soln)} + 2Cl^{-}_{(soln)} + 3(H_2O)$$

(a)

$$A_\alpha B_\beta \overset{K}{\rightleftharpoons} \alpha A_{(soln)} + \beta B_{(soln)} \qquad K_{sp} = [A]^\alpha [B]^\beta \qquad S_{A_\alpha B_\beta} = \sqrt[\alpha+\beta]{K_{sp}/\alpha^\alpha \beta^\beta}$$

(b)

Scheme 2. Chemical equilibria in solution (a) and general equation to calculate the co-crystal solubility (b) [1b]

Ionic Co-Crystals -- *PIR·LiCl·2(H₂O)* (1) *PIR·LiBr·2(H₂O)* (2)

Solubility in water

Method 1. Solubility in water was investigated preparing suspensions of Ionic co-crystals (ICC), stirred for one week; the solid phase of each one was checked every 24 h and considered at the equilibrium with aqueous solution, once the solid phase was stable for at least 72 h. The characterization of the solid phase, performed with XRPD and DSC measurements, showed no transition of the ICCs to the drug (PIR), suggesting that all ICCs under investigation are less soluble

than the piracetam (see SI – figures S6,S7,S13,S14). The concentration values, listed in table 2, showed a spread between [PIR] and [salts], especially for **2**; the fact that the stoichiometric ratio in solid is not reflected in solution is due to the hygroscopicity of the alkali and alkaline earth metals halide.

Method 2.The weighing process of the salts, stored in presence of P_2O_5, is crucial; to overcome the problems relative to the hygroscopicity of the salts, the eutectic approach was applied. This method developed by Rodriguez et al. [1], consists on reaching the eutectic point, in which both solid phases are in equilibrium with solution (ternary system); this is an invariant point with pH and temperature constant[1,4]. It should not to be confused with the original term "eutectic", which is used to describe, the transformation on cooling from an homogeneous liquid to a two-phases solid. The eutectic approach is useful to determine readily the concentration at the equilibrium of co-crystal components, when the solubility of co-crystal is higher than that of the pure drug. In our case (ICCs are less soluble than the piracetam), this method is still useful as we can calculate, accurately, the solubility of the ICCs regardless of drug:salt ratio in solution. There are various methods to reach the eutectic point [1b]; we adopted that in which the experiments were conducted by adding an excess of ICC and PIR at the same time in 8 mL glass vials.

The eutectic concentrations (C_{eu}), corresponding at the eutectic point, were confirmed by XRPD and DSC analysis of the solid state (see SI – figure S8,S9,S17,S18) and monitored with UV-spectroscopy and ICP-OES; each of the isolated solid phase contains a mixture of **1**+**Pir** (Form III) and **2**+**PIR** (Form III), corroborating that the equilibrium mixtures are both stable in solution. Table 2 lists the concentration values (C_{eu}) of co-crystals components as well as the solubility constants (K_{sp}) relative to the slurry of ICCs (method 1) and the eutectic approach (method 2) carried out on **1** and **2**. K_{sp} values are in good agreement with each other (calcultated from method 1 and 2), corroborating the goodness of the measurements performed applying both methods. The fact that the $[salts]_{eu}$ is below the $[PIR]_{eu}$ confirm, one time again, that **1** and **2** are less soluble than pure piracetam, according to the eutectic constant (K_{eu}) rules [1d]. K_{eu} (see figure 1), is a good indicator of co-crystal solubility and stability; its value is below 1.0 when the co-crystal is congruently saturated (less soluble than the pure drug)[1]; this assumption is valid for co-crystals with stoichiometric ratio 1:1.

In figure 1 is shown a clear relationship between cocrystal components and cocrystal solubility. This suggests that K_{eu} values increase with the increasing of the solubility ratio salt/PIR, suggesting the possibility to design specific solution properties -like solubility- choosing right co-crystal components, as required.

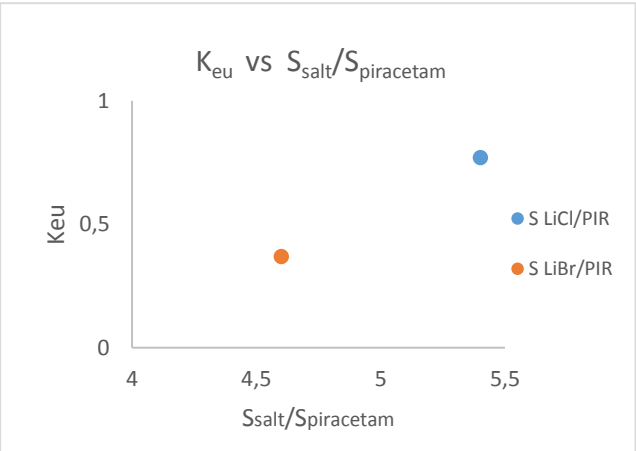

$$K_{eu} = [coformer]_{eutectic} / [drug]_{eutectic}$$

Figure 1. Qualitative relationship between K_{eu} and the intrinsic solubility ratio salts/piracetam.

Ionic Co-Crystals – *$PIR_2 \cdot CaCl_2 \cdot 2(H_2O)$*) (3) and *$PIR_2 \cdot SrCl_2 \cdot 3(H_2O)$*) (4)

Solubility in water

Upon kneading of piracetam with $SrCl_2 \cdot 6(H_2O)$, a new crystalline phase was produced (different from that present in the literature [ref.]) and attributed to an ICC with a different degree of hydration [$PIR_2 \cdot SrCl_2 \cdot 3(H_2O)$ – see SI – figures S50,S51]. Solubility in water was calculated performing slurry of **3** and **4** respectively (method 1). Each solid phase obtained was monitored through XRPD and DSC analysis; no transition to the pure drug was observed, confirming that also **3** and **4** are less soluble than the pure drug. Solubility in water of **3** was also investigated using the eutectic approach (method 2)— see SI – figures S10-12,S15,S16,S19; the results are in good agreement with that obtained from method 1 (see table 2). Unfortunately, it was not possible to apply the eutectic approach also on the ICC **4.**

Co-formers that increase solubility of piracetam

$[PIR]_{eu}$ of **2**, unlike that referred to **1**, reached a value significantly higher than the intrinsic solubility of piracetam. In this regard, a suspension of piracetam in water was prepared and subsequent addition of LiBr caused an improvement of solubility of piracetam, up to a complete dissolution of the precipitate. Solute-solute and solvent-solute interactions stabilize the supersaturated solution, at least for one week, up to a concentration limit of piracetam more than twice the intrinsic solubility ($8{,}7 \times 10^{0} \pm 1 \times 10^{-1}$ M). Beyond this concentration, crystallization of **2** occurred because it is less soluble than the drug (see SI – figure S48), acting as a limiting reagent for the stability of the system (Figure 2). Adding more piracetam to the system, we were able to build experimentally the solubility curve of **2** reaching the eutectic point ($7{,}8 \times 10^{0} \pm 4 \times 10^{-2}$ M), in which both solid phases of **2** and piracetam were in equilibrium with the aqueous solution [see Si – figure S49]. The relative concentration values of LiBr were calculated starting from the K_{sp} calculated from method 1.

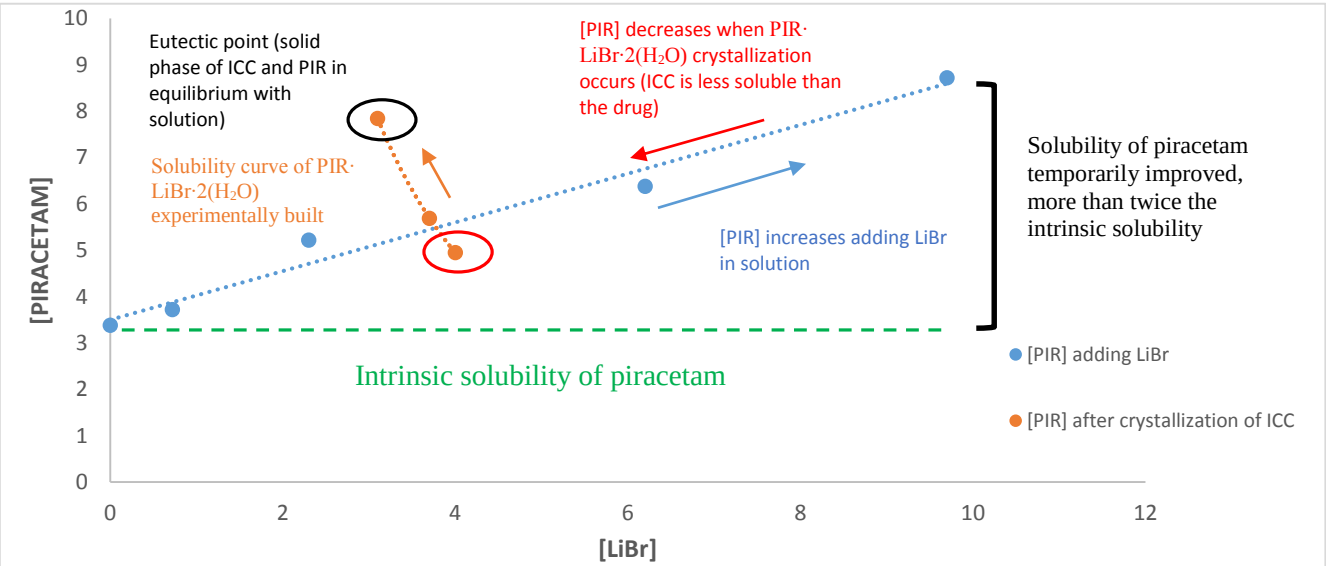

Figure 2. Slurry experiment of piracetam with addition of LiBr.

$CaCl_2$, on the other hand, has almost no effect on the drug solubility, with $[PIR]_{eu}$ ($4{,}9 \times 10^{0} \pm 7 \times 10^{-3}$ M) slightly above PIR solubility in pure solvent ($3{,}7 \times 10^{0} \pm 3 \times 10^{-3}$ M). The solubilizing effect on the drug appears to depend on the solubility of the salts. The $[salts]_{eu}$ values follow the salts solubility (LiCl ~ LiBr > $CaCl_2$); this trend is partially reversed if we consider the improvement of drug solubility represented by the value of $[PIR]_{eu}$ (LiBr > $CaCl_2$ > LiCl) – see Table 2 [1b]. In figure 3 are

shown the solubility curves calculated from method 2 (for **1**, **2** and **3**) and from method 1 (for **4**); **2** is the most soluble, followed by **1**, **4** and **3**. It is evident that, keeping invariant the molecule of interest and the nature of the interactions in solution, the type of salt affects the solubility of the co-crystal. Lithium chloride and lithium bromide, being more soluble than calcium chloride and strontium chloride, influence more the equilibria in solution in terms of solute-solute and solvent-solute interactions, increasing the stability in solution of the ICCs.

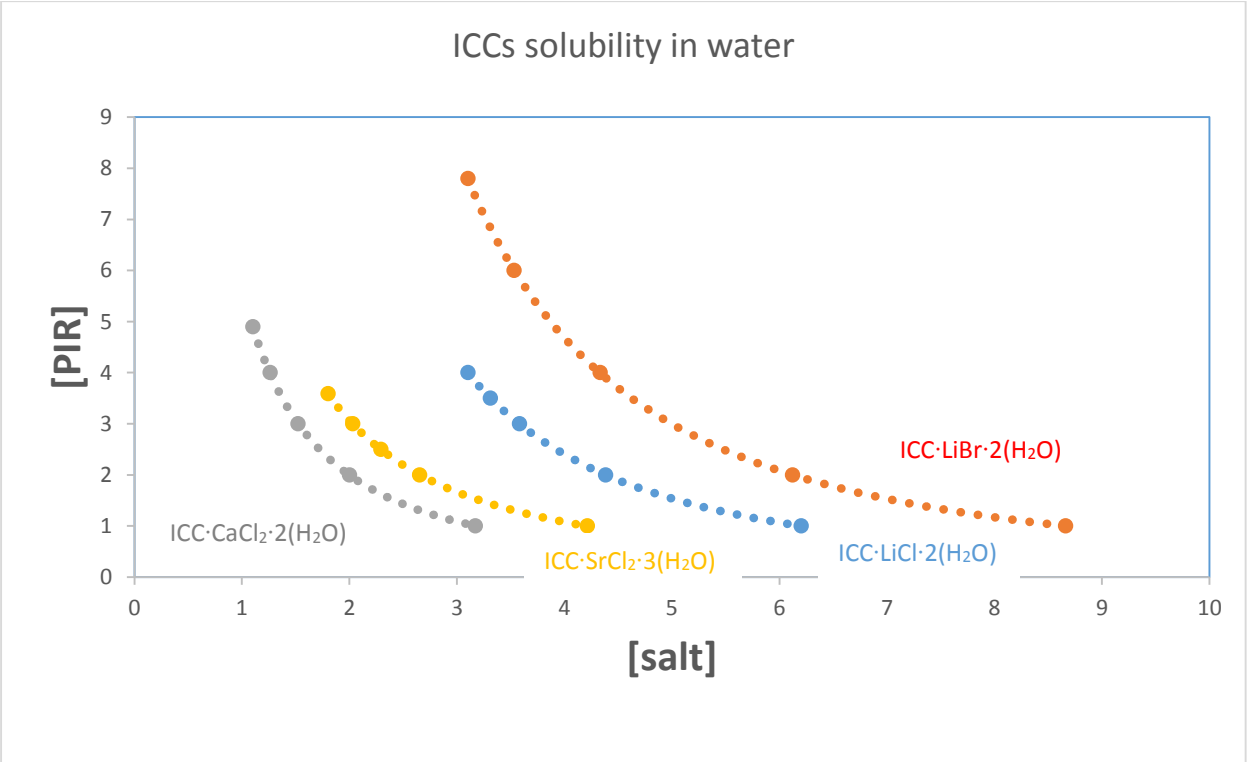

Figure 3. Solubility curves calculated from eutectic measurements (for **1**, **2** and **3**) and from slurry of ICC (**4**).

Ionic Co-Crystals – 1-2-3-4 – Solubility in ethanol

Slurry experiments (method 1) of **1**,**2**,**3**,and **4** were carried out. The solid phase of each sample was daily monitored through XRPD and DSC analysis, up to no changes were observed for at least 72h (see SI – figures S20-S27). Slurry experiments (13 days) of **4** showed a complete transition from **4** to another unknown phase probably corresponding to a crystalline phase with different degree of hydration (see SI – Figure S23). Analogously to the ICCs in aqueous media, no transition to the drug was observed, suggesting that all ICCs are less soluble than the drug. In table 3 are listed the

experimental results, and the solubility ratios of $Sdrug_{cc}/Sdrug_{intrinsic}$ relative to **1** and **2** are 3,7 and 3,8 respectively. There is a remarkable solubilizing effect of piracetam more evident than in water. This is probably due to the lower intrinsic solubility of piracetam in ethanol than in water, combined with the presence of traces of water (0,2% of water-Sigma Aldrich reference) and of the salts (LiCl and LiBr). Figure 4 shows the solubility curves calculated from method 1 of **1**, **2**, **3** and **4**; also in this case, **1** and **2** (figure 4a) are more soluble than **3** and **4** (figure 4b)**.** The same hypothesis advanced about the solubility of the ICCs in water, is also valid in this case.

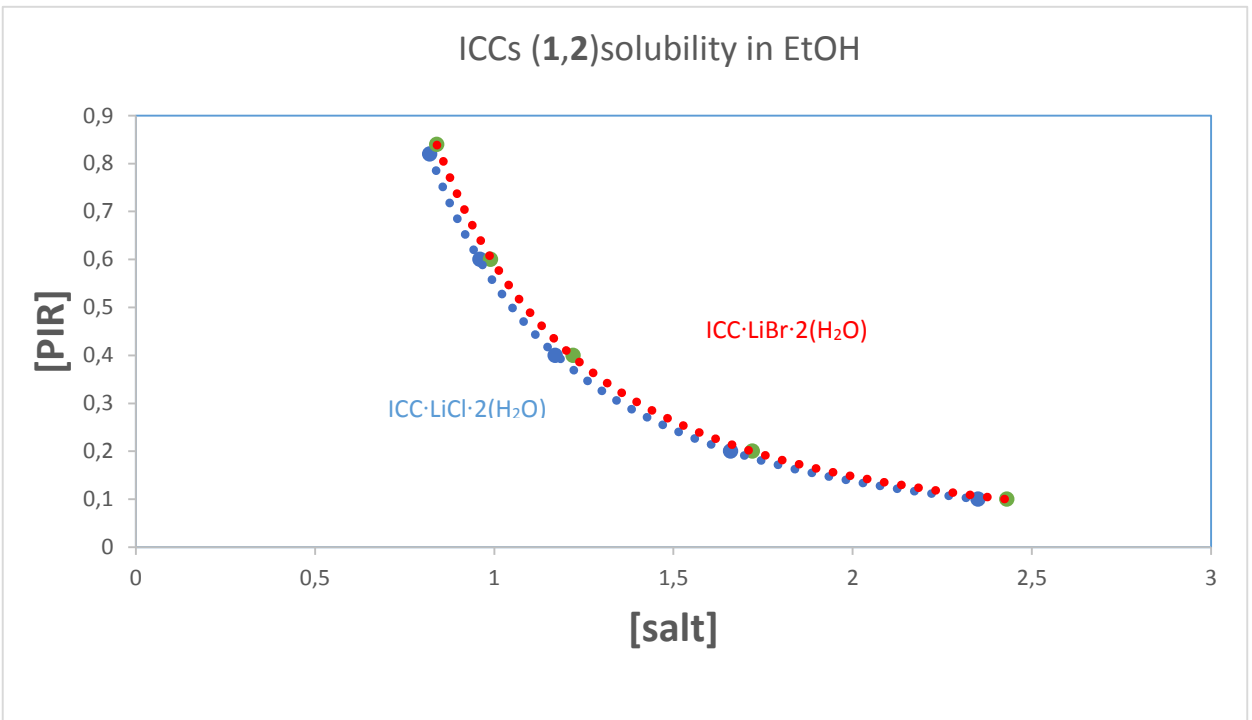

(a)

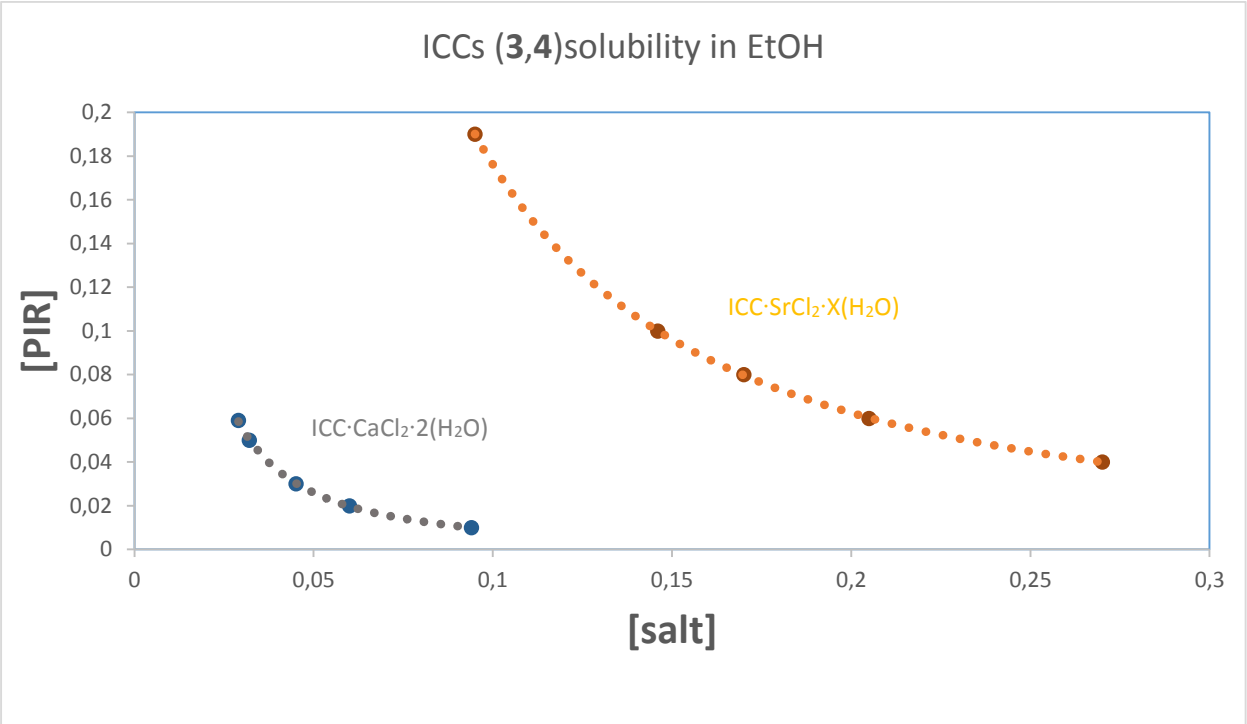

(b)

Figure 4. Solubility curves in EtOH calculated from method 1 on (a) **1**, **2** and (b) **3** and ICC·$SrCl_2$·X(H_2O).

Deliquescence relative humidity: stability studies

Piracetam together with **1, 2, 3** and **4** were stored (for 8 days) at different relative humidity levels (RH%), in order to measure the deliquescence relative humidity. The deliquescence point corresponds to the critical relative humidity (DHR), at which the solid starts to dissolve up to saturation. [5]

The DHR% values of piracetam as well as that of ICCs are shown in figure 5. Piracetam, although highly soluble in water, has an high deliquescence point (85%). This is very interesting because deliquescent materials are typically crystalline solids that are highly water soluble.[5b,c] DHR% values of ICCs lie between that of piracetam and the relative salt, keeping high the value of deliquescent point (**1**-53%, **2**-54%, **3**-78%, **4**-55%). There are additional changes in slope for the systems **1**, **2** and **4** probably due to the kinetics of dissolution at DRH point. The solid phase, relative

to each saturated solution, was investigated by XRPD and DSC; no transition to other crystalline phases occurred (see SI – figures S28-S47).

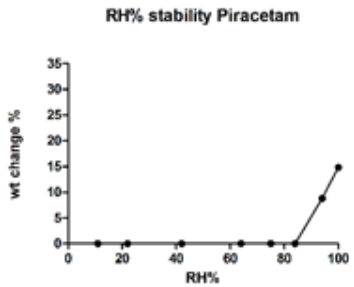

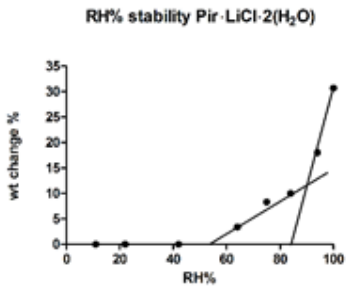

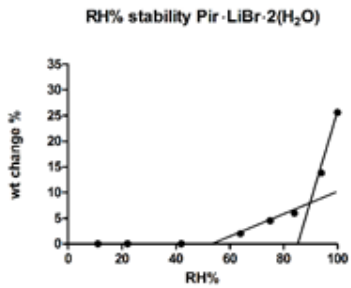

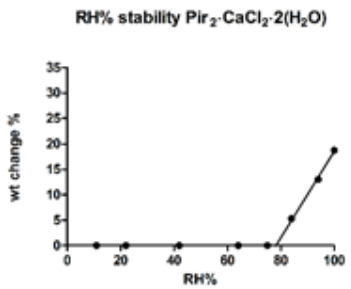

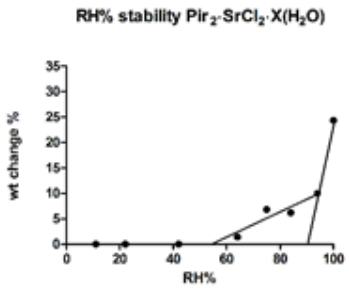

	HR_1 %	HR_2%
Piracetam	85%	-
PIR·LiCl·2(H_2O)	53%	92%
PIR·LiBr·2(H_2O)	54%	91%
PIR_2·$CaCl_2$·2(H_2O)	78%	-
PIR_2·$SrCl_2$·3(H_2O)	55%	93%

Figure 5. Deliquescence point of piracetam,**1**,**2**,**3** and **4**.

These experimental results have been compared with DHR% predicted from the Ross equation[5], optimized for a mixture. All ICCs, except for 4, are composed by high deliquescent salts and, according to the Ross equation, the deliquescent point should be lower than that of the mixture components; indeed, there is a spread between experimental and predicted values for **1**,**2** and **3** (see table 4). Experimental deliquescence point of all ICCs is an ”averaged” value between the DHR values of the co-crystal components. Ross suggested an empirical interaction parameter (χ) to represent the contribution of solute-solute and solvent-solute interactions to the DHR value of the product. χ parameter corresponds to the ratio $DHR\%_{(observed)}$/ $DHR\%_{(calculated)}$; the ratio is much greater than one for **1**, **2** and **3** but not for **4**, for which it is closed to one (table 4). This probably happens because the components are co-crystallized, but also for the hygroscopicity of the salts. LiCl, LiBr and $CaCl_2$, unlike of $SrCl_2$, are hygroscopic and they are stabilized in term of hygroscopicity,

upon co-crystallization with piracetam. This is a clear example of how the solution chemistry is reflected in the solid-state properties, suggesting the possibility to formulate deliquescent drugs, exploiting the stabilization effect due to the co-crystallization with non-hygroscopic active molecules without using further excipients.

Table 4. DHR% observed *vs* predicted

	DHR_1% (observed)	DHR% (predicted)	χ
Piracetam	85		
PIR·LiCl·2(H_2O)	53	9,3	5,7
PIR·LiBr·2(H_2O)	54	5,1	10,6
PIR_2·$CaCl_2$·2(H_2O)	78	25,5	3,1
PIR_2·$SrCl_2$·3(H_2O)	55	60,3	0,91

2.3.4 Conclusions

All ICCs are less soluble than the pure piracetam, both in H_2O and EtOH. Slurry (method 1) and eutectic approach (method 2) methods are consistent with each others. A solubilizing effect of the piracetam, up to four times the intrinsic solubility, was observed, upon addition in solution of inorganic salts (co-formers of piracetam in the ICCs). There is a synergic effect between the ion paring phenomenon and the solvating effect of the drug molecule in competition with water molecules for ions coordination, as it is observed in the solid state with the ICCs. Piracetam and its ICCs are stable also at high RH%; there is also a stabilization effect of co-crystallization on salts (LiCl in particular) in terms of hygroscopicity. The deliquescent point of the ICCs, predicted from Ross

equation, differs from that observed due probably to significant solute-solute interactions for PIR · LiCl · 2(H_2O), PIR · LiBr · 2(H_2O) and PIR_2 · CaCl2 · 2(H_2O); this is unsurprising, given the high concentrations involved. We can state that the main aspects of the solid state properties of ICCs are mirrored in solution, resulting in the modification of stability in solution of the drug under investigation, once co-crystallized. This proves one time again how the investigation of solid state properties can be a resource to figure out what is going on in solution and also to design in solid what we are interested to obtain in solution. Piracetam, given its intrinsic high solubility and permeability (bioavailability 100%), was used as a learning model for other systems less soluble and/or permeable, with the aim to choose right co-formers depending on the final requirements. Ionic co-crystals can be a valuable resource to improve not only the solubility but also, in certain cases, the permeability,[6] with the final aim to improve the bioavailability of the molecule of interest.

Table 2. Cocrystal eutectic concentrations ($[drug]_{eu}$ and $[ligand]_{eu}$), Component Solubilities, and Calculated Cocrystal Ksp Values, Solubilities, and Solubility Ratios in water.

Solubility ratio $[drug]s_{cc}/S_{drug}$	0,9	1,1	0,6	0,8
Ionic co-crystal solubility (M) eu	$3,4 \times 10^0$	$4,2 \times 10^0$	$1,2 \times 10^0$	-
Ionic co-crystal solubility (M) slurry	$3,6 \times 10^0$	$4,2 \times 10^0$	$1,1 \times 10^0$	$1,4 \times 10^0$
K_{sp} eutectic approach (2nd method)	$3,8 \times 10^1$ M^3	$7,5 \times 10^1$ M^3	$3,2 \times 10^1$ M^5	-
K_{sp} slurry (1st method)	$4,6 \times 10^1$ M^3	$7,7 \times 10^1$ M^3	$2,5 \times 10^1$ M^5	$7,5 \times 10^1$ M^5
S_{drug} (M)	$3,7 \times 10^0 \pm 3 \times 10^{-3}$	$3,7 \times 10^0 \pm 3 \times 10^{-3}$	$3,7 \times 10^0 \pm 3 \times 10^{-3}$	$3,7 \times 10^0 \pm 3 \times 10^{-3}$
S_{ligand} (M)	$19,9 \times 10^0 \pm 3 \times 10^{-3}$	$17 \times 10^0 \pm 2 \times 10^{-4}$	$7,5 \times 10^0 \pm 3 \times 10^{-3}$	$3,5 \times 10^0 \pm 2 \times 10^{-4}$
$[ligand]_{eu}$(mean ± range)	$3,1 \times 10^0 \pm 4 \times 10^{-2}$	$3,1 \times 10^0 \pm 3 \times 10^{-3}$	$1,1 \times 10^0 \pm 5 \times 10^{-3}$	-
$[PIR]_{eu}$(M) (mean ± range)	$4 \times 10^0 \pm 1 \times 10^{-2}$	$7,8 \times 10^0 \pm 4 \times 10^{-2}$	$4,9 \times 10^0 \pm 7 \times 10^{-3}$	-
$[ligand]_{slurry}$ (M) (mean ± range)	$3,8 \times 10^0 \pm 4 \times 10^{-2}$	$3,6 \times 10^0 \pm 3 \times 10^{-2}$	-	-
$[PIR]_{slurry}$(M) (mean ± range)	$3,1 \times 10^0 \pm 2 \times 10^{-2}$	$5,8 \times 10^0 \pm 4 \times 10^{-3}$	$2,9 \times 10^0 \pm 4 \times 10^{-3}$	$3,6 \times 10^{-1} \pm 3 \times 10^{-2}$
Solvent	H_2O	H_2O	H_2O	H_2O
A:B	1:1	1:1	2:1	2:1
Ionic co-crystal	$PIR \cdot LiCl \cdot 2(H_2O)$	$PIR \cdot LiBr \cdot 2(H_2O)$	$PIR_2 \cdot CaCl_2 \cdot 2(H_2O)$	$PIR_2 \cdot SrCl_2 \cdot 3(H_2O)$

Table 3. Cocrystal components concentrations, component Solubilities, Calculated Cocrystal Ksp Values, Solubilities, and Solubility Ratios in EtOH.

Solubility ratio [drug]s_{cc}/S_{drug}	3,7	3,8	0,2	0,7
Ionic co-crystal solubility (M) slurry	$8,2 \times 10^{-1}$	$8,4 \times 10^{-1}$	$2,2 \times 10^{-2}$	$7,2 \times 10^{-2}$
K_{sp} slurry ICC (1st method)	5,5 x 10-^{1} M^3	$5,9 \times 10^{-1}$ M^3	$8,4 \times 10^{-8}$ M^5	$3,1x\ 10^{-5}$ M^5
S_{drug} (M)	$2,2 \times 10^{-1} \pm 2 \times 10^{-4}$	$2,2 \times 10^{-1} \pm 2 \times 10^{-4}$	$2,2 \times 10^{-1} \pm 2 \times 10^{-4}$	$2,2 \times 10^{-1} \pm 2 \times 10^{-4}$
S_{ligand} (M)	$7,4 \times 10^{0} \pm 3 \times 10^{-3}$	$7,3 \times 10^{0} \pm 2 \times 10^{-4}$	$2,3 \times 10^{0} \pm 3 \times 10^{-3}$	$2,2 \times 10^{-1} \pm 2 \times 10^{-4}$
$[ligand]_{slurry}$ (M) (mean ± range)	-	-	-	-
$[PIR]_{slurry}$(M) (mean ± range)	$8,2 \times 10^{-1} \pm 3 \times 10^{-3}$	$8,4 \times 10^{-1} \pm 4 \times 10^{-3}$	$5,9 \times 10^{-2} \pm 7 \times 10^{-6}$	$1,9 \times 10^{-1} \pm 6 \times 10^{-4}$
Solvent	Ethanol	Ethanol	Ethanol	Ethanol
A:B	1:1	1:1	2:1	2:1
Ionic co-crystal	$PIR{\cdot}LiCl{\cdot}2(H_2O)$	$PIR{\cdot}LiBr{\cdot}2(H_2O)$	$PIR_2{\cdot}CaCl_2{\cdot}2(H_2O)$	$PIR_2{\cdot}SrCl_2{\cdot}X(H_2O)$

SUPPORTING INFORMATION

XRPD patterns of piracetam and the ICCs - PIR·LiCl·2(H_2O)(**1**), PIR·LiBr·2(H_2O) (**2**), PIR_2·$CaCl_2$·2(H_2O) (**3**) and PIR_2·$SrCl_2$·3(H_2O) (**4**). [2]

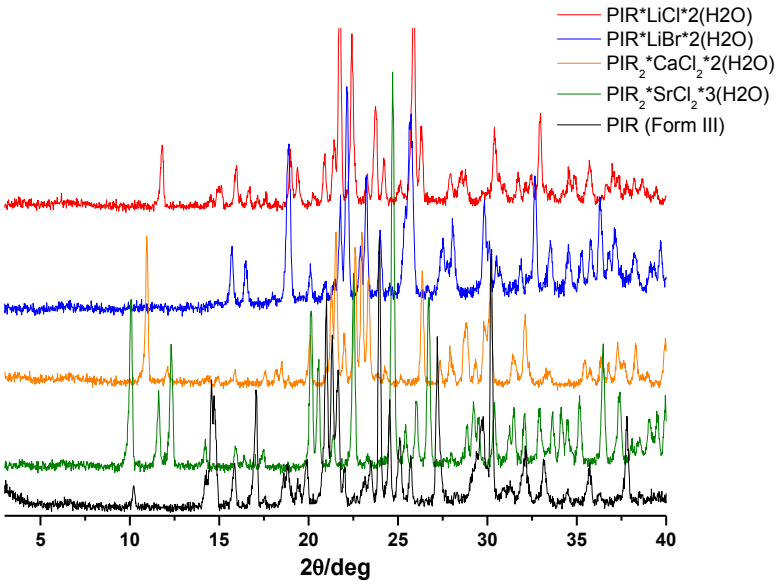

Figure S1. X-ray powder diffraction patterns observed for **Piracetam** (**PIR**, form III), **1**, **2**, **3** and **4** .

DSC measurements (3-6 mg - sealed pan) of the ICCs - PIR·LiCl·2(H_2O)(**1**), PIR·LiBr·2(H_2O) (**2**), PIR_2·$CaCl_2$·2(H_2O) (**3**) and PIR_2·$SrCl_2$·3(H_2O) (**4**). [2]

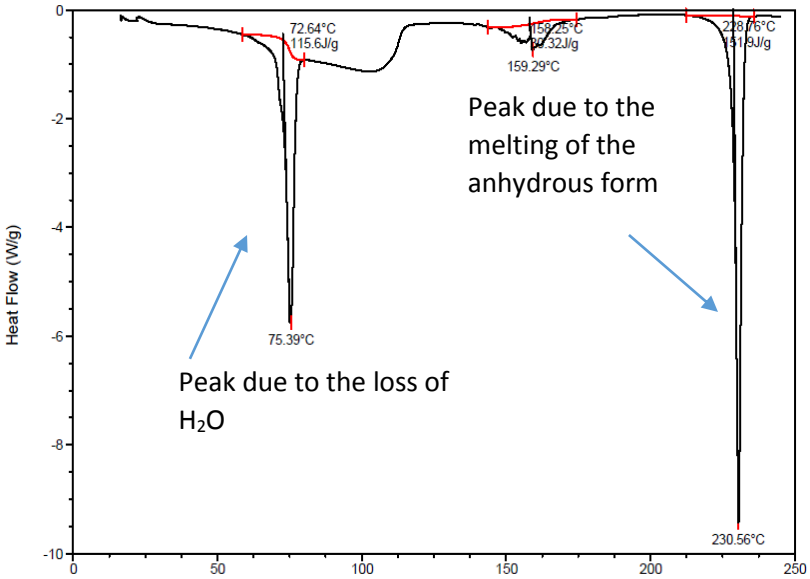

Figure S2. DSC measurement of **1**; heating rate 5°C/min

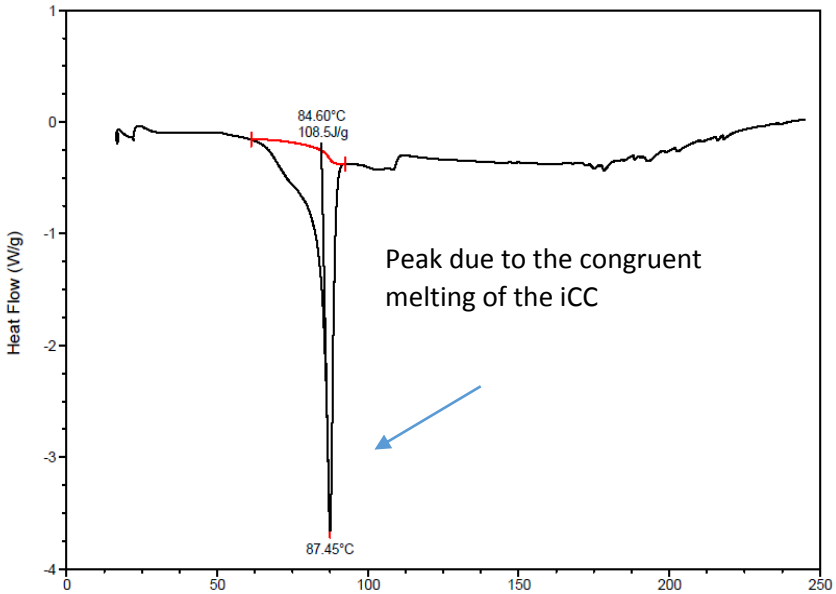

Figure S3. DSC measurement of **2.** RT → 130°C heating rate 10°C/min, 130°C → 160°C heating rate 2°C/min, 160°C → 200°C heating rate 15°C/min.

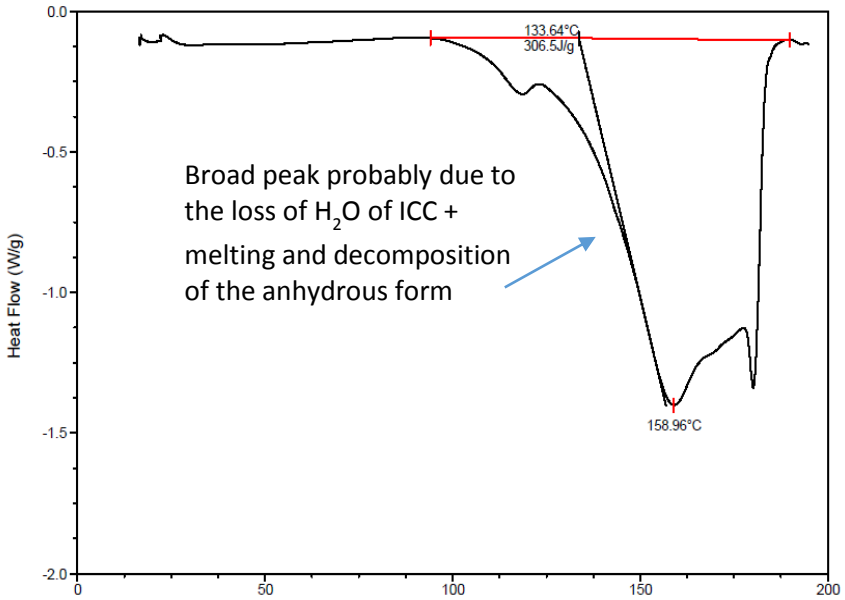

Figure S4. DSC measurement of **3;** heating rate 5°C/min.

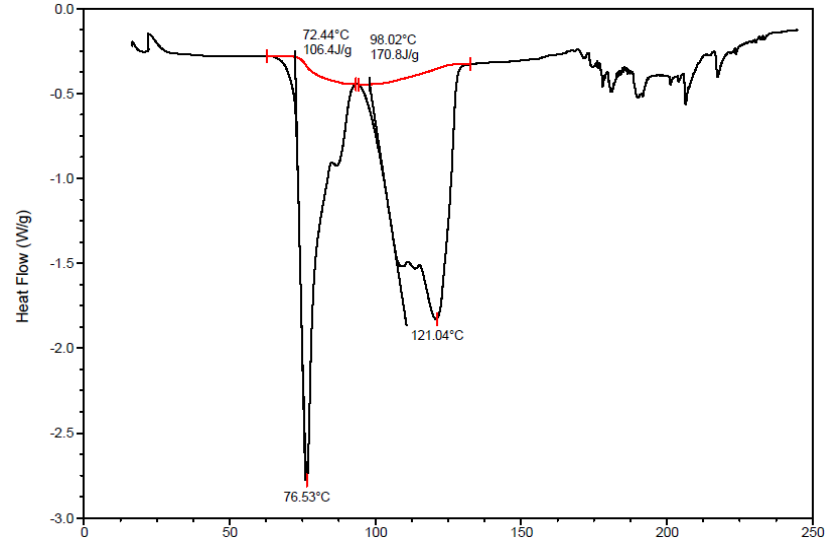

Figure S5. DSC measurement of **4;** heating rate 5°C/min.

Ionic Co-Crystals (1), (2), (3) and (4). Solubility studies in H_2O

XRPD patterns of **1** and **2**.

1st method

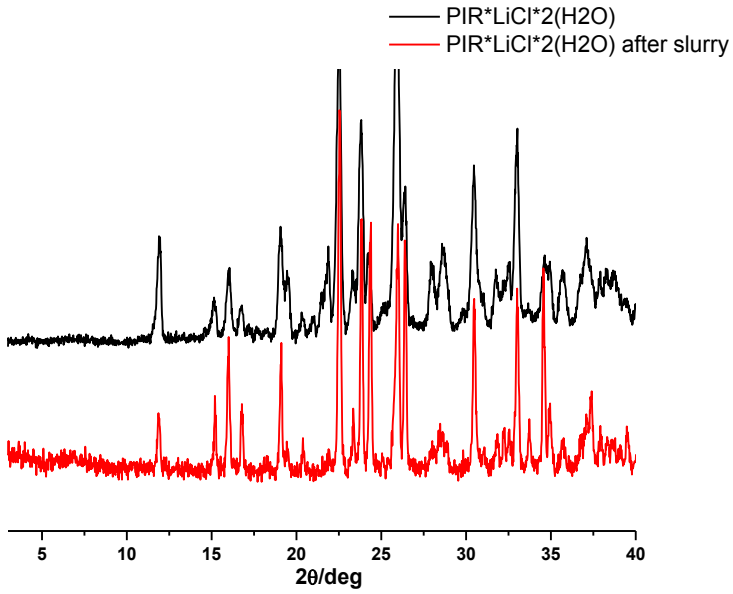

Figure S6. X-ray powder diffraction patterns observed for **1 (black trace)** and **1** after slurry in water (1st method) **(red trace)**.

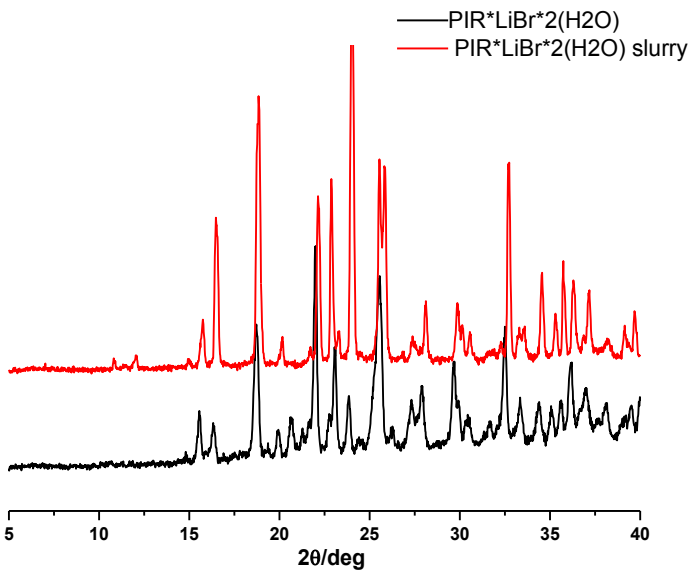

Figure S7. X-ray powder diffraction patterns observed for **2 (black trace)** and **2** after slurry in water (1st method) **(red trace).**

2nd method

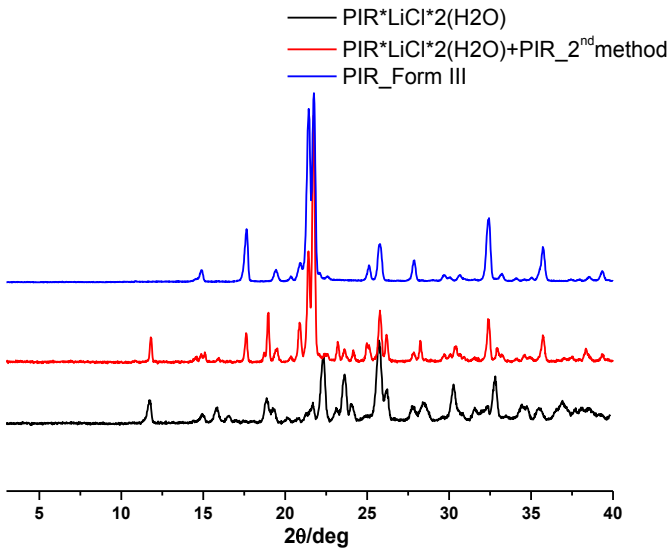

Figure S8. X-ray powder diffraction patterns observed for **1 (black trace)**, slurry in water of **1** and piracetam (2nd method- **red trace**) and **piracetam** (**PIR**- form III – **blue trace**).

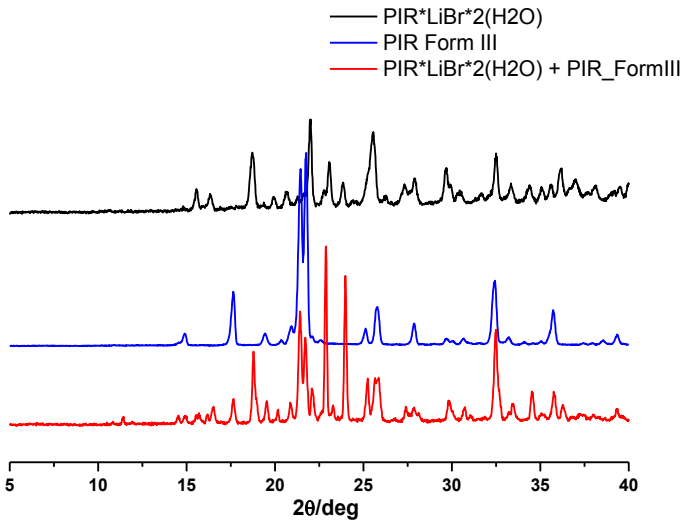

Figure S9. X-ray powder diffraction patterns observed for **2 (black trace)**, slurry in water of **2** and **piracetam** (2nd method- **red trace**) and **piracetam** (**PIR**- form III – **blue trace**).

XRPD patterns of 3 and 4.

1st method

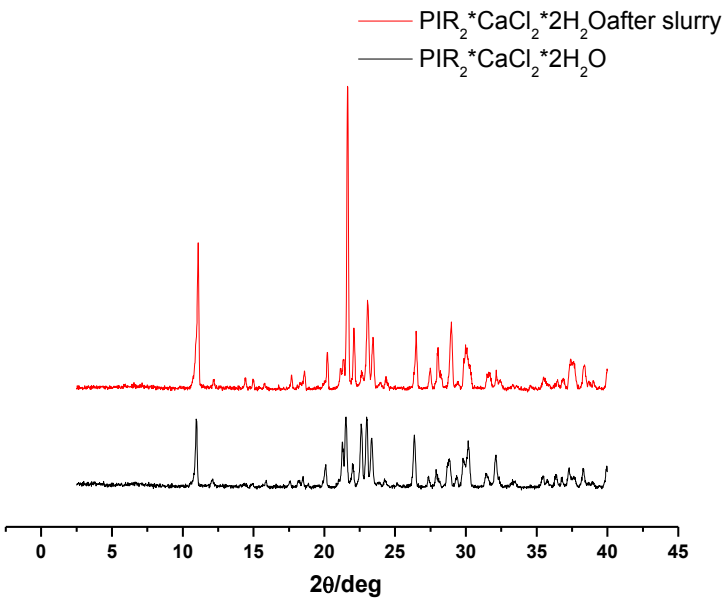

Figure S10. X-ray powder diffraction patterns observed for **3 (black trace)** vs **3** after slurry in water (1st method) **(red trace)**.

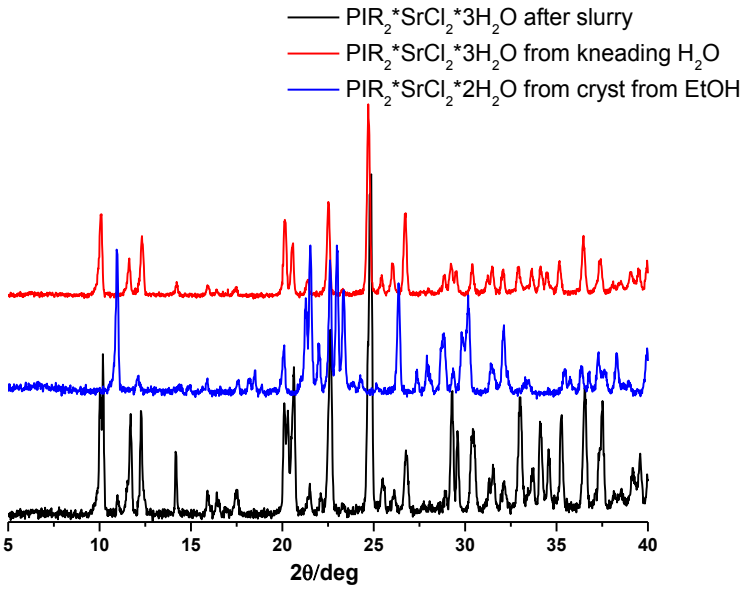

Figure S11. X-ray powder diffraction patterns observed for **4 (red trace), 4** after slurry in water (1st method) **(black trace)** and **$PIR_2SrCl_2 \cdot 2H_2O$ (blue trace)**.

2nd method

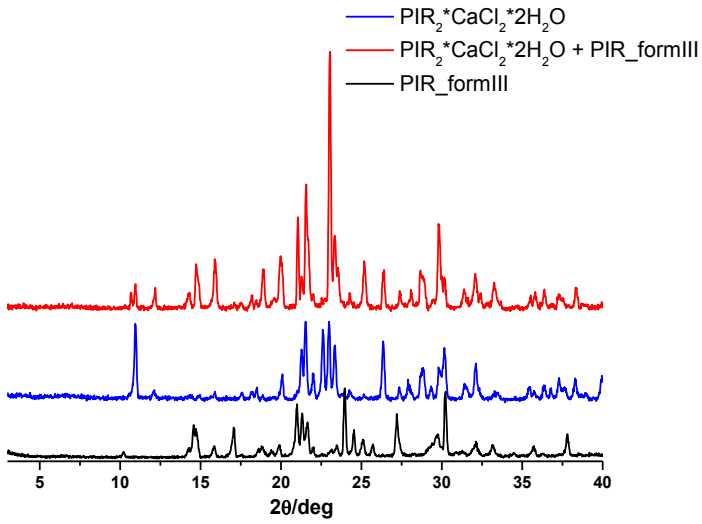

Figure S12. X-ray powder diffraction patterns observed for **3 (blue trace)**, slurry in water of **3** and piracetam (2nd method- **red trace**) and **piracetam** (**PIR**- form III – **black trace**).

DSC measurements of 1, 2, 3 and 4.

1st Method

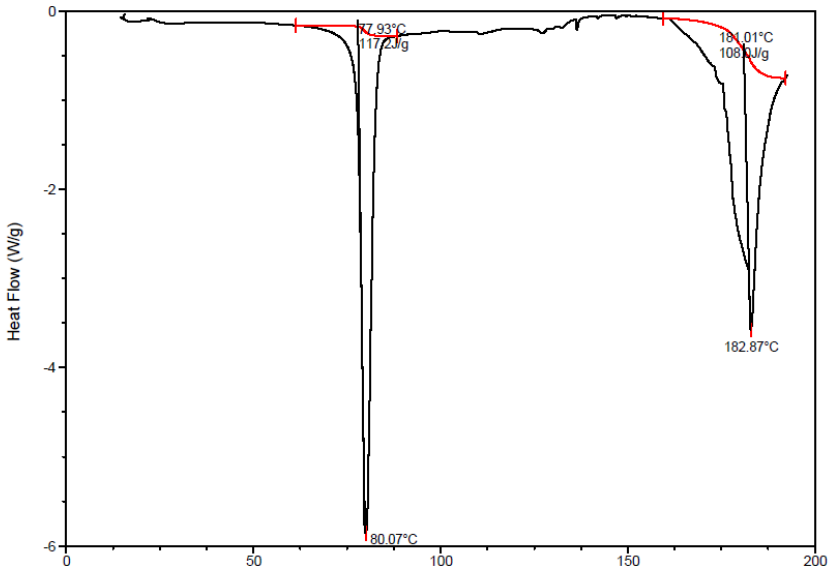

Figure S13. DSC measurement of **1**; RT → 130°C heating rate 10°C/min, 130°C → 160°C heating rate 2°C/min, 160°C → 200°C heating rate 15°C/min.

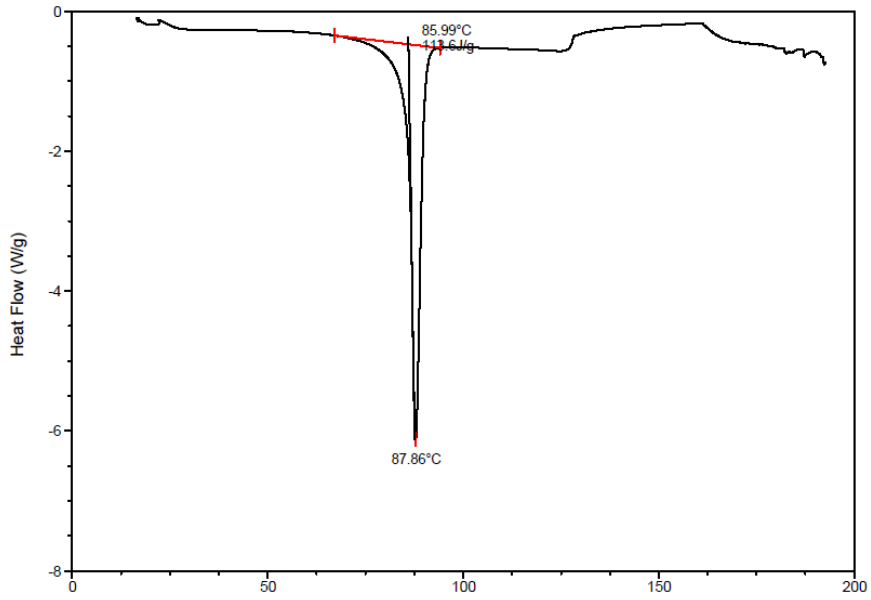

Figure S14. DSC measurement of **2.** RT → 130°C heating rate 10°C/min, 130°C → 160°C heating rate 2°C/min, 160°C → 200°C heating rate 15°C/min.

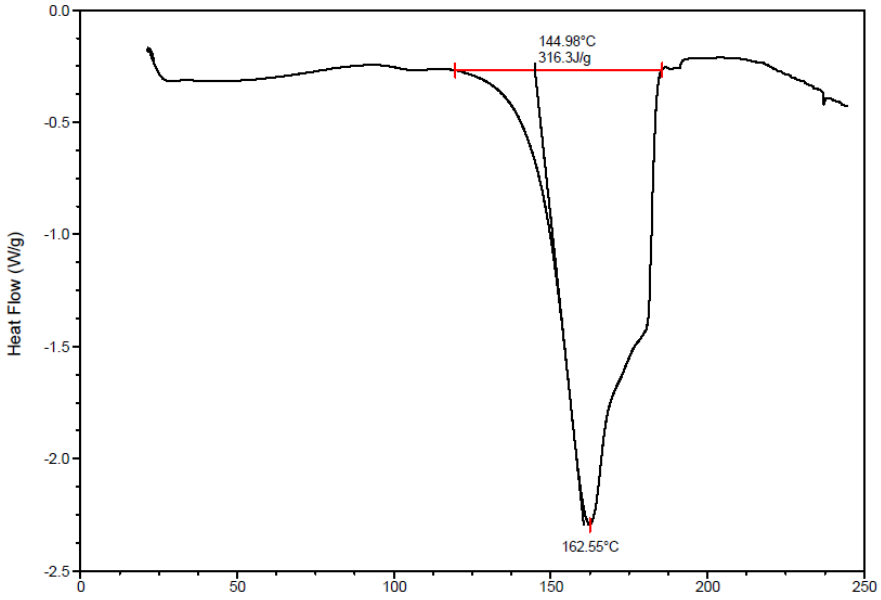

Figure S15. DSC measurement of **3;** heating rate 5°C/min.

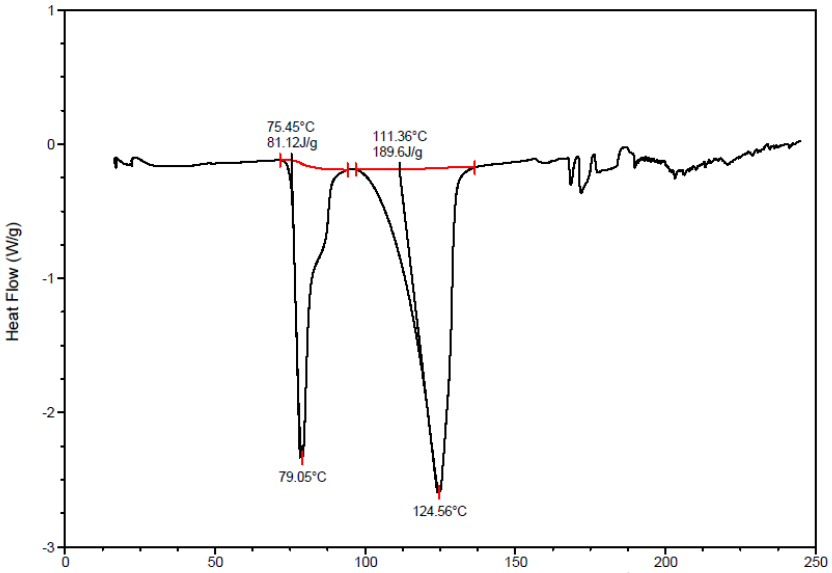

Figure S16. DSC measurement of **4;** heating rate 5°C/min.

2nd Method

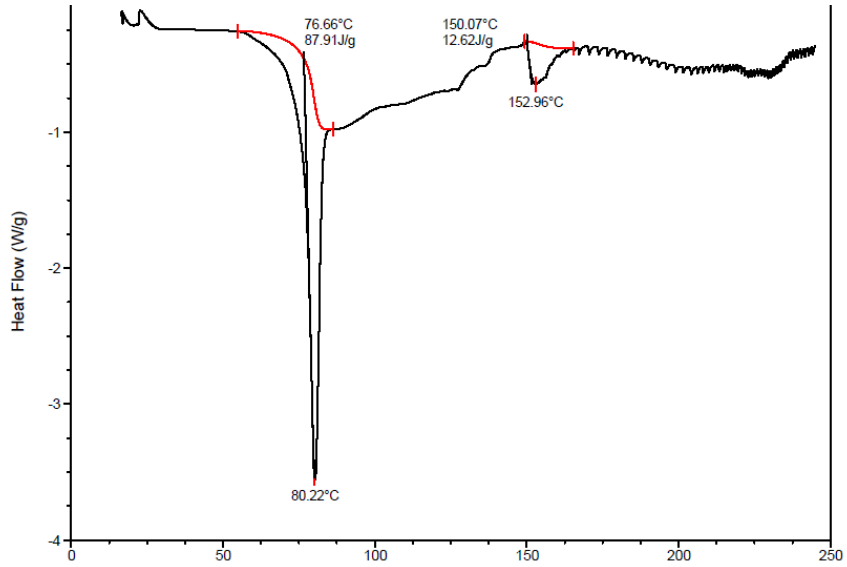

Figure S17. DSC measurement of **1 + PIR ;** heating rate 5°C/min.

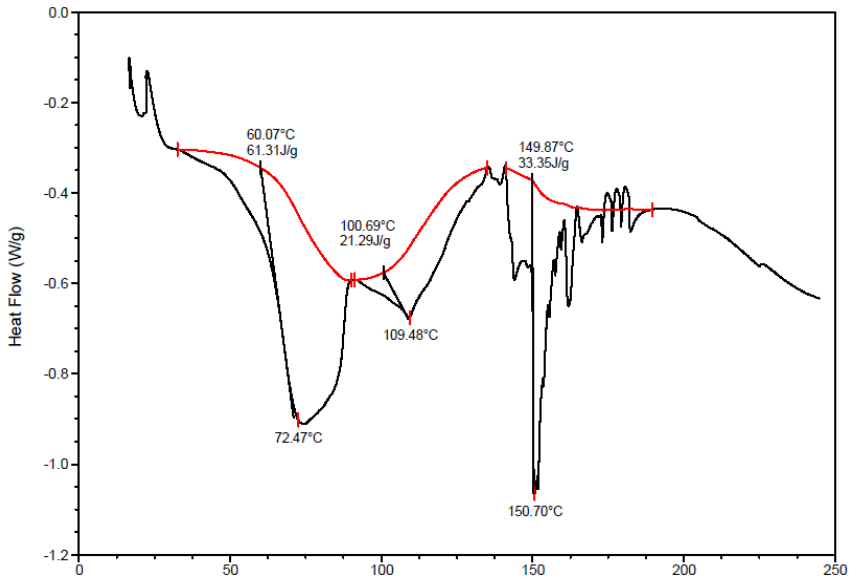

Figure S18. DSC measurement of **2 + PIR ;** heating rate 5°C/min.

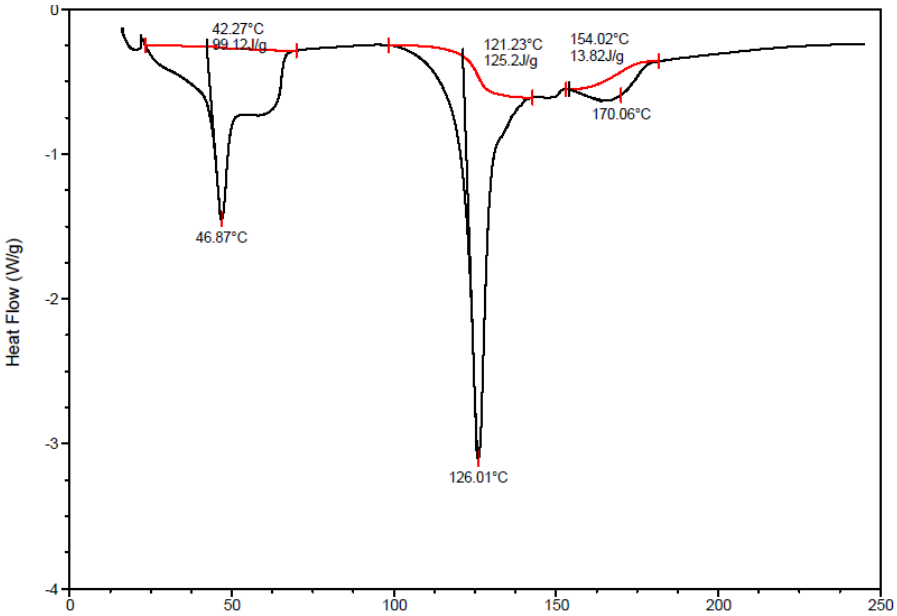

Figure S19. DSC measurement of **3 + PIR ;** heating rate 5°C/min.

Ionic Co-Crystals (1), (2), (3) and (4). <u>Solubility studies in EtOH</u>

XRPD patterns of **1**, **2**, **3** and **4.**

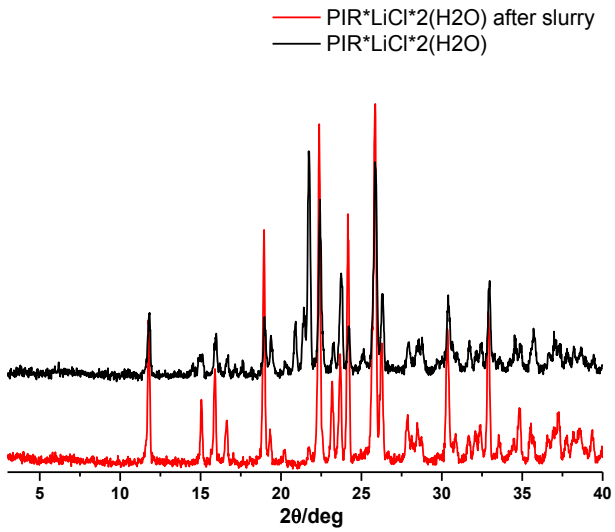

Figure S20. X-ray powder diffraction patterns observed for **1 (black trace)** vs **1** after slurry in ethanol (1st method) **(red trace)**.

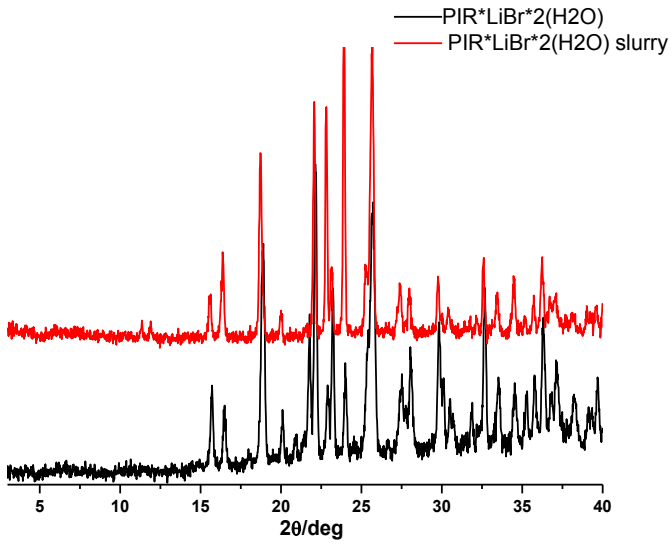

Figure S21. X-ray powder diffraction patterns observed for **2 (black trace)** vs **2** after slurry in ethanol (1st method) **(red trace)**.

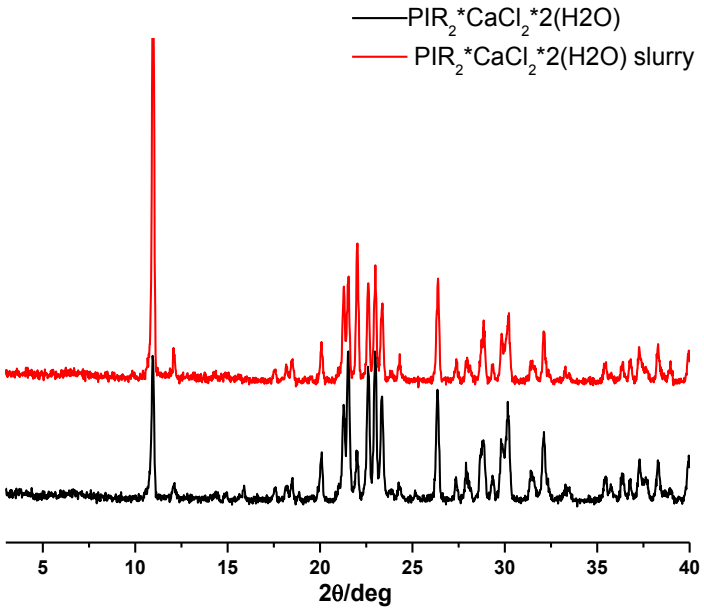

Figure S22. X-ray powder diffraction patterns observed for **3 (black trace)** vs **3** after slurry in ethanol (1st method) **(red trace)**.

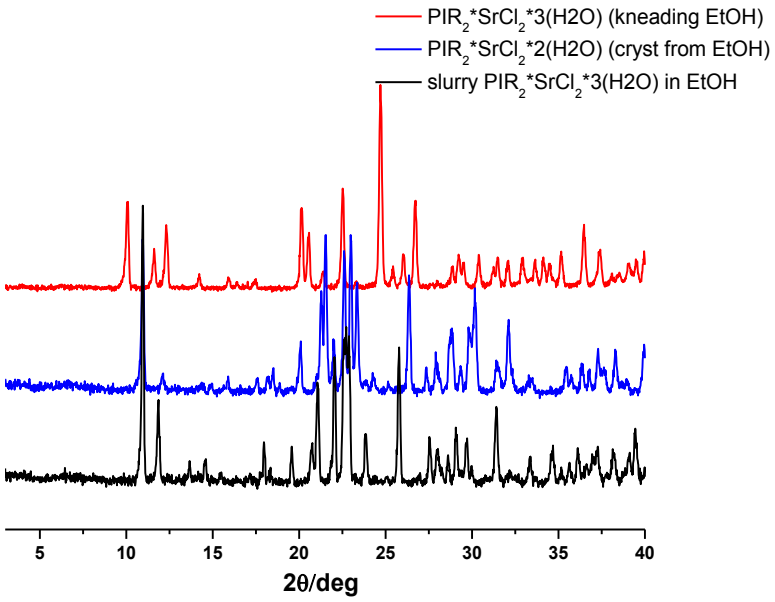

Figure S23. X-ray powder diffraction patterns observed for **4 (red trace), phase X** after slurry of **4** in ethanol (13days - 1st method) **(black trace)** and **$PIR_2SrCl_2{\cdot}2H_2O$ (blue trace)**.

DSC measurements of 1, 2, 3 and 4.

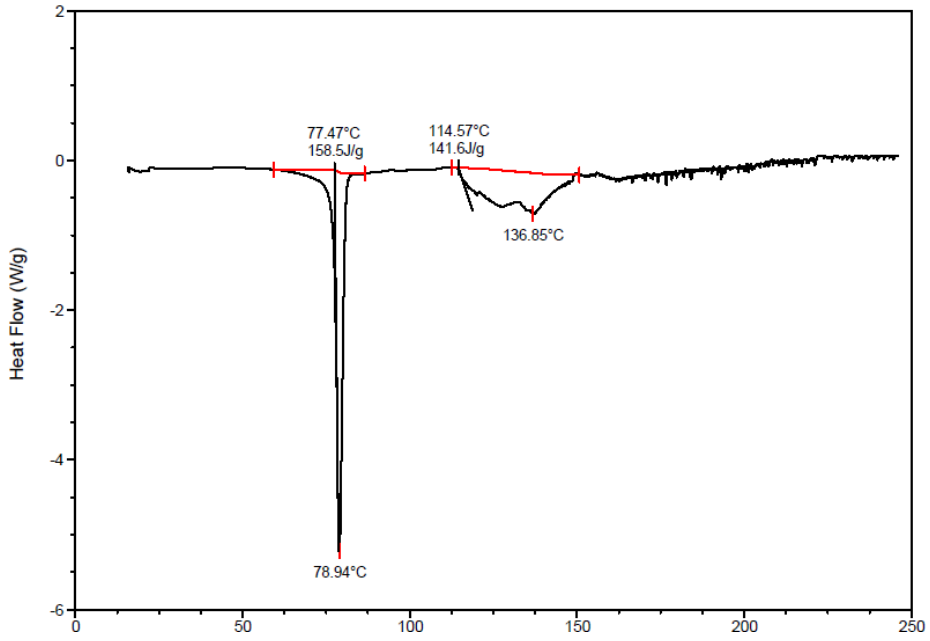

Figure S24. DSC measurement of 1 **after slurry in ethanol** ; heating rate 5°C/min.

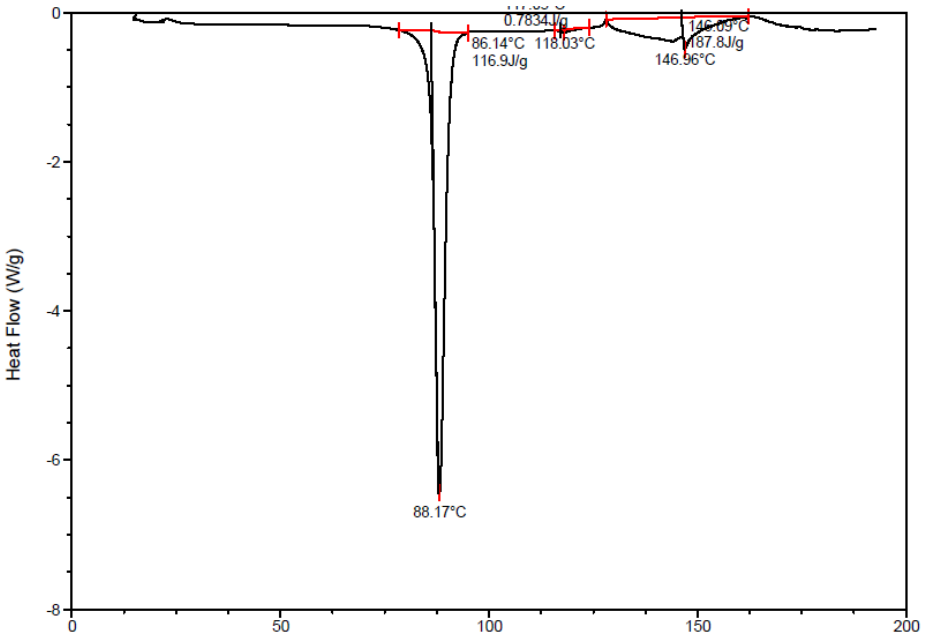

Figure S25. DSC measurement **of 2 after slurry in ethanol**; RT → 130°C heating rate 10°C/min, 130°C → 160°C heating rate 2°C/min, 160°C → 200°C heating rate 15°C/min.

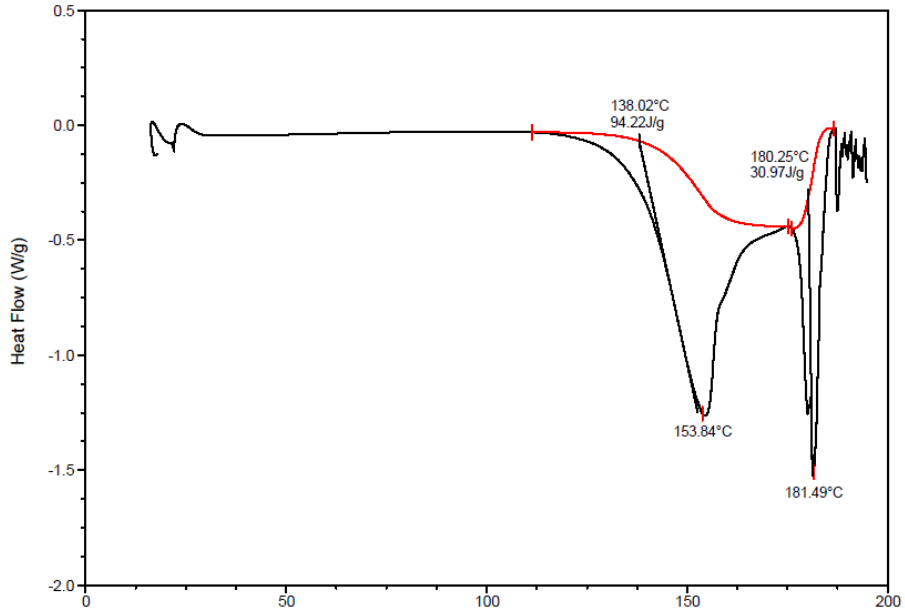

Figure S26. DSC measurement **of 3 after slurry in ethanol**; heating rate 5°C/min.

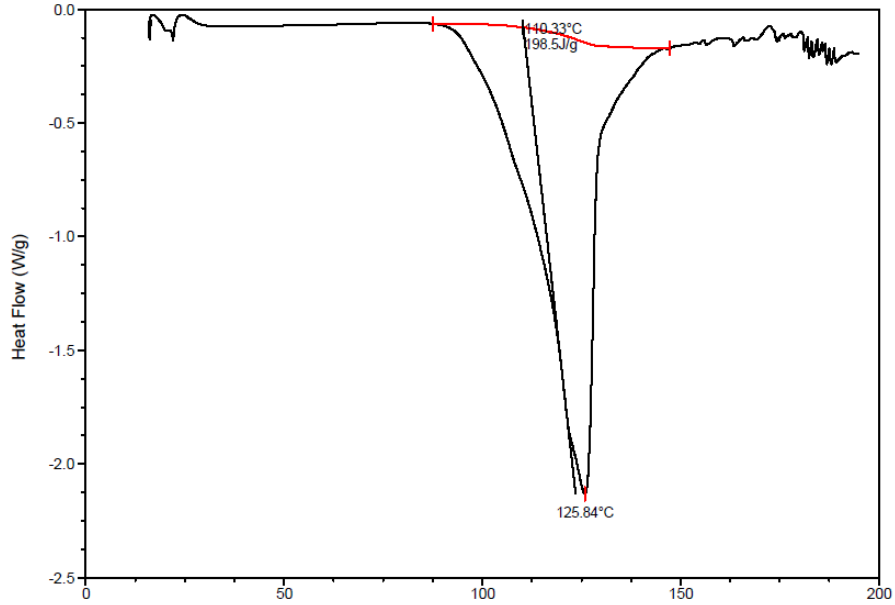

Figure S27. DSC measurement of 4 after slurry in ethanol (13days)**; heating rate 5°C/min.**

Deliquescence relative humidity: stability studies

XRPD patterns of **1**, **2**, **3** and **4.**

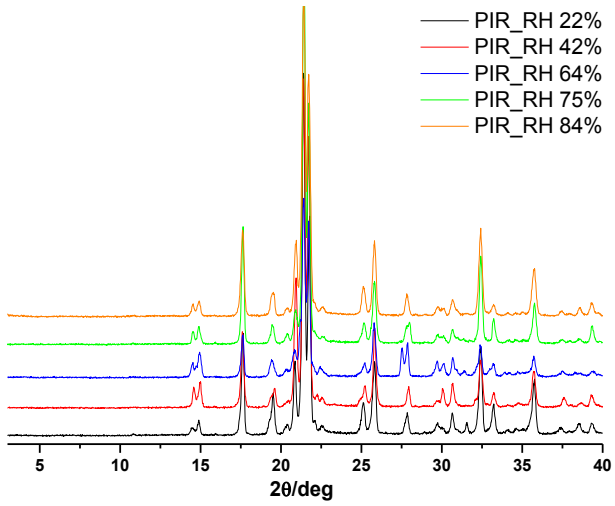

Figure S28. X-ray powder diffraction patterns observed for **PIR** exposed to **RH 22% (black trace), RH 42% (red trace), RH 64% (blue trace)**, **RH 75% (green trace), RH 84% (orange trace)**

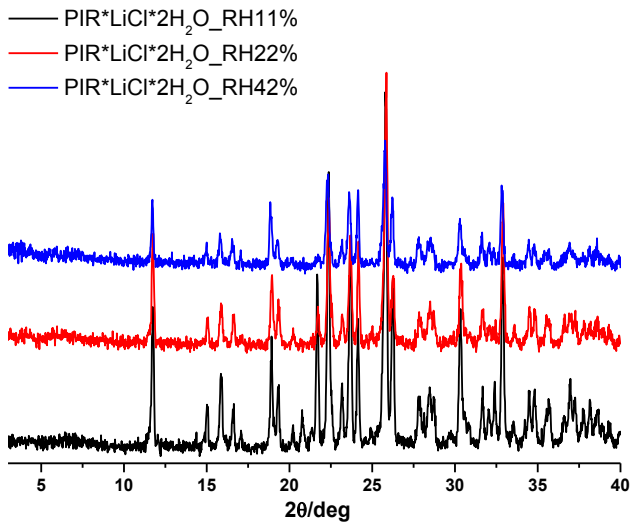

Figure S29. X-ray powder diffraction patterns observed for **1** exposed to **RH 11% (black trace), RH 22% (red trace)** and **RH 42% (blue trace)**.

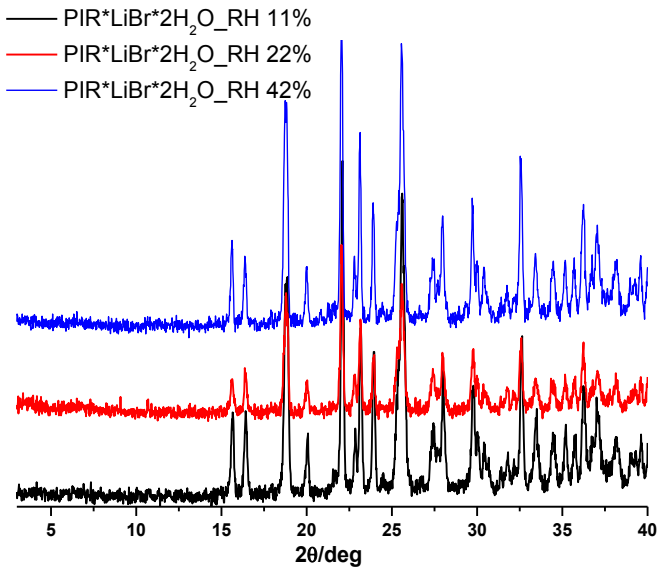

Figure S30. X-ray powder diffraction patterns observed for **2** exposed to **RH 11% (black trace), RH 22% (red trace)** and **RH 42% (blue trace)**.

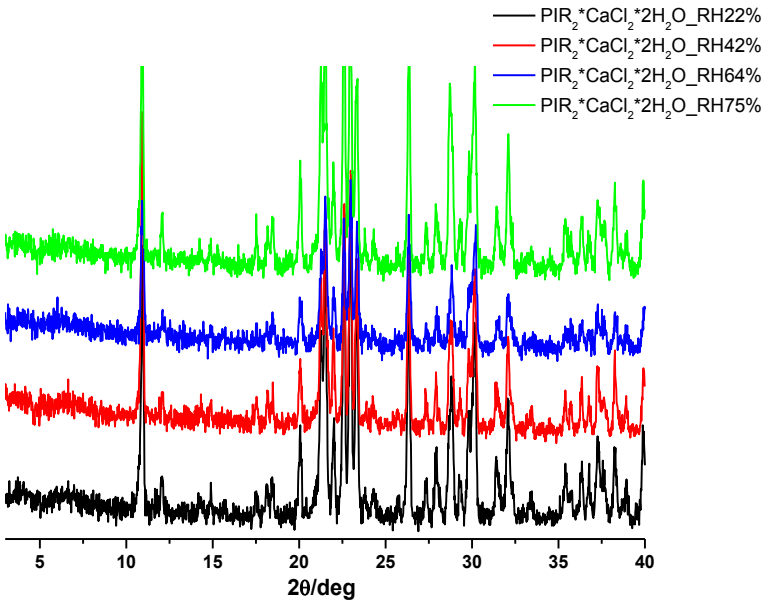

Figure S31. X-ray powder diffraction patterns observed for **3** exposed to **RH 22% (black trace), RH 42% (red trace), RH 64% (blue trace)** and **RH 75% (green trace)**.

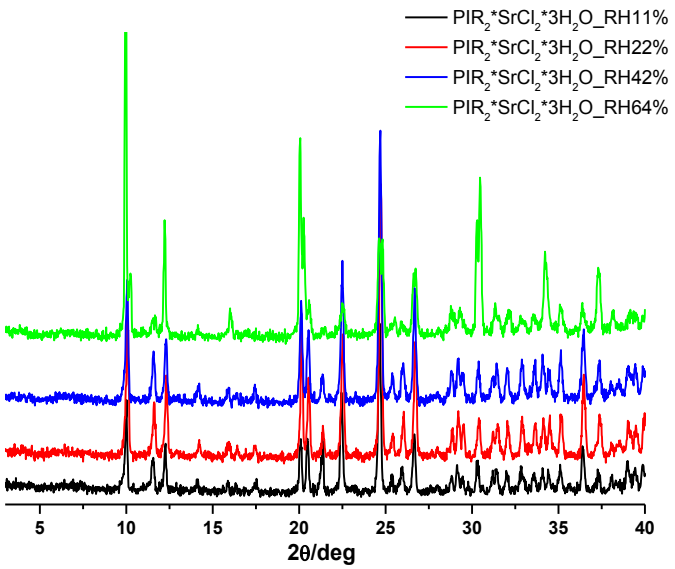

Figure S32. X-ray powder diffraction patterns observed for **4** exposed to **RH 11% (black trace), RH 22% (red trace)** and **RH 42% (blue trace)** and **RH 64% (green trace)**.

*DSC measurements of **1, 2, 3** and **4.***

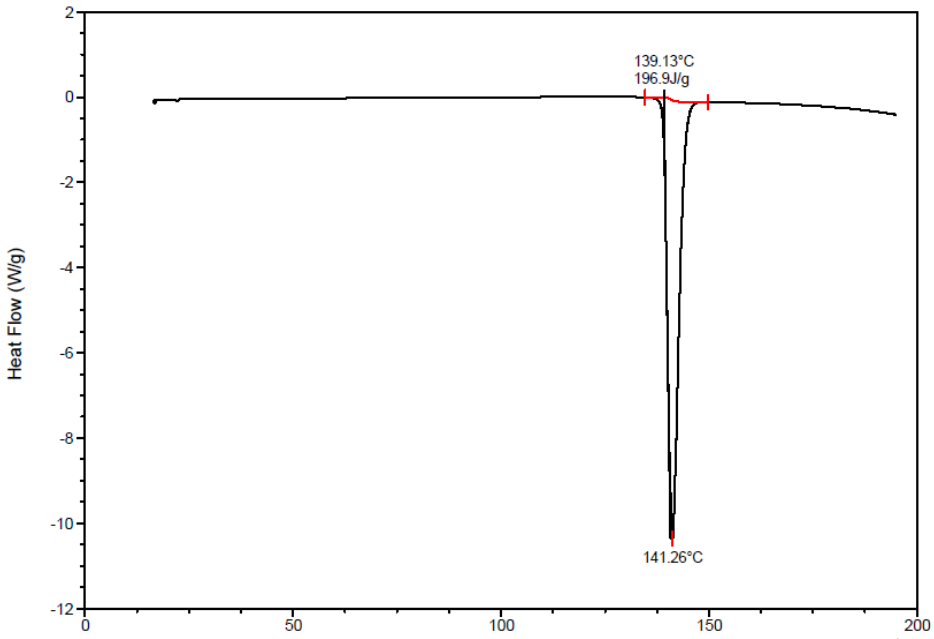

Figure S33. DSC measurement of PIR **exposed to RH 22%;** heating rate 5°C/min.

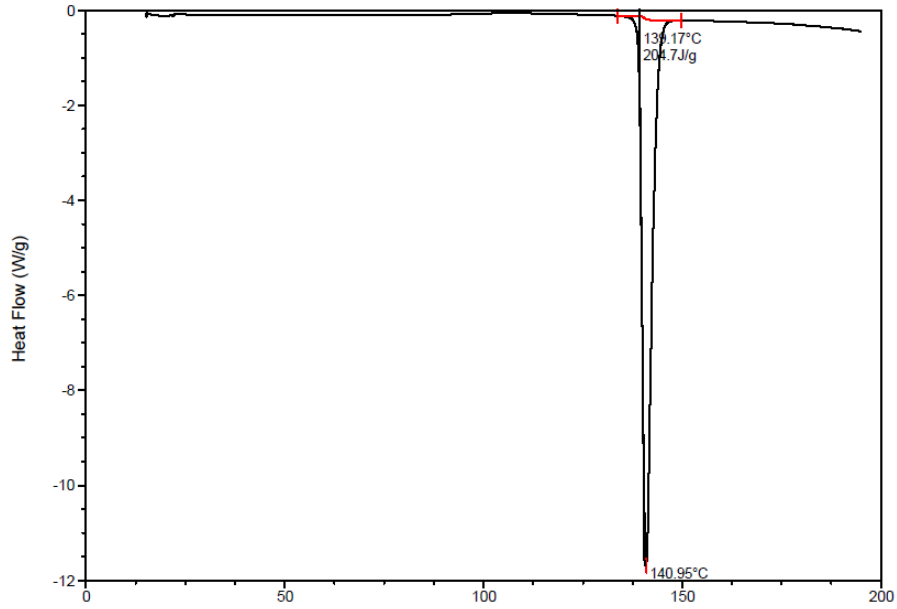

Figure S34. DSC measurement of **PIR exposed to RH 42%**; heating rate 5°C/min.

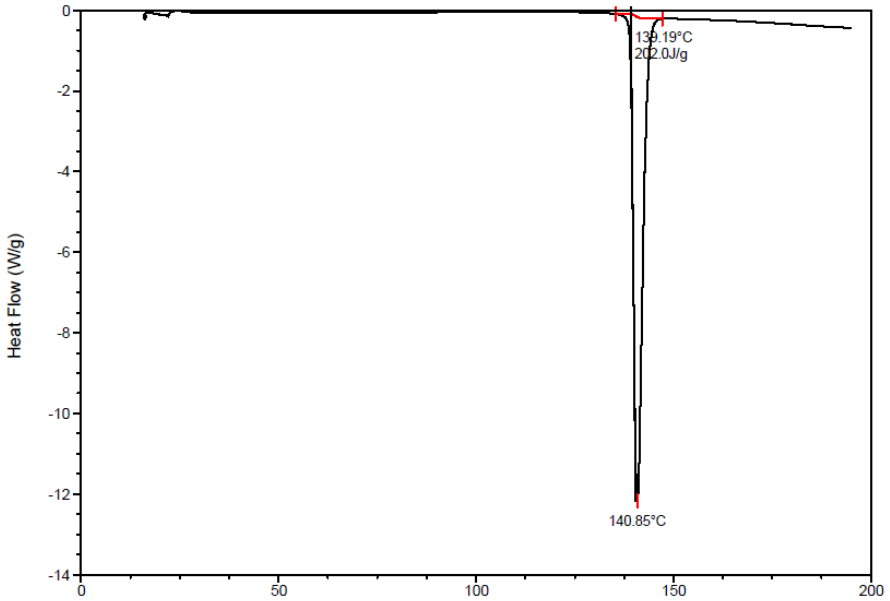

Figure S35. DSC measurement of **PIR exposed to RH 64%**; heating rate 5°C/min.

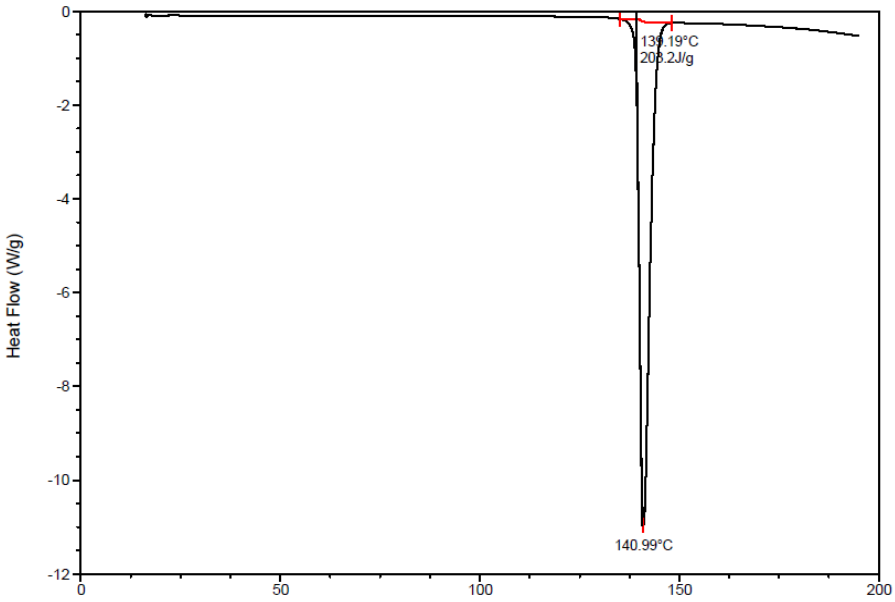

Figure S36. DSC measurement of PIR **exposed to RH 84%**; heating rate 5°C/min.

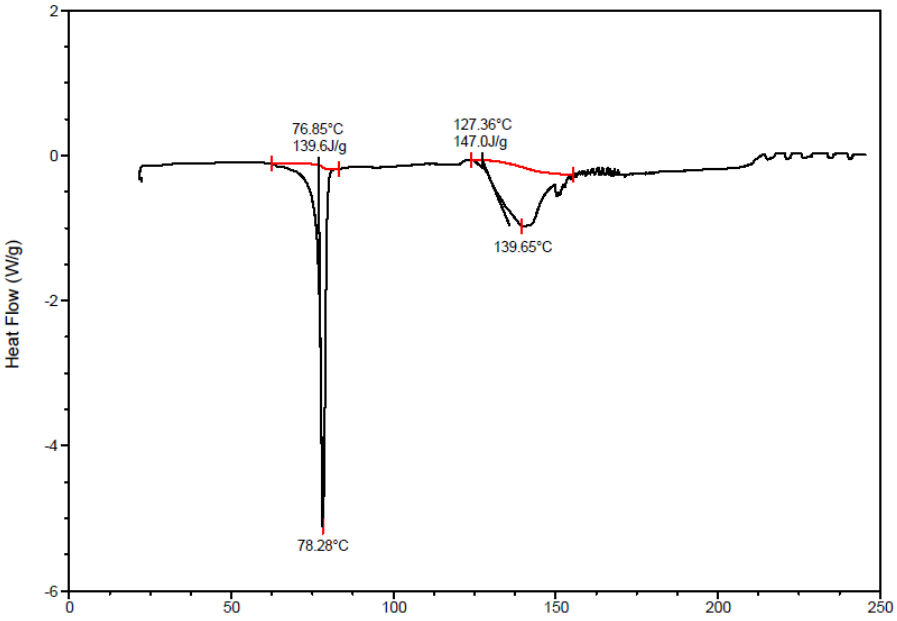

Figure S37. DSC measurement of **1 exposed to RH 11%;** heating rate 5°C/min.

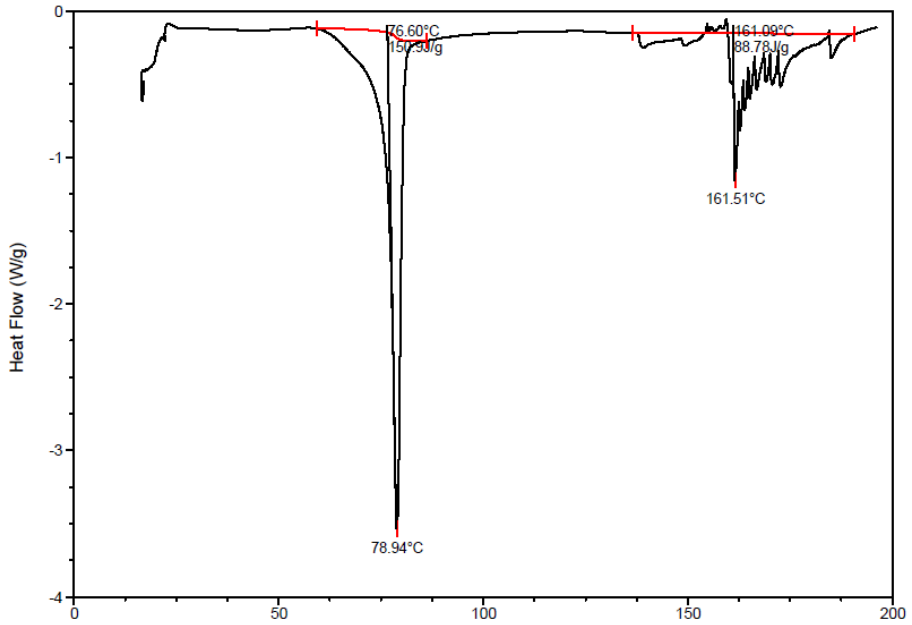

Figure S38. DSC measurement of 1 **exposed to RH 22%;** heating rate 5°C/min.

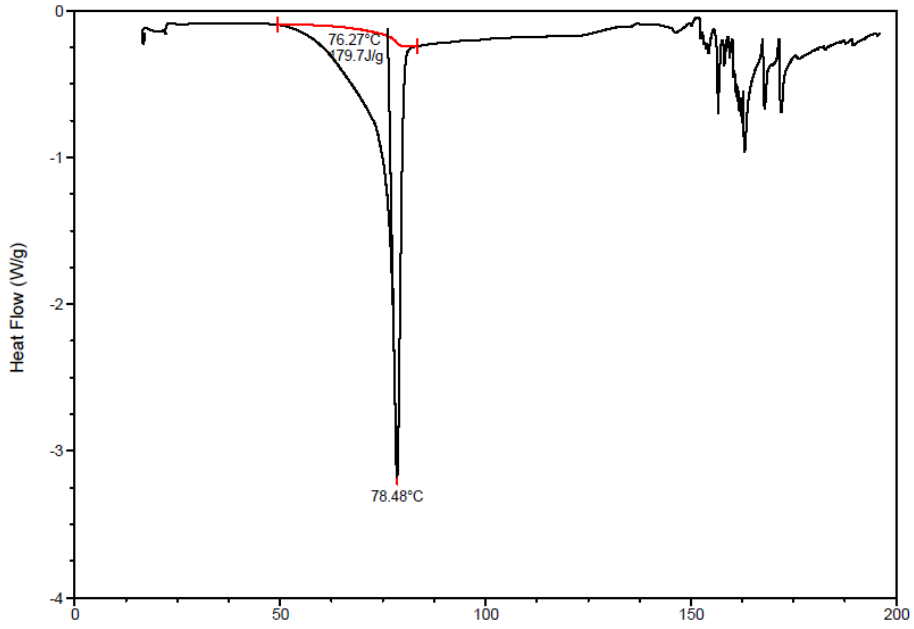

Figure S39. DSC measurement of 1 **exposed to RH 42%;** heating rate 5°C/min.

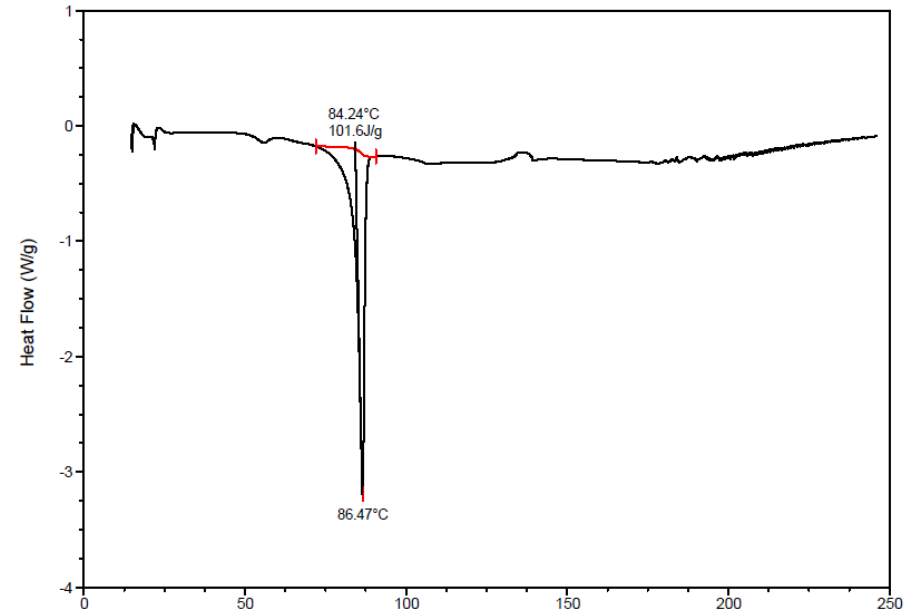

Figure S40. DSC measurement of 2 **exposed to RH 11%**; heating rate 5°C/min.

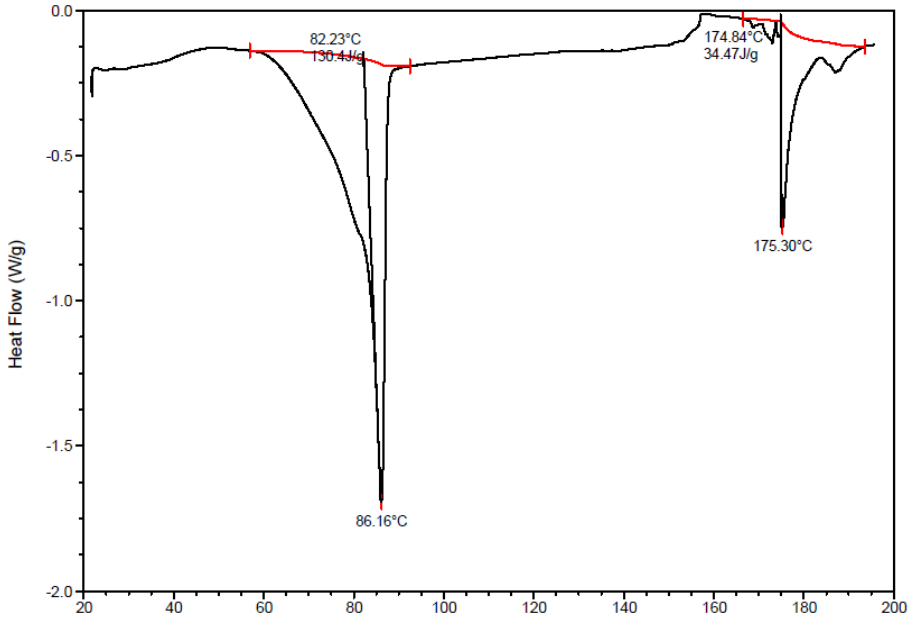

Figure S41. DSC measurement of 2 **exposed to RH 22%;** heating rate 5°C/min.

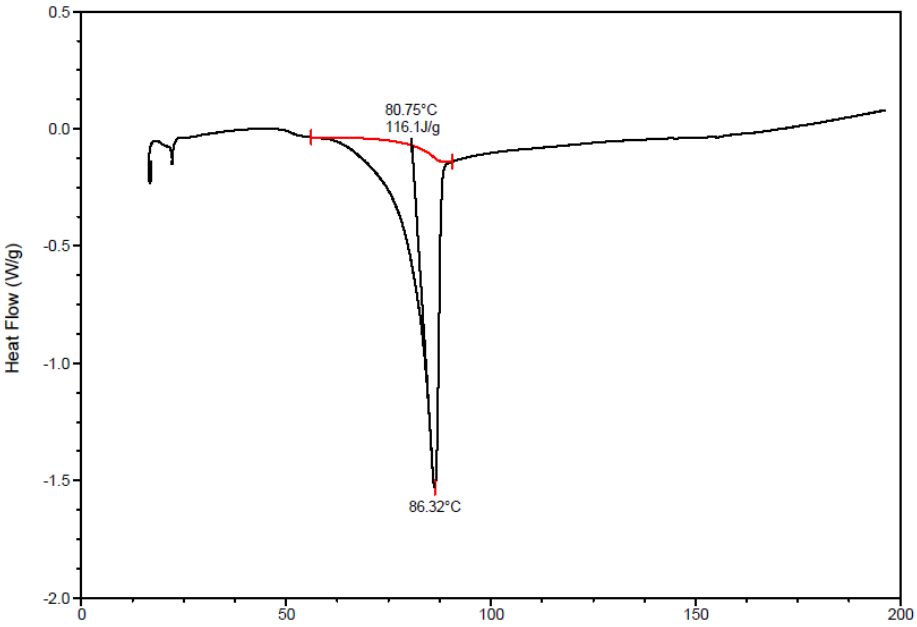

Figure S42. DSC measurement of **2 exposed to RH 42%;** heating rate 5°C/min.

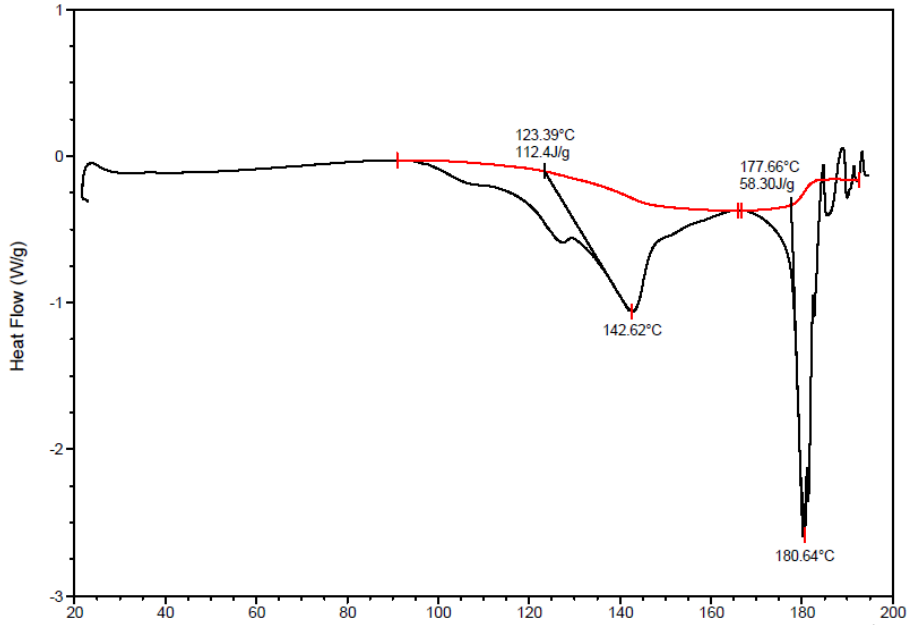

Figure S43. DSC measurement of 3 **exposed to RH 22%;** heating rate 5°C/min.

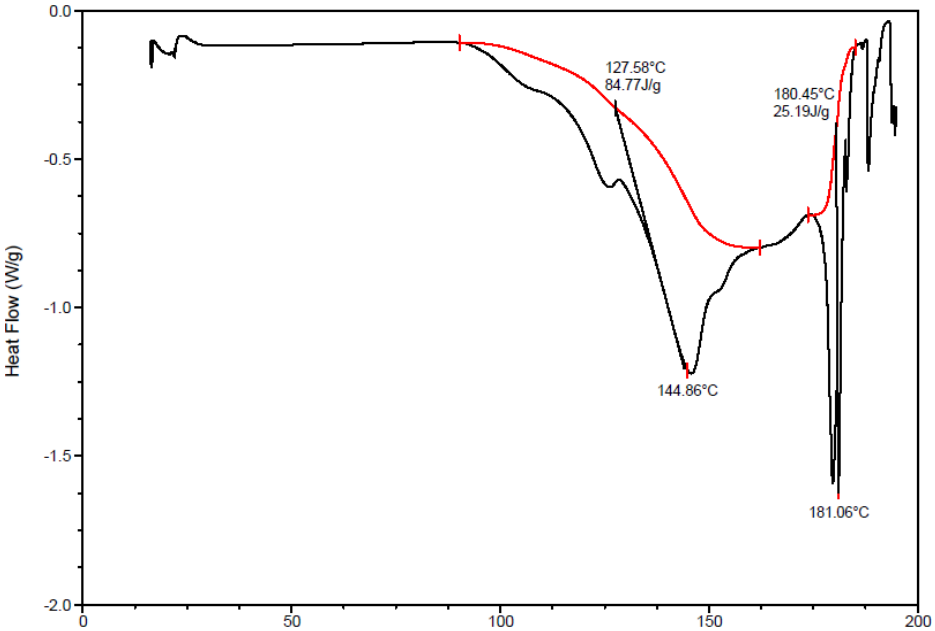

Figure S43. DSC measurement of 3 exposed to RH 42%; heating rate 5°C/min.

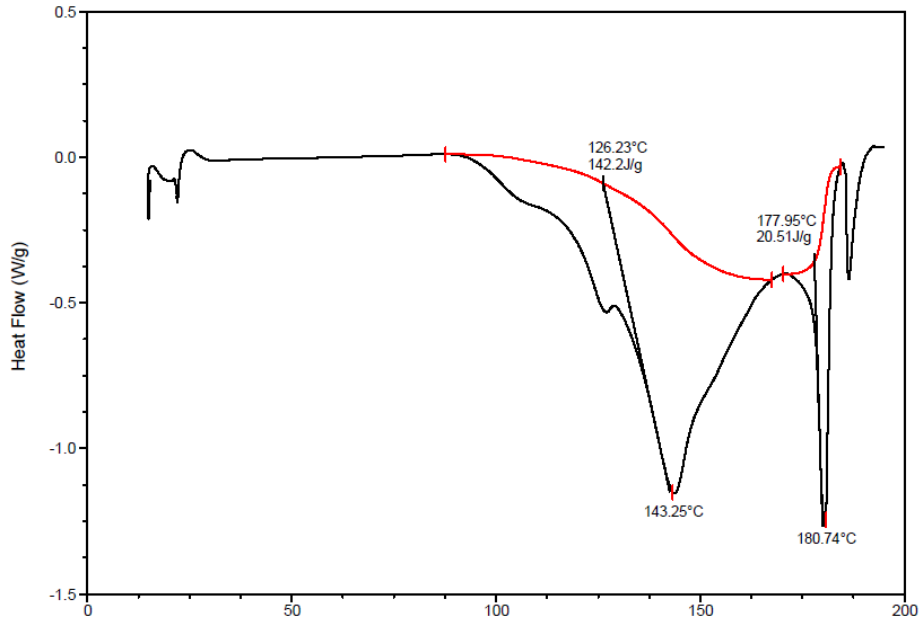

Figure S44. DSC measurement of 3 **exposed to RH 64%;** heating rate 5°C/min.

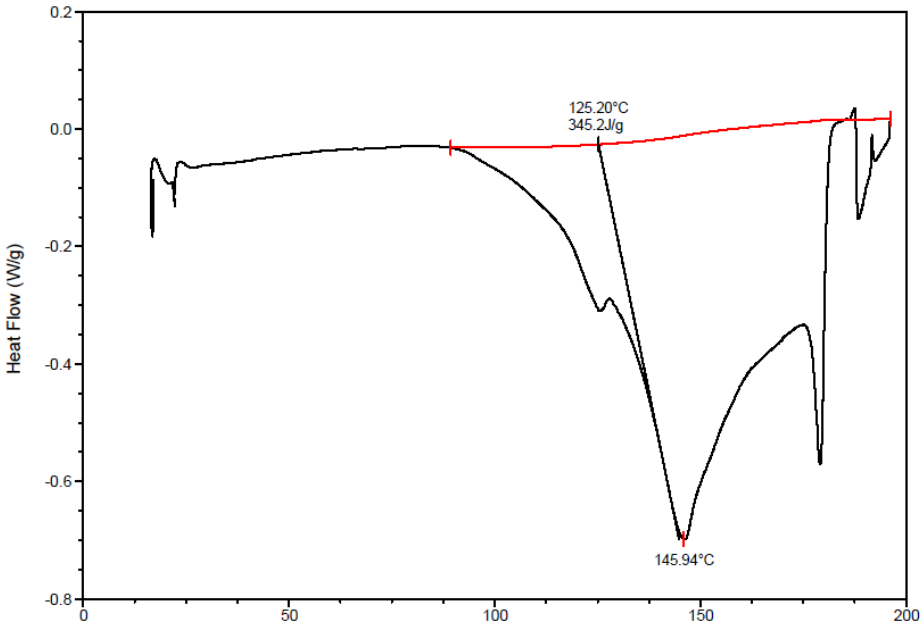

Figure S45. DSC measurement of 3 **exposed to RH 75%;** heating rate 5°C/min.

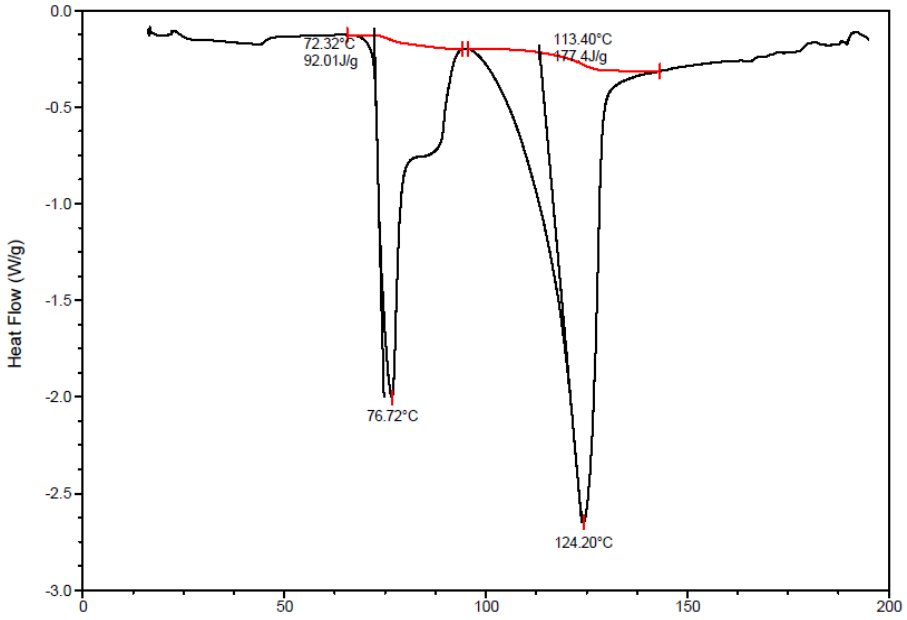

Figure S46. DSC measurement of 4 exposed to RH 22%; heating rate 5°C/min.

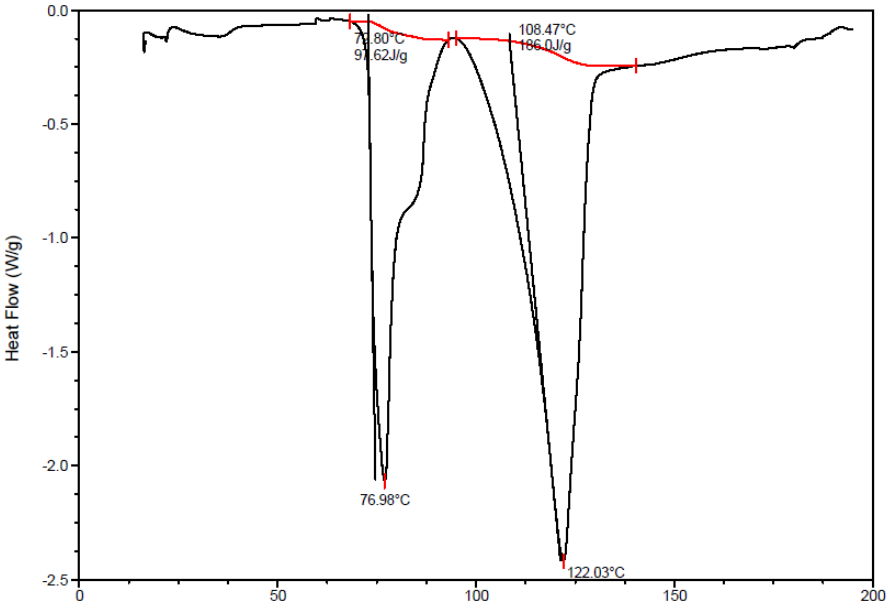

Figure S47. DSC measurement of 4 exposed to RH 42%; heating rate 5°C/min.

Co-formers that increase the solubility of piracetam

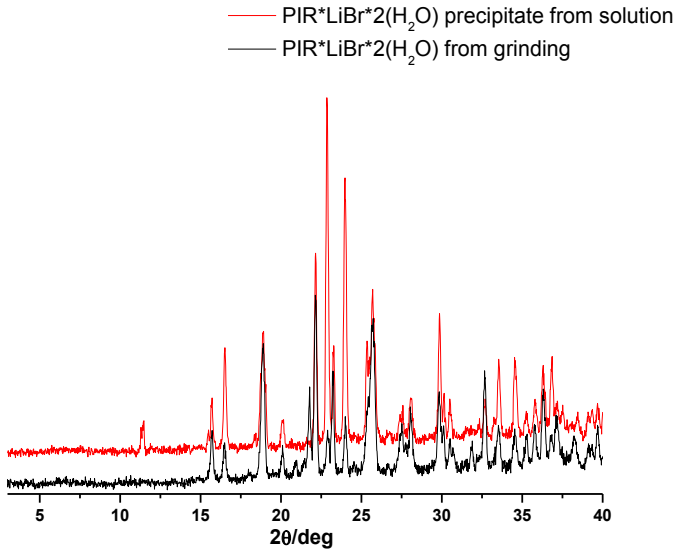

Figure S48. X-ray powder diffraction patterns observed for **2 (black trace)** and **2 precipitate from aqueous solution (red trace)**.

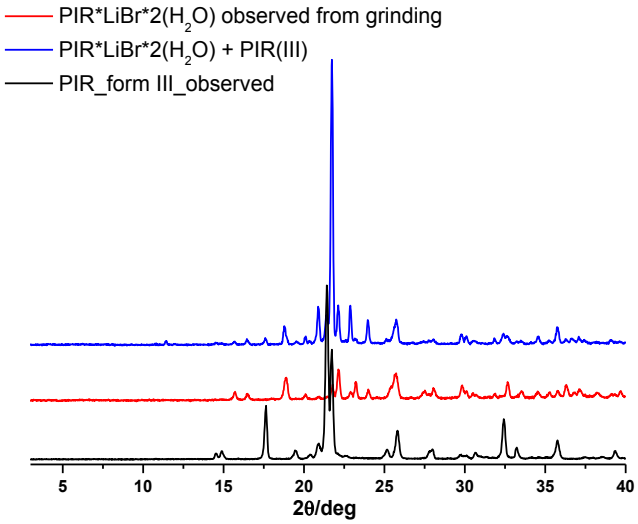

Figure S49. X-ray powder diffraction patterns observed for **PIR-Form III (black trace), 2 (red trace) and 2 + PIR-form III (blue trace).**

Crystal structure determination of $PIR_2{\cdot}SrCl_2{\cdot}3(H_2O)$ from single crystal data (crystallized from H_2O)

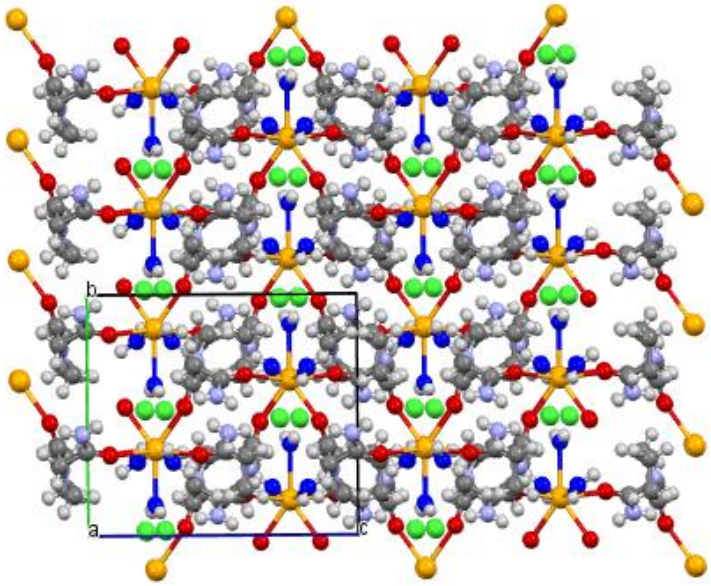

Figure S50. Crystalline packing of **4** – view down the a-axis.

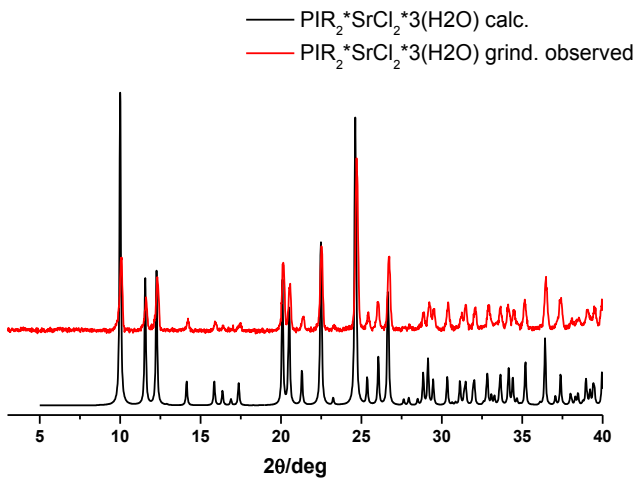

Figure S51. X-ray powder diffraction patterns calculated for **4 (black trace)** and observed for **4 (red trace)**.

REFERENCES:

[1] (a) Nehm, S. J.; Rodriguez-Spong, B.; Rodrìguez-Hornedo, N. *Cryst.Growth Des.* **2006**, 6 (2), 592–600; (b) David J. Good and Naìr Rodrìguez-Hornedo *Crystal Growth & Design,* **2009** 9 (5), 2252-2264; (c) Good, D.J., Rodriguez-Hornedo, N.,. Cocrystal eutectic constants and prediction of solubility behavior. *Crystal Growth & Design* **2010**, 1028–1032. (d) Amjad Alhalaweh, Anders Sokolowski, Naír Rodríguez-Hornedo, and Sitaram P. Velaga; *Cryst. Growth Des.* **2011**, 11, 3923–3929; (e) Ranjit Thakuriaa, Amit Deloria, William Jonesa, Maya P. Lipert, Lilly Roy, Nair Rodriguez-Hornedo, *International Journal of Pharmaceutics* 453 (**2013**) 101– 125

[2] (a) Braga, D.; Grepioni, F.; Maini, L.; Prosperi, S.; Gobetto, R.; Chierotti, M. R. *Chem.Commun*. **2010**, 46, 7715–7717.(b) D. Braga, F. Grepioni, G. I. Lampronti, L. Maini and A. Turrina, Cryst. Growth Des., **2011**, 11, 5621–5627. (c) D. Braga, F. Grepioni, L. Maini, G. I. Lampronti, D. Capucci and C. Cuocci, CrystEngComm, **2012**, 14, 3521–3527. (d) D. Braga, F. Grepioni, L. Maini, D. Capucci, S. Nanna, J. Wouters, L. Aerts and L. Quéré, *Chem. Commun*., **2012**, 48, 8219–8221 (e) J. Wouters, F. Grepioni, D. Braga, R. M. Kaminski, S. Rome, L. Aerts and L. Quéré, *CrystEngComm*, **2013**, 15, 8898–8902. (f) Fabrizia Grepioni, Johan Wouters, Dario Braga, Saverio Nanna, Baptiste Fours,Gérard Coquerel, Geraldine Longfils, Sandrine Rome, Luc Aerts and Luc Quéré, *CrystEngComm,* **2014**,16, 5887–5896

[3] (a) Maher, A.; Croker, D.; Rasmuson, A. C.; Hodnett, B. K. *J. Chem.Eng. Data* **2010**, 55, 5314–5318; (b) Anthony Maher, Denise M. Croker, Åke C. Rasmuson, and Benjamin K. Hodnett *Cryst. Growth Des*. **2012**, 12, 6151−6157; (c) Anthony Maher, Åke C. Rasmuson, Denise M. Croker, and Benjamin K. Hodnett *J. Chem. Eng. Data* **2012**, 57, 3525−3531; (d) Anthony Maher, Colin C. Seaton, Sarah Hudson, Denise M. Croker, Åke C. Rasmuson, and Benjamin K. Hodnett *Cryst. Growth Des*. **2012**, 12, 6223−6233.

[4] (a) Jacques, J.; Wilen, S. H. Enantiomers, Racemates, and Resolution.; Krieger Publishing Company: Malabar, FL, **1991**; (b)Klussmann, M.; White, A. J. P.; Armstrong, A.; Blackmond, D. G. Angew. Chem., Int. Ed. **2006**, 45 (47), 7985–7989.

[5] Adnan K. Salameh1 and Lynne S. Taylor1,Pharmaceutical Research, Vol. 22, No. 2, February **2005**; (b) G. Zografi. States of water associated with solids. Drug Dev. Ind. Pharm. 14:1905–1926 (**1988**); (c) G. Zografi and B. Hancock. Water-solid interactions in pharmaceutical systems. In T. Nagai (ed.), Topics in Pharmaceutical Sciences 1993, Proceedings of International Congress on Pharmaceutical Sciences f.I.P., Medpharm Scientific, Stuttgart, Germany **1994**, pp. 405–419.

[6] Christian A. Heinen, Stefan Reuss, Gordon L. Amidon, and Peter Langguth *Mol. Pharmaceutics* **2013**, 10, 3989−3996.

*2.4 COMBINING PIRACETAM AND LITHIUM SALTS: IONIC CO-CRYSTALS AND CO-DRUGS?**

Ionic co-crystals of piracetam with the inorganic salts LiCl and LiBr were synthesized through solid state reactions (grinding and kneading) and from solution as well. Ionic co-crystal are crystalline materials composed by organic molecule and inorganic salts of alkaline and alkaline earth metals, and stabilized by synergic action of organic and inorganic interactions. Crystallization from water solutions of piracetam with LiCl and LiBr yield crystalline materials of PIR·LiCl·2(H_2O) and PIR·LiBr·2(H_2O) respectively. PIR·LiBr·2(H_2O) was found to be isomorphous with PIR·LiCl·2(H_2O). Kneading of Piracetam with LiCl produced two crystalline phases corresponding to PIR·LiCl·2(H_2O) and the relative anhydrous form. The physical-chemical properties of these two crystalline forms in addition to PIR·LiBr·2(H_2O) have been studied and characterized by single crystal and powder X-ray diffraction at variable temperatures, DSC, TGA, hot stage microscopy (HSM) and intrinsic dissolution rate (IDR). The ionic co-crystals studied have different properties with respect to pure components especially in terms of thermal stability. Moreover, it was observed that the thermal relationships between hydrate and anhydrous form of the ionic co-crystals with LiCl also depend on the method for preparation and/or on the conditions of measurements. It confirms, on the other hand, that the thermal techniques used to characterize the systems of interest are complementary each other and give only a part of the overall information. In this regard, also the role of the intrinsic properties of the crystalline phase such as crystallinity and size (milli metric or micrometric) of the crystals is important and it is still a forefront topic open at new perspective.

*D. Braga, F. Grepioni, L. Maini, D. Capucci, S. Nanna, J. Wouters, L. Aerts and L. Quéré, *Chem. Commun.*, **2012**, 48, 8219–8221

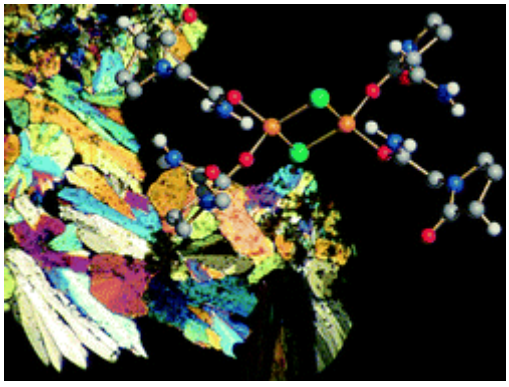

For copyright reasons only the link to the original article is reported here:

http://pubs.rsc.org/en/content/articlelanding/2012/cc/c2cc33855f#!divAbstract

*2.5 IMAZAMOX: A QUEST FOR POLYMORPHIC MODIFICATIONS OF A CHIRAL AND RACEMIC HERBICIDE**

Chiral and racemic imazamox was characterized and assessed in solid state. In detail, crystal structure of four polymorphs of chiral imazamox were solved and thermally characterized. Moreover, we were able to identify the thermodynamically stable forms at room and high temperatures. In addition, the adoption of salts in the crystallization media has had positive effects, allowing the production of new polymorphs with different morphologies/sizes of the crystal. Potential polymorphs in agrochemical field, induced by different crystallization environment, can be interesting in the process of identifying stable forms during industrial production processes.

*Dario Braga , Laura Chelazzi, Fabrizia Grepioni , Saverio Nanna, Katia Rubini, Marco Curzi, Stefano Giaffreda, Heidi E. Saxell, Matthias Bratz, and Tiziana Chiodo, Cryst. Growth Des., 2014, 14 (3), pp 1430–1437

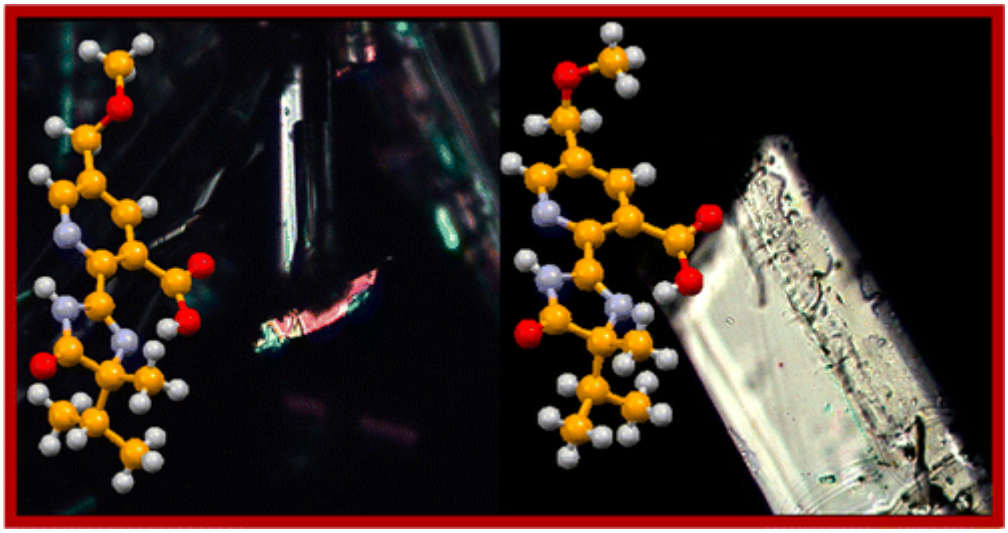

For copyright reasons only the link to the original article is reported here:

http://pubs.acs.org/doi/abs/10.1021/cg4019025

*2.6 BENTAZON: EFFECT OF ADDITIVES ON THE CRYSTALLIZATION OF PURE AND MIXED POLYMORPHIC FORMS OF A COMMERCIAL HERBICIDE**

After polymorph screening studies on the bentazon molecule, two different polymorphs, Forms II and III (Form I already reported in literature), were isolated and characterized with X-ray single crystal diffraction, X-ray powder diffraction (XRPD), variable temperature X-ray powder diffraction (VTXRPD), differential scanning calorimetry (DSC), and hot-stage microscopy (HSM). Unlike the pharmaceutical field, the investigation of agrochemical compounds in solid state is very interesting, being a relatively unexplored field. Indeed, a better understanding of the solid state properties of these unexplored crystalline forms can represent a resource for the industry and a challenge for solid-state chemists.

Dario Braga, Fabrizia Grepioni , Laura Chelazzi, Saverio Nanna, Katia Rubini, Marco Curzi, Stefano L. Giaffreda, Heidi E. Saxell, Matthias Bratz, and Tiziana Chiodo, Cryst. Growth Des., 2014, 14 (11), pp 5729–5736.

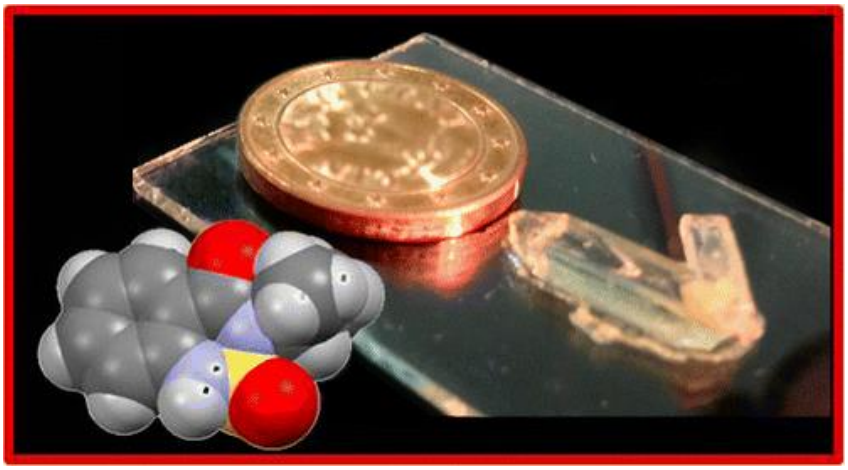

For copyright reasons only the link to the original article is reported here:

http://pubs.acs.org/doi/abs/10.1021/cg500980j

*2.7 IONIC CO-CRYSTALS OF RACETAMS: SOLID-STATE PROPERTIES ENHANCEMENT OF NEUTRAL ACTIVE PHARMACEUTICAL INGREDIENTS VIA ADDITION OF MG^{2+} AND CA^{2+} CHLORIDES**

Mechanochemical and solution based reactions between brivaracetam (BRV) or seletracetam (SEL) and calcium or magnesium salts ($CaCl_2$ and $MgCl_2$) have been conducted yielding ionic co-crystals. These new materials showed different/improved physical-chemical properties with respect to pure drug in terms of thermal stability, hygroscopicity and crystal morphology. Furthermore, the relationship between crystal structures and properties was investigated. "$BRV_2{\cdot}MgCl_2{\cdot}4H_2O$ and $SEL_2{\cdot}MgCl_2{\cdot}4H_2O$ co-crystals present an octahedral coordination of Mg2+ within polymeric chains, forming a crystal lattice constituted by lipophilic multilayers". After co-crystallization of BRV and SEL with $MgCl_2$ and $CaCl_2$ changes in the morphology of the crystals were observed as well as different thermal stability was observed respectively. All ionic co-crystals were characterized via a combination of solid-state techniques, i.e. single crystal and powder X-ray diffraction, variable temperature X-ray diffraction, DSC, TGA and hot-stage microscopy (HSM). In addition to thermal stability, changes in hygroscopicity and crystal morphology were observed; indeed, these differences could play a key role not only in the industrial production processes but also in the storage operations.

**Fabrizia Grepioni, Johan Wouters, Dario Braga, Saverio Nanna, Baptiste Fours, Gérard Coquerel, Geraldine Longfils, Sandrine Rome, Luc Aertse and Luc Quére, CrystEngComm, 2014,16, 5887-5896.*

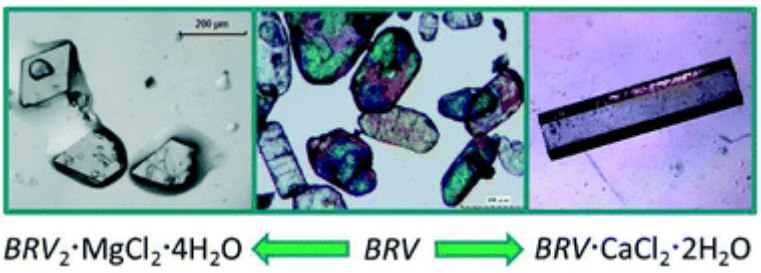

For copyright reasons only the link to the original article is reported here:

http://pubs.rsc.org/en/content/articlelanding/2014/ce/c4ce00409d#!divAbstract

SUMMARY

The aim of this PhD thesis was:

"Optimization of molecular and crystalline forms of drugs, agrochemicals, pesticides in relation to activity, bioavailability, patentability and to the fabrication of polymorphs, solvates, co-crystals with green chemistry methods"

During these three years, each project carried out concerned a part of the overall target. Below are summarized the main results obtained for each project.

Folic acid: an investigation of solid-state properties and crystal forms.

The structure of folic acid was solved by XRPD and the high temperature phase was reported. "Amorphous Salts" and "amorphous ionic co-crystals" of folic acid with inorganic salts were synthesized by solvent free methods and characterized by TGA/DSC and their intrinsic dissolution rate were tested. This study highlights the importance of using different routes of preparation to obtain "new" APIs. In particular, the solid-solid reaction can be used to produce new forms with different physical chemical properties. This aspect together with the possibility to obtain stable amorphous phase over time, without changing the chemical entity, could be an interesting way to obtain new useful results in the pharmaceutical field.

Folic acid revisited: a synergic computational, spectroscopic and structural approach in the solid-state.

In this paper was pointed out how the synergic combination of different techniques at the solid state could be a power-full tool to solve complicated structural problems. The structure of folic acid was solved with X-ray powder diffraction and ab initio calculations reporting for the first time the Raman spectra with peaks assignment too.

Ionic co-crystals of piracetam: from solid to solution

All ICCs are less soluble than the pure piracetam both in H2O and EtOH. Slurry (method 1) and eutectic approach (method 2) methods are consistent each others. A solubilizing effect of the piracetam, until four times the intrinsic solubility, was observed, adding in solution inorganic salts (co-formers of piracetam in the ionic co-crystals - ICCs). There is a synergic effect between ion paring

phenomenon and the solvating effect of the drug molecule in a competition with water molecules for ions coordination, as it is observed in solid state with the ICCs. Piracetam and its ICCs are stable also at high RH%; there is also a stabilization effect of co-crystallization on salts (LiCl in particular) in terms of hygroscopicity. The deliquescent point of the ICCs, predicted from Ross equation, differs from that observed due probably to significant solute-solute interactions for PIR · LiCl · 2(H2O), PIR · LiBr · 2(H2O) and PIR2 · CaCl2 · 2(H2O); this is unsurprising, given the high concentrations involved. We can state that the main aspects of the solid state properties of ICCs are mirrored in solution, resulting in the modification of stability in solution of the drug under investigation, once co-crystallized. This proves one time again how the investigation of solid state properties can be a resource to figure out what is going on in solution and also to design in solid what we are interested to obtain in solution. Piracetam, given its intrinsic high solubility and permeability (bioavailability 100%), was used as a learning model for other systems less soluble and/or permeable, with the aim to choose right co-formers depending on the final requirements. Ionic co-crystals can be a valuable resource to improve not only the solubility but also, in certain cases, the permeability, with the final aim to improve the bioavailability of the molecule of interest.

Combining piracetam and lithium salts: ionic co-crystals and co-drugs?

Ionic co-crystals of piracetam with the inorganic salts LiCl and LiBr were synthesized through solid state reactions (grinding and kneading) and from solution as well. Ionic co-crystal are crystalline materials composed by organic molecule and inorganic salts of alkaline and alkaline earth metals, and stabilized by synergic action of organic and inorganic interactions. Crystallization from water solutions of piracetam with LiCl and LiBr yield crystalline materials of PIR·LiCl·2(H_2O) and PIR·LiBr·2(H_2O) respectively. PIR·LiBr·2(H_2O) was found to be isomorphous with PIR·LiCl·2(H_2O). Kneading of Piracetam with LiCl produced two crystalline phases corresponding to PIR·LiCl·2(H_2O) and the relative anhydrous form. The physical-chemical properties of these two crystalline forms in addition to PIR·LiBr·2(H_2O) have been studied and characterized by single crystal and powder X-ray diffraction at variable temperatures, DSC, TGA, hot stage microscopy (HSM) and intrinsic dissolution rate (IDR). The ionic co-crystals studied have different properties with respect to pure components especially in terms of thermal stability. Moreover, it was observed that the thermal relationships between hydrate and anhydrous form of the ionic co-crystals with LiCl also depend on the method for preparation and/or on the conditions of measurements. It confirms, on the other hand, that the thermal techniques used to characterize the systems of interest are complementary each other and

give only a part of the overall information. In this regard, also the role of the intrinsic properties of the crystalline phase such as crystallinity and size (milli metric or micrometric) of the crystals is important and it is still a forefront topic open at new perspective.

Imazamox: A Quest for Polymorphic Modifications of a Chiral and Racemic Herbicide

Chiral and racemic imazamox was characterized and assessed in solid state. In detail, crystal structure of four polymorphs of chiral imazamox were solved and thermally characterized. Moreover, we were able to identify the thermodynamically stable forms at room and high temperatures. In addition, the adoption of salts in the crystallization media has had positive effects, allowing the production of new polymorphs with different morphologies/sizes of the crystal. Potential polymorphs in agrochemical field, induced by different crystallization environment, can be interesting in the process of identifying stable forms during industrial production processes.

Bentazon: Effect of Additives on the Crystallization of Pure and Mixed Polymorphic Forms of a Commercial Herbicide

After polymorph screening studies on the bentazon molecule, two different polymorphs, Forms II and III (Form I already reported in literature), were isolated and characterized with X-ray single crystal diffraction, X-ray powder diffraction (XRPD), variable temperature X-ray powder diffraction (VTXRPD), differential scanning calorimetry (DSC), and hot-stage microscopy (HSM). Unlike the pharmaceutical field, the investigation of agrochemical compounds in solid state is very interesting, being a relatively unexplored field. Indeed, a better understanding of the solid state properties of these unexplored crystalline forms can represent a resource for the industry and a challenge for solid-state chemists.

Ionic co-crystals of racetams: solid-state properties enhancement of neutral active pharmaceutical ingredients via addition of Mg2+ and Ca2+ chlorides

Mechanochemical and solution based reactions between brivaracetam (BRV) or seletracetam (SEL) and calcium or magnesium salts ($CaCl_2$ and $MgCl_2$) have been conducted yielding ionic co-crystals. These new materials showed different/improved physical-chemical properties with respect to pure drug in terms of thermal stability, hygroscopicity and crystal morphology. Furthermore, the

relationship between crystal structures and properties was investigated. "$BRV_2 \cdot MgCl_2 \cdot 4H_2O$ and $SEL_2 \cdot MgCl_2 \cdot 4H_2O$ co-crystals present an octahedral coordination of Mg2+ within polymeric chains, forming a crystal lattice constituted by lipophilic multilayers". After co-crystallization of BRV and SEL with $MgCl_2$ and $CaCl_2$ changes in the morphology of the crystals were observed as well as different thermal stability was observed respectively. All ionic co-crystals were characterized via a combination of solid-state techniques, i.e. single crystal and powder X-ray diffraction, variable temperature X-ray diffraction, DSC, TGA and hot-stage microscopy (HSM). In addition to thermal stability, changes in hygroscopicity and crystal morphology were observed; indeed, these differences could play a key role not only in the industrial production processes but also in the storage operations.

The results relative to the published papers and those that are going to be published are in agreement to the initial target of my PhD. It would be interesting to extend these study to further investigations within the formulation field in the pharmaceutical and agrochemical industry. Indeed, the synthesis of new materials by adopting the principles of synthesis of green chemistry is an important aspect, as respect for the environment is fundamental in order to produce innovative and sustainable crystalline forms on a large-scale. Accordingly, the studies carried out during my PhD can be a stimulus to introduce innovative methods in the formulation field simplifying the conventional industrial processes (using a small number of excipients) and changing the physical-chemical properties with respect to the current formulations.